

FRAGILITY ESTIMATES FOR RC BUILDINGS

Thesis

Submitted in partial fulfilment of the requirements for the
degree of

DOCTOR OF PHILOSOPHY

by

C. M. RAVI KUMAR



**DEPARTMENT OF CIVIL ENGINEERING
NATIONAL INSTITUTE OF TECHNOLOGY KARNATAKA, SURATHKAL
MANGALORE – 575025
AUGUST, 2016**

DECLARATION

I hereby declare that the Research Thesis entitled “**Fragility Estimates for RC Buildings**” which is being submitted to the **National Institute of Technology Karnataka, Surathkal** in partial fulfilment of the requirements for the award of the Degree of **Doctor of Philosophy in Civil Engineering** is *a bonafide report of the research work carried out by me*. The material contained in this Research Thesis has not been submitted to any University or Institution for the award of any degree.

C. M. RAVI KUMAR

Register No. - **110649CV11F01**

Department of Civil Engineering

Place: NITK-Surathkal

Date: 05/08/2016

C E R T I F I C A T E

This is to *certify* that the Research Thesis entitled “ **Fragility Estimates for RC Buildings**” submitted by Mr. **C. M. Ravi Kumar** (Register Number: **110649CV11F01**) as the record of the research work carried out by him, is *accepted as the Research Thesis submission* in partial fulfilment of the requirements for the award of degree of **Doctor of Philosophy**.

Prof. D. Venkat Reddy
Department of Civil Engineering,
(Research Supervisor)

Prof. K. S. Babu Narayan
Department of Civil Engineering,
(Research Supervisor)

Prof. D.V. Reddy
Department of Civil Engineering
Chairman – DRPC



Dedicated to
The cherished memories of my guru and
Most Revered Engineering Teacher
Prof. Srichand
(1942-2012)
Sri Jayachamarajendra College of
Engineering, Mysore

ACKNOWLEDGEMENT

I express my profound and grateful veneration to my research supervisors **Prof. K. S. Babu Narayan** and **Prof. D. Venkat Reddy**, Department of Civil Engineering, NITK, Surathkal. **Prof. K. S. Babu Narayan** taught me many subjects at the postgraduate level (M-Tech) and supervised the Ph.D work. He is the fountain source of my inspiration; I would like to thank him for his valuable guidance. I am also, thankful to **Prof. D. Venkat Reddy** for the encouragement, support, and visionary ideas he provided during my research work.

I am very greatly indebted to RPAC members, **Prof. A. Vasudev Adhikari**, Department of Chemistry and **Prof. Subhash C. Yaragal**, Department of Civil Engineering, for their critical comments, evaluation and suggestions during the course of work.

I am immensely grateful to **Dr. G.R. Reddy**, **Dr. Akanshu Sharma**, Reactor Safety Division, Atomic Bhabha Research Centre, Mumbai, **Dr. Ramesh Babu**, Central Power Research Institute, Bengaluru, and **Dr. Pradeep Kumar Ramancharla**, IIT, Hyderabad for their excellent guidance on pushover experiments and analysis. I acknowledge their help with gratitude.

I am deeply thankful to **Dr. Katta Venkatramana**, Dean (Academic) and **Dr. K.N. Lokesh**, Director for their valuable suggestions. I wish to express my deep gratitude to **Prof. D.V. Reddy**, Head of the Department of Civil Engineering and Chairman, DRPC and **Prof. B. R. Jayalekshmi**, Secretary, DRPC and Former Secretary, DRPC, **Prof. S. Shrihari** for providing all facilities and help during my research work.

I would like to thank **Dr. H. Ramesh**, Department of Applied Mechanics, **Mr. M. H. Prashanth**, Department of Civil Engineering and friends **Dr. Premanand Shenoy**, **Mr. Rajendra Prabhu**, **Mr. Mithun**, **Mr. Nanda Kishore** and **Supriya Kulkarni** for their help, encouragement for successful completion of this research work.

I gratefully acknowledge the authorities of **Visvesvaraya Technological University; Belagavi** for deputing me to NITK, Surathkal for Ph.D degree under Quality Improvement Programme and I am obliged to **Quality Improvement Programme, All India Council for Technical Education, Govt. of India**, for providing me the fellowship.

Finally, I would like to share this moment of happiness with my parents, **Late C. Marjja** and **M. Susheelamma** for their constant encouragement. I am grateful to my wife, **Smt. Pallavi Ravi** and my sons, **Arjun** and **Aryan**, who had to endure many inconveniences during the course of my Ph.D programme. I also express my deepest gratitude to many, not mentioned here, for their support in countless ways throughout my research work.

C.M. Ravi Kumar

Place: NITK,Surathkal

Date: 05/08/2016

ABSTRACT

Fragility curves are commonly used to estimate the vulnerability of structures to earthquakes. The seismic fragility of a structure is expressed through a family of ‘fragility’ curves, which plot the conditional probabilities of failure against varying intensities of the seismic hazard. The failure probability of the structure can be defined for multiple limit states. The thesis derives such fragility curves for the reinforced concrete frame structure with variation in material strength, accounting for the nonlinear behaviour of the system. A performance-based seismic design is applied to the case study building, which enables to have predefined multiple performance levels. In order to validate the performance-based design method against seismic excitations, seismic fragility curves are developed based on the demand models. “Fragility Estimates for Reinforced Concrete Buildings” is a parametric study, which has been attempted for which experimental pushover data is available.

The objective of this research has three main phases. The first is to propose a simplified methodology to assess the expected seismic damage in reinforced concrete buildings. This simplified approach is summarised and applied to reference four storeyed building assumed to be located in zone-IV of IS: 1893(2002). In order to do so, the seismic behaviour of the building was studied by considering variation in material strength. Exhaustive review of literature has been done to understand the state of the art, to identify the points needing further research and then to perform seismic fragility estimates for RC buildings. Often nonlinear pushover analysis of RC building is required for establishing building capacity and fragility curves. This thesis presents a procedure for establishing the required fragility curves for various damage states, in particular for the damage states, based on nonlinear pushover analysis results. A solution is proposed for overcoming the difficulty encountered when determining the median spectral displacements for the damage states.

Second phase of the study deals with usage of variation in material strength. The variations in strength of materials were generated considering partial safety factors for material strength. The thesis focuses on the structural fragility of reinforced concrete

buildings under monotonic loading. Methodology has been adopted to quantify the effect of variation in material strength on prediction of capacity of structure. The capacity and demand assessment are addressed in detail with regard to RC frame treating concrete as confined and unconfined. Thus, thirty five models of moment resisting frames in each case were produced to represent the RC building stock. Each generated frame was subjected to pushover analyses using SAP2000. After seismic fragility estimates, more discussions are presented with regard to applying the performance based approach.

Third phase of work considers the usage of Indian Strong Ground Motion. The variations of material strength for M20 grade of concrete, 20-30 N/mm² and for Fe 415 steel, 520-600 N/mm² are taken. Different models were created and non-linear static analyses of the reference building stocks are performed with two different modelling approaches. All the created models are subjected to Indian strong ground motion records. Twenty Indian ground motions are selected, scaled to different levels of intensity represented by peak ground acceleration. The fragility curves, damage thresholds were obtained. A method is defined for obtaining the yielding and collapse capacity of the analyzed structure using curves. The fragility curves for yielding and collapse damage levels are developed by statistically interpreting the results of the non-linear static analyses.

In this work, an available test result of a full scale four storeyed RCC structure under monotonic load profile till failure was used. The test was conducted using tower testing facility at Central Power Research Institute (CPRI), Bengaluru along with NITK, Surathkal and in association with Reactor Safety Division, Bhaba Atomic Research Centre, Mumbai that provided a base shear versus roof displacement plot (experimental pushover curve). The result of the study is estimated fragility curves for typical reinforced concrete designed without seismic detailing; the obtained results clearly reveal the deformation capacity. Parametric study shows that probability of failure for the RC buildings varies with variation in material strength. The effectiveness of the results is demonstrated by their application to a structural model. Additionally, the fragility curves related to various damage states were estimated. It is

concluded that the proposed procedure offers a viable alternative to existing approaches. The experimental investigation results were utilized and compared with that of analytical investigation; very interesting conclusions have been drawn.

Key words: Variation in Material Strength, Ground Motion, Moment- Curvature Characteristics, Tower Testing Facility Performance Evaluation, Pushover Curves, Damage Thresholds, Fragility Curves.

CONTENTS

Declaration	
Certificate	
Acknowledgements	
Abstract	
Contents	i
List of Figures	v
List of Tables	ix
Nomenclature	xi
1 INTRODUCTION	1
1.1 GENERAL	1
1.2 NEED AND SCOPE OF THE THESIS	2
1.3 ORGANIZATION OF THE THESIS	2
2 REVIEW OF LITERATURE	4
2.1 INTRODUCTION	4
2.2 LITERATURE REVIEW	4
2.3 SUMMARY OF THE LITERATURE REVIEW	10
2.4 NOVELTY OF PUSHOVER TEST	11
2.5 OBJECTIVES OF THE THESIS	11
3 PUSHOVER TEST –AN EXPERIMENTAL INVESTIGATION	13
3.1 INTRODUCTION	13
3.2 DESCRIPTION OF THE STRUCTURE	13
3.3 SECTION PROPERTIES OF BEAMS AND COLUMNS	15
3.4 DESIGN OF FOUNDATION	16
3.5 DETAILS OF SLAB	16
3.6 DETAILS OF JOINTS	18
3.7 MATERIAL PROPERTIES	18

3.8	TOWER TESTING FACILITY	20
3.9	LOADING PATTERN	20
3.10	LOADING SEQUENCE	21
3.11	EXPERIMENTAL RESULTS FOR AS-BUILT STRUCTURE	22
	3.11.1 Pushover Curves	22
4	ANALYTICAL INVESTIGATION	31
4.1	INTRODUCTION	31
4.2	METHODOLOGY FOR SEISMIC FRAGILITY ESTIMATES	31
4.3	ANALYTICAL INVESTIGATION	39
	4.3.1 Introduction	39
	4.3.2 Material Properties	39
	4.3.3 The Nonlinear Analysis: A Parametric Study	40
4.4	STRUCTURAL MODELLING	40
	4.4.1 Beams and Columns	40
	4.4.2 Beam-Column Joints	40
	4.4.3 Slab	41
4.5	MODELLING APPROACHES	41
	4.5.1 Introduction	41
	4.5.2 Stress-strain curve for concrete and steel	41
	4.5.3 Kent and Park Model and Modified Kent and Park Model	42
	4.5.4 Unified Stress-Strain Approach Proposed by Mander	43
	4.5.5 Stress – strain models pertaining to confined concrete	43
	4.5.6 Procedure to develop moment – curvature relationship	44
	4.5.6.1 Moment – curvature characteristics considering IS: 456	46

5	RESULTS AND DISCUSSIONS	49
5.1	INTRODUCTION	49
5.2	DYNAMIC PROPERTIES OF THE STRUCTURE	49
5.3	PARAMETRIC STUDY – I (UN-CONFINED CONCRETE SECTION)	50
5.3.1	Moment – curvature characteristic	50
5.3.2	Pushover Analysis Results for Buildings with Unconfined Concrete section	52
5.3.2.1	Comparison of Results in Terms of Pushover Curves	53
5.3.2.2	Performance evaluation of building	55
5.4	PARAMETRIC STUDY –II (CONFINED CONCRETRE SECTION)	56
5.4.1	Moment of Curvature Relationship	56
5.4.2	Pushover Analysis Results (Confined Concrete section)	58
5.4.2.1	Mander’s Model	58
5.4.2.2	Kent and Park Model	60
5.4.2.3	Performance evaluation of building	62
5.5	PARAMETRIC STUDY – III (CODE PROPOSED AND USER DEFINED RESPONSE SPETRA)	65
5.5.1	Moment Curvature Relationship for Code proposed and user defined property	65
5.5.1.1	Code proposed property	65
5.5.1.2	User Defined Response Spectra	67
5.5.2	Pushover analysis results for code proposed and user defined response spectra	68
5.5.2.1	Code proposed response spectra	68
5.5.2.2	User Defined Response Spectra	70
5.5.2.3	Comparison of POA results for Code Proposed and User Defined Response Spectra	74

5.5.3 Performance point results	77
5.5.3.1 Code proposed response spectra	78
5.5.3.2 User defined response spectra	79
5.6 FRAGILITY CURVES OF INVESTIGATED RC BUILDINGS	80
5.6.1 Fragility Curves in terms of Spectral Displacement: Unconfined Concrete Section	80
5.6.1.1 Damage state thresholds for unconfined concrete section	84
5.6.2 Fragility Curves in terms of Spectral Displacement confined concrete Section	86
5.6.2.1 For Mander's Model	86
5.6.2.2 Kent and Park model	89
5.6.2.3 Comparison of damage thresholds for confined concrete section	91
5.3.3 Fragility Curves in terms of Spectral Displacement: Code Proposed and User Defined Response Spectra	94
5.6.3.1 Comparison of Damage State Thresholds for Code Proposed and Used Defined Response Spectra	101
6 CONCLUSIONS AND SCOPE FOR FUTURE WORK	105
6.1 CONCLUSIONS	105
6.2 SCOPE FOR FUTURE WORK	112
REFERENCES	113
APPENDIX-I	121
APPENDIX-II	122
APPENDIX - III	124
LIST OF PUBLICATIONS	125
BIODATA	127

LIST OF FIGURES

Fig. No.	Description	Page No.
3.1	Overall geometry of the structure (a) Floor plan (b) Roof plan (c) Elevation of the structure	14
3.2	Details of various structural systems (a) Details of floor beams (b) Details of roof beams (c) Details of columns	15
3.3	Additional reinforcement under cross beams	15
3.4	Typical lap and anchorage details	15
3.5	General layouts of columns on raft	16
3.6	Reinforcement details for floor/roof slab	17
3.7	Typical non-conforming joint details	18
3.8	Tower testing facility at CPRI Bangalore	20
3.9	Schematic of loading pattern along the height of building	21
3.10	Structure during the test	21
3.11	Pushover curve for CL 16 side (Akanshu Sharma et al., 2010)	23
3.12	Pushover curve for CL 20 side (Akanshu Sharma et al., 2010)	23
3.13	Failure mode of CL 16	24
3.14	Failure mode of CL 20	24
3.15	Failure mode of CL 15	24
3.16	Failure mode of CL 19	24
3.17	Failure mode of Beam BF 205	25
3.18	Failure mode of Beam BF 205	25
3.19	Torsional failure of beam BF 225 while testing	26
3.20	Torsional failure of beam BF 225 after removal of loose concrete	26
3.21a	Joint failure of CL 19 at First floor during the test	27
3.21b	State of joint of CL 19 at first floor after removal loose concrete	27
3.22	State of joint of CL 19 at second floor after removal of loose concrete	28
3.23	Joint failure of CL 16 due to bond at first floor level	28
3.24	Joint failure of CL 16 due to bond at second floor level	29

3.25	Joint failure of CL 20 due to joint shear, beam flexure and bond at second floor	30
3.25	State of joint of CL 20 at second floor after removal of loose concrete	30
4.1	Overall geometry of the structure	32
4.2	Nonlinear analysis procedures	32
4.3	Capacity spectrum methods (Nikos D. Lagaros, 2012)	32
4.4	Idealized component load deformation curve with control points A to E (after NEHRP Guidelines for Seismic Rehabilitation of Buildings, FEMA 1997a)	35
4.5	Figure 4.5 Capacity curve for elastic-perfectly-plastic structural behaviour (Borzi et al., 2006)	35
4.6	Damage state thresholds on bilinear capacity spectrum	36
4.7	Stress-strain curve for (a) concrete, and (b) steel	41
4.8	Kent and Park Stress-Strain Model	42
4.9	Modified Kent and Park Stress-strain Model	42
4.10	Mander Stress-Strain Model Proposed For Monotonic Loading	43
4.11	Flow chart to develop moment curvature relationship	46
4.12	Stress – strain curve for concrete	47
4.13a	Stress – strain diagram of steel (Fe415)	47
4.13b	Stress – strain curve for (Fe415) steel	48
5.1	Normalised mode shape of structure	49
5.2	Moment curvature relationship for beams (Unconfined model)	51
5.3	Moment curvature relationship for columns (Unconfined model)	51
5.4	Comparison of results provided by SAP2000 with experimental pushover curve (X-direction)	54
5.5	Moment curvature relation for Beam BF204 and Column CL-15 for $f_{ck}=20\text{MPa}$ and varying tensile strength of steel (Mander Model)	57

5.6	Moment curvature relation for BF204 and CL 15 for $f_{ck}=20\text{MPa}$ and varying tensile strength of steel (Kent & Park Model)	58
5.7	Comparison of analytical results for varying values f_{ck} and $f_y=520\text{MPa}$ with experimental pushover curve	60
5.8	Comparison of analytical pushover curves with experimental pushover curve	62
5.9	Moment curatur relationship for BF 204 for $f_{ck} = 20 \text{ MPa}$ and varying f_y values (code specified)	66
5.10	Moment curatur relationship for CL 15 and 19 for 20 MPa and varying f_y values (code specified)	66
5.11	Moment curatur relationship for BF 204 for $f_{ck} = 20 \text{ MPa}$ and varying f_y values (user defined)	67
5.12	Moment curatur relationship for CL 15 and 19 for 20 MPa and varying f_y values (user defined)	67
5.13	Comparison of analytical push over curves with experimental push over curve	70
5.14	Response spectra for selected ground motions	71
5.15	Code proposed spectra along with mean spectra of selected ground motions	72
5.16	Analytical pushover curves with experimental pushover curve	72
5.17	Pushover curve for $f_{ck} = 20\text{MPa}$, $f_y = 520\text{MPa}$	74
5.18	Pushover curve for $f_{ck} = 21.5\text{MPa}$, $f_y = 520\text{MPa}$	75
5.19	Pushover curve for $f_{ck} = 23\text{MPa}$, $f_y = 520\text{MPa}$	75
5.20	Pushover curve for $f_{ck} = 25\text{MPa}$, $f_y = 520\text{MPa}$	76
5.21	Pushover curve for $f_{ck} = 27\text{MPa}$, $f_y = 520\text{MPa}$	76
5.22	Pushover curve for $f_{ck} = 28.5\text{MPa}$, $f_y = 520\text{MPa}$	77
5.23	Pushover curve for $f_{ck} = 30\text{MPa}$, $f_y = 520\text{MPa}$	77
5.24	Capacity curve and bilinear representation of capacity curve for $f_{ck} = 20 \text{ MPa}$ and tensile strength = 520 MPa	82
5.25	Fragility curve for varying values of compressive strength and tensile strength = 520 MPa	84

5.26	Damage state thresholds for varying values of f_{ck} and tensile strength of steel = 520 MPa	85
5.27	Bilinear Capacity Curve for Mander Model ($f_{ck} = 20\text{MPa}$; $f_y = 520\text{MPa}$)	87
5.28	Fragility curve for varying values of compressive strength and tensile strength = 520 MPa	88
5.29	Bilinear Capacity Curve for Kent and Park Model ($f_{ck} = 20\text{MPa}$; $f_y = 520\text{MPa}$)	89
5.30	Fragility curve for varying values of compressive strength and tensile strength = 520 MPa	91
5.31	Damage state thresholds by both the models	92
5.32	Capacity curve for $f_{ck} = 20\text{MPa}$ and $f_y = 520\text{MPa}$ for code proposed response spectra	95
5.33	Bilinear capacity spectrum for $f_{ck} = 20\text{MPa}$ and $f_y = 520\text{MPa}$ for code proposed response spectra	95
5.34	Pushover curve for $f_{ck} = 20\text{MPa}$, $f_y = 520\text{MPa}$ for user defined response spectra	96
5.35	Bilinear capacity spectrum for $f_{ck} = 20\text{MPa}$ and $f_y = 520\text{MPa}$ for user defined response spectra	96
5.36	Fragility curves for Code Proposed Response Spectra	98
5.37	Fragility curves for User Defined Response Spectra	100
5.38	Damage state thresholds for both the properties	102

NOMENCLATURE

Abbreviations

- ADRS -Acceleration-Displacement Response Spectra
ATC – Applied Technology Council
BARC, Mumbai - Bhabha Atomic Research Centre, Mumbai
BIS- Bureau of Indian Standard
BMTPC- Building Materials and Testing Promotion Council
CPRI, Bengaluru - Central Power Research Institute, Bengaluru
CSM - Capacity Spectrum Method
DBE- Design Basis Earthquake
DCM -Displacement Coefficient Method
EDP - Engineering Demand Parameters
FEMA- Federal Emergency Management Agency
FOSM - First Order Second Moment
FS - Factor of Safety
HDMR - High Dimensional Model Representation
HYSD Bars – High Yield Strength Deformed Bars
MCE- Maximum Considered Earthquake
MDOF – Multi Degree of Freedom System
MKNP – Modified Kent and Park Model
KNP- Kent and Park Model
MDRS – Mander’s Model
MPA- Modal Pushover Analysis
NITK, Surathkal – National Institute of Technology Karnataka, Surathkal
PBSD- Performance-Based Seismic Design
PGA- Peak Ground Acceleration
PBEE - Performance-Based Earthquake Engineering
POA – Pushover Analysis
SDOF - Single Degree of Freedom

SPT -Standard Penetration Test

SSI - Soil Structure Interaction

RC- Reinforced Concrete

RSD- Reactor Safety Division

Notations

DI = Mean damage index

E_C - Elastic Modulus of the Concrete

E_s - Elastic Modulus of the Steel

EI -Flexural Rigidity

f_c -Maximum Stress

f_{ck} - Characteristic Strength of Concrete

f_y – Tensile Strength of Steel

g- Acceleration due to gravity

H_i = Height of a storey between the storey level i and (i+1) levels.

I- Importance Factor

I_{eff} – Effective Moment of Inertia

I_g – Gross Moment of Inertia

R – Capacity

R- Earthquake Reduction Factor

$1/R$ -The curvature

S_a - Spectral Acceleration

S_d - Spectral Displacement

S_a/g -Spectral Coefficient

T- Time Period(s)

V- Vulnerability

V_B - Seismic Base Shear

Z- Zone Factor

μ = Ductility factor

$S_{d,u}$ or d_u = Spectral Displacement at Ultimate Point

$S_{d,y}$ or d_y = Spectral Displacement at Yield Point

CHAPTER 1

INTRODUCTION

1.1 GENERAL

Fragility analysis is an exercise to determine the damage thresholds which usually are classified as slight, moderate, extensive and collapse on some prefixed performance levels. Probabilities of exceeding a particular damage level plotted against damage measure provide the fragility curve. These curves are of immense help in assessing structural safety or probable seismic damages.

The very philosophy of seismic design requires structures to behave elastically during minor earthquake, elasto plastically if quakes are moderate and plastically accommodating target deformations without collapsing when quakes are of large magnitude. Codes have done their best to account for these requirements by way of suggesting design basis earthquake, response reduction factors and ductile detailing specifications.

Current research focuses on Performance-Based Seismic Design (PBSD) which attempts to understand post elastic and plastic behaviour of structures that are not identifiable by an elastic analysis.

Displacement controlled procedures for seismic performance evaluation are gaining popularity as they can track formation and propagation of structures yield and quantify force capacities with displacement demand.

Though performance based seismic design look very attractive for performance appraisal a lot depends on addressing issues of geometric and material modelling. Never the less researchers are attempting to resolve these issues to redefine and refine the technique.

In this work an attempt has been made to obtain fragility estimates for an RC building for which experimental pushover data is available.

1.2 NEED AND SCOPE OF THE THESIS

Data of an experimental investigation on a four storied RC building (**Akanshu Sharma et al., 2010**) have been acquired and for the same geometry and material data, analytical investigations have been carried out to obtain fragility curve. Results of the two investigations have been compared and sensitivity of the analysis results to material strength parameters have been investigated.

A few available strong motion data have been used to get response spectrum and the same has been adopted for POA to compare the results with code specified response spectra. Appraisal of various geometry and material modelling technique has been made, and unresolved issues have been highlighted and scope for future studies has been suggested.

1.3 ORGANIZATION OF THE THESIS

The thesis has been organized in six chapters. First chapter is introductory that discusses about background and need of fragility curves. It also emphasizes on defining the problem. Later organization of thesis included.

Second chapter reports a review of literature and introduces objectives and scope of the research.

Third chapter provides available pushover test data, conducted at Central Power Research Institute (CPRI), Bengaluru. The reported results have been acquired for validation.

The analytical methodology and parameters required have been outlined. The details of parametric study and modelling approaches have been discussed. For the acquired

results of experimental data, analytical investigations have been carried out to obtain fragility curve in Fourth chapter.

Fifth chapter deals with results and discussions, mainly validation of experimental results with that of analytical results.

Sixth chapter summarizes the findings of this study followed by recommendations for future research.

CHAPTER 2

REVIEW OF LITERATURE

2.1 INTRODUCTION

A brief review of literature has been reported. This literature review focuses on recent contributions related to studies on fragility estimates of RC buildings. The findings of previous research are given in chronological order.

2.2 LITERATURE REVIEW

Fragility estimate requires extensive computer simulations to account for the randomness of both input motion as well as response characteristics. **Seong-Hoon Jeonga et al. (2007)** had done investigations on this. An approach consists of set of fragility relationships are derived based on response characteristics of stiffness, strength and ductility. An exact solution for a generalized SDOF system was developed and employed to construct a response database of coefficients. Once the response quantities for structural systems are defined, the fragility relationships for various limit states were also established without any modification in the simulation procedure. The uncertainty associated with modelling approaches is quantified by conducting comparisons between the approaches to MDOF systems.

Gencturk et al. (2008) proposed a Methodology for fragility analysis of buildings. This procedure consists of four components, namely (i) capacity of building; (ii) earthquake demand; (iii) structural assessment and (iv) fragility curve generation. Each of these elements is handled rigorously in order to arrive at reliable fragility relationships. The capacity of the building is represented using either analytically-derived or expert-opinion or based on pushover curve. Earthquake demand is modelled by synthetically generated site specific ground motions. Structural assessment is carried out using an advanced Capacity Spectrum Method (CSM). Fragility curves are presented in two different formats, conventional and HAZUS-

procedure. The proposed methodology is applied to different types of buildings. Fragility relationships are proposed as a reliable tool for earthquake loss assessment.

Practical method based on pushover analyses was proposed by **Faella et al. (2008)**. Two procedures aimed at applying well-known methods for seismic reliability evaluation of structures are outlined as possible generalization of the so called IN₂ method. Response spectra are the key feature of the two methods. A sample application of both procedures has confirmed that application of static analyses resulting in conservative evaluation of seismic risk and reliability of structures.

Angelo Marinilli (2008) had carried out the stochastic analysis of reinforced concrete frames under seismic loads. Seismic performances of a structure are highly dependent on the mechanical properties of materials. Stochastic approach is used to evaluate the effect of variability of such mechanical properties on seismic performance of structures. Simplified analyses were performed based on Point Estimate Method, considering compressive strength of concrete and yield strength of steel as independent stochastic variables. Seismic performance of frame structures was evaluated with pushover analyses. Results obtained with Point Estimate Method were validated with results obtained with Monte Carlo Simulation Method. It was concluded that Point Estimate Method can be used to perform stochastic analyses of structures under seismic actions. More refined results can be obtained, which requires a greater amount of numerical evaluation of seismic responses.

Fragility curves represents the structure's response, which may exceed the performance limit of a given ground motion intensity. Conventional methods for computing building fragilities are either based on statistical extrapolation or based on Monte Carlo simulation. The Monte Carlo technique requires a relatively large number of simulations in order to obtain a reliable estimate of the fragilities. In view of this, High Dimensional Model Representation (HDMR) technique was proposed by **Vipin Unnithan et al. (2008)**, which simplifies the process of fragility computation. It is used to replace performance-function with an explicit functional relationship, fitting a functional approximation, thereby reducing the numerical analyses.

Reliability Analysis for seismic performance assessment of concrete reinforced buildings was presented by **El Ghoulbzouri Abdelouafi et al. (2009)**. Surface response concept is introduced to derive explicitly the failure function in order to compute reliability index of reinforced concrete buildings. The failure function is considered to be the maximum inter-story displacement. Two random variables namely material resistance variations of concrete and steel were introduced. Ductility is also taken as hidden variable. The failure is evaluated in order to identify the building surface response by polynomial regression. A parametric study regarding seismic performance reliability was conducted as function of ductility ratio.

Stochastic approach for developing seismic fragility function of structures was described by **Nasserasadi et al. (2009)**. Fragility function of structures is one of the major requirements of seismic loss estimation in seismic risk evaluation. Initially, comprehensive and simplified stochastic methods are presented for development of fragility functions. Later, the effect of damage threshold uncertainty on fragility functions is estimated. It shows that the results of stochastic approach are almost comparable with that of previous studies.

Pushover analysis on typical RCC structure by applying different lateral load patterns using ETABS and SAP2000 was performed by **Abhilash et al. (2009)**. The lateral load patterns used here are uniform load distribution and equivalent lateral force distribution as per FEMA-257, lateral loads from response spectrum analysis as per IS-1893(2002) and the lateral load pattern as per upper-bound pushover analysis (UBPA) method. Commonly applied load patterns are inverted triangle and uniformly distributed load. To study the effect of lateral load patterns in pushover analysis, the guidelines like FEMA- 257 and 356 were adopted, which will provide guidelines for lateral loads. It is concluded that, for all the four type loadings the performance points are very close. Performance is very close for Uniform loading from FEMA and IS-1893 loading. Similarly Equivalent Lateral loading (FEMA) and UBPA loading performance appears to be same. This is due to the close similarity between the load patterns. Different loading pattern shows only slight change in performance point in regular building.

Simplified methodology for developing drift-based fragility curves for low-to-medium rise buildings in seismic zones was presented by **Ruiz-Garcia et al. (2010)**. Drift-based fragilities are derived from stiffness-and-strength for an equivalent single-degree-of-freedom system subjected to a set of earthquake ground motions scaled to peak displacement demands associated with damage states. For assessing the seismic vulnerability of structures for estimating the earthquake-induced damages based on an engineering demand parameter like structural damage.

To estimate the structural performance based on code-based seismic demand and capacity details were presented by **Fatemeh Jalayer et al. (2010)**. To characterize the uncertainties in material properties and in construction, simulation method has been preferred for structural resistance. The simulation-based methods allow for suitable grouping of uncertain parameters in order to build a simplified model for correlation. A Bayesian framework has been adopted to update the uncertainties and the structural reliability. This take into account for more information gathered as a result of destructive or non-destructive tests and inspections on the structure.

Seismic performance evaluation of reinforced concrete buildings was performed by **Pavan Kumar et al. (2010)**. Three methods namely capacity spectrum method (CSM), displacement coefficient method (DCM), modal pushover analysis (MPA) are adopted for estimating seismic inelastic displacement. Using these methods seismic performance of reinforced concrete buildings was evaluated. The validation of these methods has been done with models reported in literature.

The non-linear response of RCC control frame and the retrofitted RCC frame using Finite Element Modelling under the incremental loading has been carried out by **Beena Kumari et al. (2010)**. The study was carried out with the intention to investigate the relative importance of several factors in the non-linear finite element analysis of RCC frames. These include the variation in load displacement graph, the crack patterns, propagation of the cracks, the crack width and the effect of the non-linear response of control frame and deformed frame.

Vulnerability and risk evaluation for a reinforced concrete frame based on the capacity spectrum method was carried by **Ioanaolteanu et al. (2011)**. Vulnerability

and risk assessment was carried out through simulation based approach. A 2-D reinforced concrete frame, designed according to the Romanian norm was studied. The capacity curve obtained with a non-linear static analysis, fragility curves were plotted and an average damage index for the performance point of the structure was calculated. With the use of simulation method the influence of uncertainties in the damage states thresholds are estimated. The obtained results for 10% and 20% coefficients of variation of the damage states thresholds are simulated as random variables.

The development of fragility functions for Reinforced Concrete bare frame as well as in-filled frame buildings was studied by **Alexandra Papailia (2011)**. The buildings considered for the study are regular configurations both in plan and elevation. Buildings designed for seismic loading and for gravity loads are discussed. Later, the frame buildings are considered with or without masonry infills. The variable parameters are the number of storeys (2, 5 and 8) and the level of seismic design and ductility level. Additional studies are carried out considering the effect of the material properties and span of the building. Further the seismic performance of systems with frames of different stiffness is also examined. The analysis gives the median value of the fragility curve corresponding to the damage measure. The dispersion value of the fragility curve takes into account explicitly the model uncertainty for the estimation of the damage states. For better fragility estimates, model uncertainty and the dispersion of material and geometric properties are considered.

Simplified fragility analysis of RCC building frame for preliminary estimate of its failure was presented by **Rehan A. Khan et al. (2011)**. The risk analysis procedure uses the format considers band limited white noise at the bed rock as the seismic input. The RCC building frame is modelled as 2D frame using pushover analysis. The risk evaluation procedure includes uncertainties of the response due to variation of ground motion, material property, modelling and method of analysis and those of the capacity due to the variation of ductility factor and damage concentration effect. This method is applied to a 5-storey RCC building frame for obtaining its fragility curves using First Order Second Moment (FOSM). The fragility curves takes into account of number of parametric variations. The parameter includes soil conditions and

coefficient of variation of the uncertainty factors. The study concludes that the parameters considered have considerable effect on the fragility estimates.

The non-linear response of RCC frame using SAP2000 under monotonic loading has been carried out by **Rohit Bansal et al. (2011)** with the intention to investigate the relative importance of several factors in the non-linear analysis of RCC frames. This includes the variation in load -displacement graph.

Seismic fragility estimates using analytical functions using performance based approach was performed by **Lu D.G et al. (2012)**. Four categories of seismic fragility are defined namely, seismic demand fragility, structural capacity fragility, seismic damage fragility, and seismic loss fragility. The analytical formulae of seismic demand and damage fragility functions are derived. The analytical relationships of the median and the dispersion of the two kinds of fragility models are established. Then the seismic performance of the code-conforming reinforced concrete buildings is evaluated based on analytical functions.

Fragility analysis of reinforced concrete structures with fill walls is performed by **Nikos D Lagaros (2012)**. For this purpose a fuzzy-based fragility assessment framework for evaluating 3D framed structures is proposed taking into account various sources of uncertainty. In particular, randomness on the material properties and on the seismic demand is considered. The proposed framework requires the development of a fuzzy nonlinear static analysis model in order to define the limit states. The fragility curves are expressed in the form of a two-parameter lognormal distribution.

Analytical formulations of two types of seismic fragility functions namely seismic demand fragility and seismic damage fragility are derived by **Dagang Lu et al. (2013)**. Using suitable intensity measure (IM) and damage measure (DM), the well-known Cornell's IM- and displacement-based formulations for seismic risk assessment are obtained based on analytical functions of fragility. It is found that the widely used formulations using engineering demand parameters (EDPs) as well as DM-based approaches are two specific cases for IM-based risk evaluation. To investigate the effects of the derived fragility parameters on the seismic performance

of five-storey reinforced concrete (RC) frame designed according to the Chinese codes has been used as a case study. The result of study indicates that the capacity randomness and the selection of earthquake IMs have obvious influences on seismic fragility and risk. It is also found that the fragility curve for different limit states in 50 years of design life span satisfies the requirements of Chinese code.

Yeudy F. Vargas (2013) had done the investigations on the use of simplified deterministic nonlinear static procedures for assessing the seismic response of buildings and evaluated the influence of uncertainty in strength of materials. In this the Seismic risk assessment of reinforced concrete building, considering mechanical properties of materials and the seismic action are considered as random variables was obtained. The Monte Carlo method is then used to analyze the structural response of the building. The obtained results show that significant uncertainties are expected; uncertainties in the structural response increase with the severity of the seismic actions. Lastly, it was concluded that major influence in the randomness of the structural response is due to randomness of the seismic action.

Reliability analysis of the designed buildings has been carried out by **Haran Pragalath D C et al. (2014)** after considering the possible uncertainties. In this the author found that, the seismic performance assessment requires simulation based procedures due to the uncertainties involved. The major uncertainties are in the material properties of concrete and steel, time history of ground motions, building geometries etc. The seismic performance of the buildings depends on these uncertainties. Reliability assessment of RC structures is established by combining the fragility curve and hazard curve.

2.3 SUMMARY OF THE LITERATURE REVIEW

From review of literature it is evident that understanding structural behaviour in elastic and post elastic ranges are essential to make earthquake resistant design more meaningful. Quantifying capacity and demand and establishing performance level is a complicated exercise owing to difficulties in geometric and material modelling that is close to reality. Uncertainties associated with material properties, size, shape and

geometry of elements and structure as a whole, selection of the appropriate technique for determination of demand, further complicate the structural appraisal.

This work is an attempt to understand, qualitatively and quantitatively these issues by way of an analytical investigation and comparison of the results of the investigation with observations and performance data available for particular pushover test and to suggest techniques for enhancement of seismic performance appraisal.

2.4 NOVELTY OF PUSHOVER TEST

The role of non-linear equivalent static (pushover) analyses is being more and more recognized as a practical tool for the evaluation of the seismic response of structures. Pushover analyses are therefore increasingly being considered within modern seismic codes, both for design of new structures and for assessment of existing ones.

The experiment, which was used to examine the applicability of these pushover methods, was performed in the four storeyed frame of the extensive ROUND ROBIN Exercise. This test was conducted at CPRI, Bengalure in association with NITK, Surathkal and BARC, Bombay.

One of the main purposes of the work has been to verify the computer simulations by means of experimental data in order to establish the reliability of the analytical studies for various parametric studies. The main properties of the experimentally observed building response are described and analyzed in Chapter 3. The related analytical model, used for the analytical studies is presented in Chapter 4. The last, Chapter 5 is devoted to the comparison of the experimental results and analytical results.

2.5 OBJECTIVES OF THE THESIS

The objectives of study are to:

- i) Propose a simplified methodology to assess the expected seismic damage in reinforced concrete buildings keeping salient features of IS: 1893 (2002) code as well as IS 15988: 2013 code, from a probabilistic point of view.
- ii) Examine various aspects of vulnerability derivation process for fragility estimate of reference RC building located in Zone-IV of IS: 1893-2002 by

considering probability of variation in strength and Indian strong ground motion as uncertainties.

- iii) Obtain the capacity curves, damage states and fragility curves and to establish the curves describing expected seismic damage to the structure as a function of a seismic hazard characteristic.
- iv) Usage of experimental results conducted at Central Power Research Institute, Bengaluru and compare the analytical results with that of experimental results.

CHAPTER 3

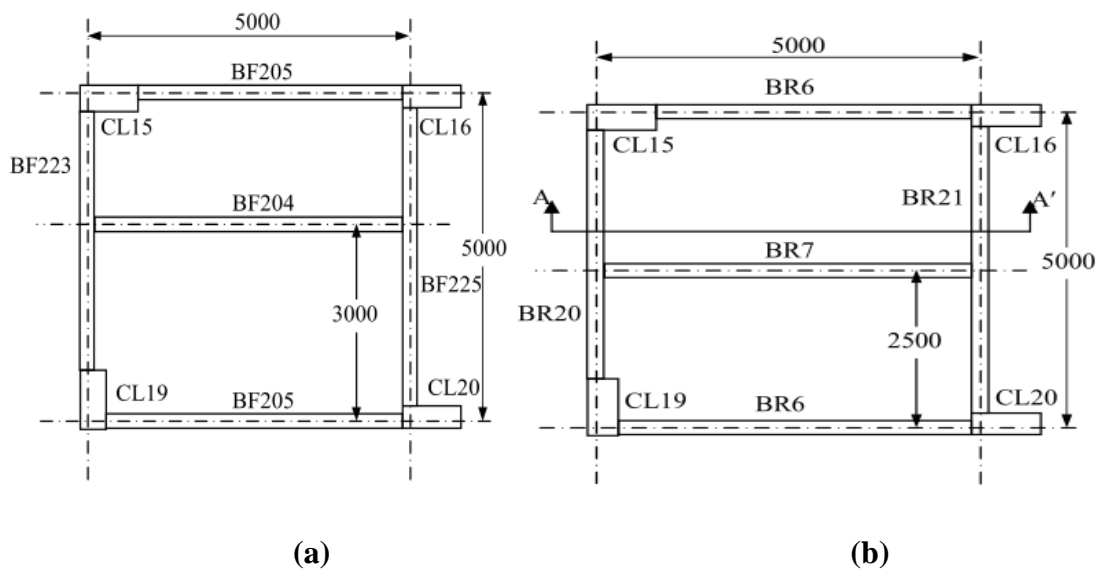
PUSHOVER TEST – AN EXPERIMENTAL INVESTIGATION

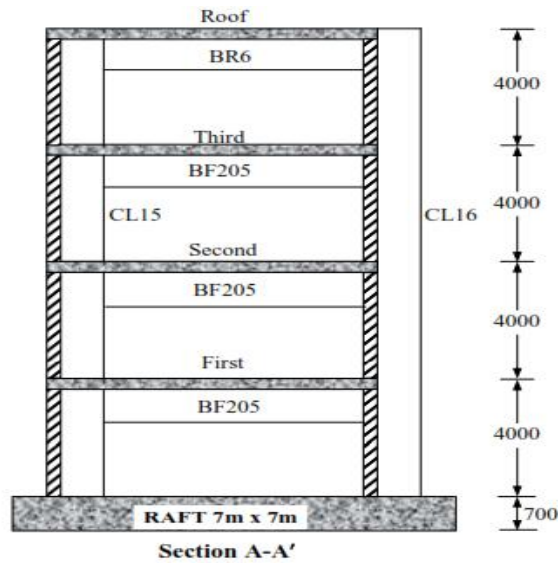
3.1 INTRODUCTION

This chapter provides the details of experimental pushover test on prototype reinforced concrete structure. The details of building description for the study, construction, loading arrangement and tested results have been provided herein.

3.2 DESCRIPTION OF THE STRUCTURE

The structure considered for the study is a four storied single bay RCC framed structure. The storey height is 4m (total building height = 16m) and the bay width in each direction is 5m. Figure 3.1 shows the roof plan, floor plan and the sectional elevation of the structure. Floor plan is same for all the floors. The structure is supported on an RCC raft, which in turn will be supported on rock bed using rock grouting. Details of various structural systems say (a) Details of floor beams (b) Details of roof beams (c) Details of columns are indicated in Figure 3.2. The figures in brackets beside the name of the section indicate the size of the section as (Breadth \times Depth).

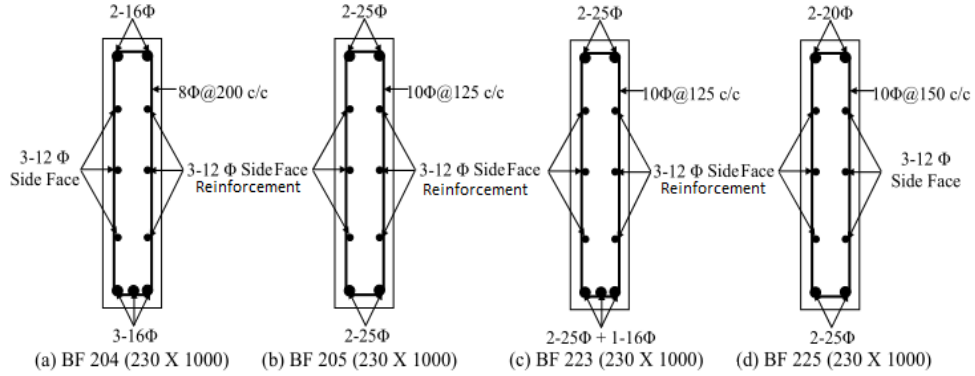




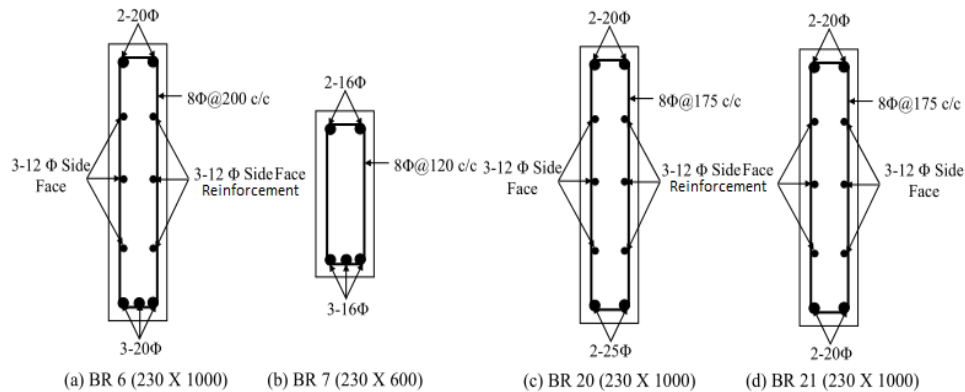
(c)

Figure 3.1 Overall geometry of the structure (a) Floor plan (b) Roof plan

(c) Elevation of the structure (Akanshu Sharma et al. 2010)



(a)



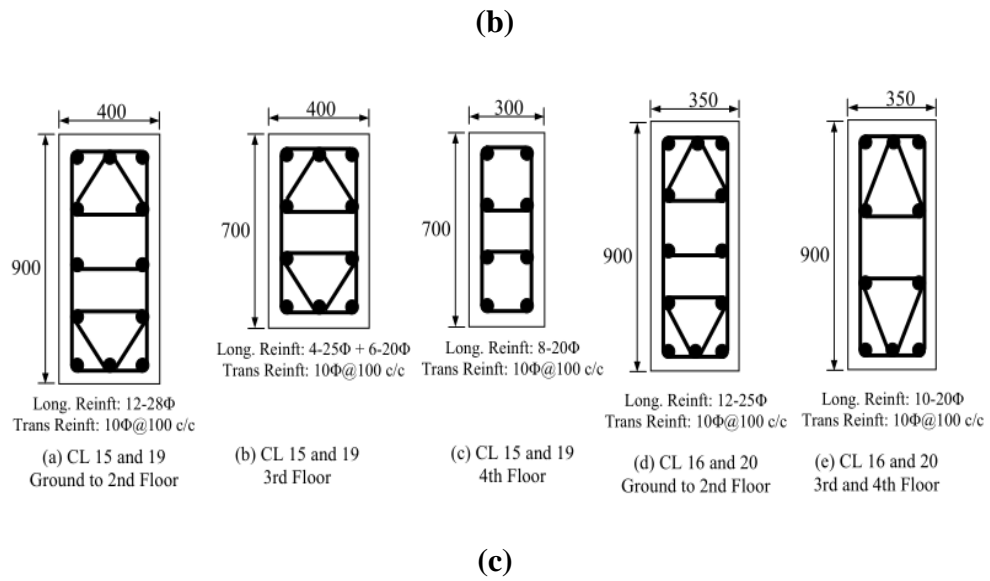


Figure 3.2 Details of various structural systems (a) Details of floor beams

(b) Details of roof beams (c) Details of columns (Akanshu Sharma et al., 2010)

All dimensions are given in ‘mm’.

3.3 SECTION PROPERTIES OF BEAMS AND COLUMNS

Under the cross beams, additional reinforcements were provided as given in Figure 3.3. The details of lap and anchorage in beams are given in Figure 3.4.

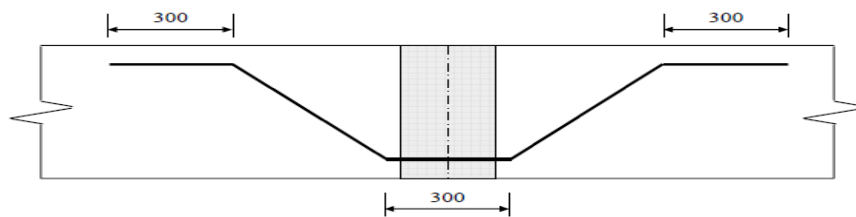


Figure 3.3 Additional reinforcement under cross beams

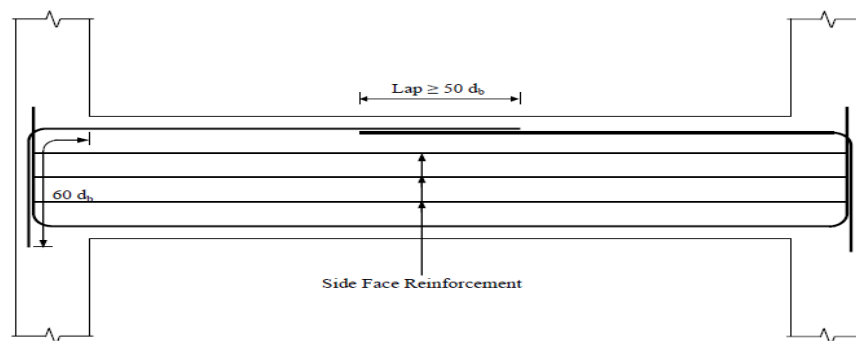


Figure 3.4 Typical lap and anchorage details

3.4 DESIGN OF FOUNDATION

The raft is proportioned in such a way that the clear overhang of the raft is equal to 750 mm from the face of each column on both sides (Figure 3.5). The length of each bolt was 1500mm.

Dimensions and design details of the raft are therefore,

Length of the raft, $L = 750 + 115 + 5000 + 785 + 750 = 7400\text{mm}$

Breadth of the raft, $B = 750 + 115 + 5000 + 115 + 750 = 6730\text{mm}$

Depth of the raft, $D = 700\text{mm}$

Reinforcement in the direction of loading (along length), $A_{st1} = 25\phi - 100\text{mm c/c}$

Reinforcement in perpendicular direction (along Breadth), $A_{st2} = 25\phi - 200\text{mm c/c}$

3.5 DETAILS OF SLAB

The reinforcement details for floor/roof slab are shown in Figure 3.6 and Table 3.1 below. Thickness of the slab is 120 mm.

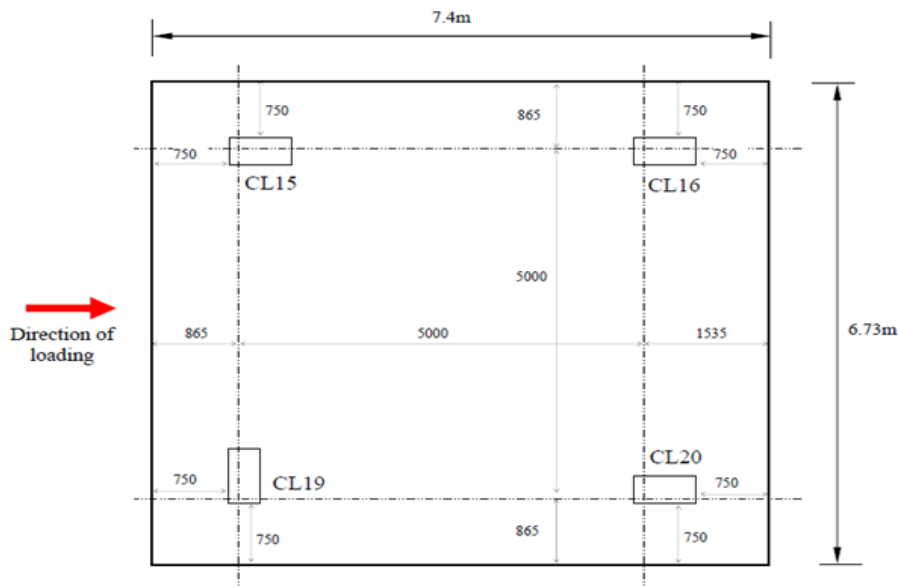


Figure 3.5 General layouts of columns on raft

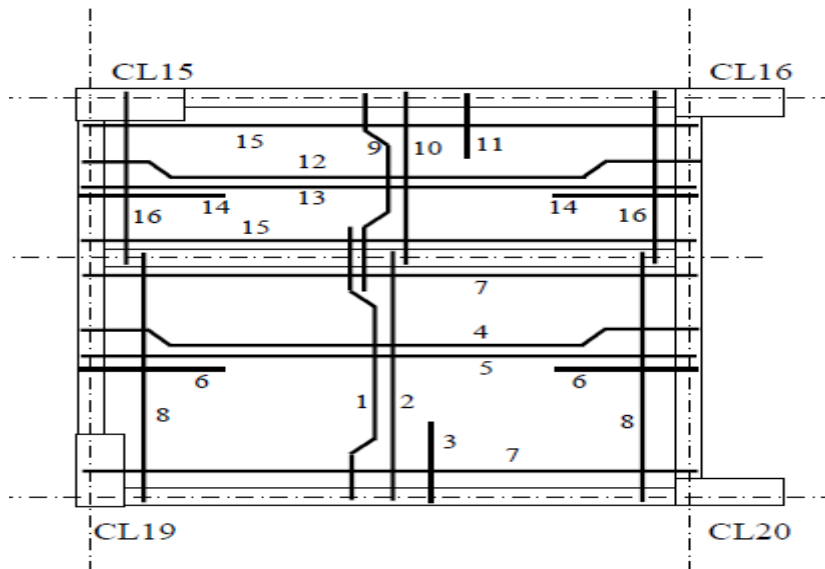


Figure 3.6 Reinforcement details for floor/roof slab

Table 3.1: Reinforcement details for floor/roof slab

Detail No.	Diameter of bar (mm)	C/C Spacing (mm)	Type/ Location
1	10 Φ	450	a\w CKD
2	10 Φ	450	Bottom
3	10 Φ	450	Top
4	10 Φ	500	a\w CKD
5	10 Φ	500	Bottom
6	10 Φ	500	Top
7	8 Φ	250	Top (Distribution)
8	8 Φ	250	Top (Distribution)
9	10 Φ	450	a\w CKD
10	10 Φ	450	Bottom

11	10 Φ	450	Top
12	10 Φ	500	a\w CKD
13	10 Φ	500	Bottom
14	10 Φ	500	Top
15	8 Φ	250	Top (Distribution)
16	8 Φ	250	Top (Distribution)

3.6 DETAILS OF JOINTS

Figure 3.7 shows a typical non-conforming joint detail as was provided in the structure. The beam longitudinal reinforcement bars were extended beyond the face of the column into the joint up to a length equal to the development length for the bar.

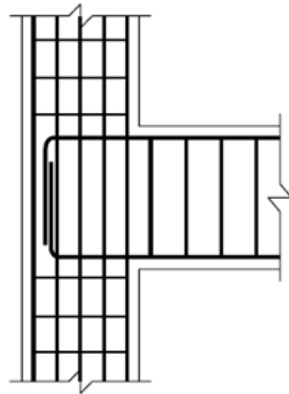


Figure 3.7 Typical non-conforming joint details

3.7 MATERIAL PROPERTIES

The material properties are, Concrete grade: M20 ($f_{ck} = 20$ MPa) and Reinforcement: HYSD bar ($f_y = 415$ MPa)

Actual material properties obtained from tests are given below. The average concrete cube strengths reported by **Akanshu Sharma et al., 2010**, from various locations are given in Table 3.2. Table 3.3 summarizes the average yield and ultimate strengths of various diameters of reinforcement bars used in structure. Three samples each for all diameter bars have been tested and reported by **Akanshu Sharma et al., 2010**.

Table 3.2: Average concrete cube strengths

Location	Average Compressive Strength (MPa)
Raft	32.88
Raft to 1st Floor	28.86
1st Floor	27.73
1st – 2nd Floor	33.30
2nd Floor	31.09
2nd to 3rd Floor	32.24
3rd Floor	29.86
3rd to 4th Floor	31.24
4th Floor (Roof)	30.56

Table 3.3: Yield and ultimate strengths of various dia. of reinforcement bars

Diameter of bar (mm)	Yield Strength (MPa)	Yield Strain	Ultimate Strength (MPa)	Ultimate Strain
8	456.06	0.00213	604.91	0.042
10	517.81	0.0022	599.94	0.030
12	539.88	0.00253	620.78	0.032
16	490.96	0.0021	615.02	0.053
20	488.93	0.00283	614.60	0.063
25	523.37	0.0031	629.49	0.057

3.8 TOWER TESTING FACILITY

Another very important and critical part was to provide arrangement for applying the loads on to the structure. As mentioned earlier, the load was to be applied using the tower testing facility at CPRI Bengaluru (Figure 3.8).



Figure 3.8 Tower testing facility at CPRI Bangalore

3.9 LOADING PATTERN

Pushover loads can be applied in inverse triangular fashion, parabolic fashion or in ratio of the first mode shape etc. In view of the existing tower test facility, it was found that the best possible control of the loading would be through the inverse triangular loading. The ratio of force at “first level: second level: third level: fourth level” will be kept as “1: 2: 3: 4” as shown in Figure 3.9. Figure 3.10 shows the photograph of the structure being tested. The load application in the ratio of 1:2:3:4 can be visualized for the same.

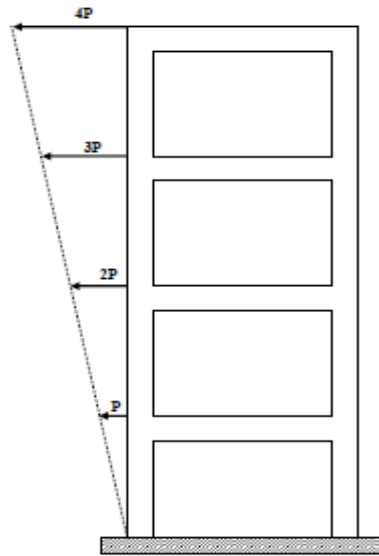


Figure 3.9 Schematic of loading pattern along the height of building



Figure 3.10 Structure during the test

3.10 LOADING SEQUENCE

Due to the loading pattern, if P is the load on the 1st floor then the base shear would be equal to $P+2P+3P+4P = 10P$. The load on the structure was gradually increased in the steps of 1t at 1st floor, which resulted in a corresponding load step of 20 t at 2nd floor, 30 t at 3rd floor and 40 t at 4th floor resulting in a load step of 10 t in Base

shear. The base shear in the first step was 10 t, in the second step 20t and so on till failure. Loading arrangement for different floors as accomplished in Figure 3.10.

3.11 EXPERIMENTAL RESULTS FOR AS-BUILT STRUCTURE

3.11.1 Pushover Curves

The pushover curves as obtained are reported for CL16 side and CL20 side are shown in Figures 3.11 and 3.12 respectively. Since the experiment was conducted under load control, the dropping part of the curves could not be obtained. It can be seen from the two figures, the maximum displacement for CL16 side was obtained as 537 mm and that on CL20 was obtained as 765 mm. This clearly demonstrates torsion due to eccentricity raised from column orientation. The difference in the curves is as expected showing more displacement on CL20 side due to less stiffness offered by CL19 in loading direction. The average top drift is therefore equal to around 4% of the total height of the building.

The structure behaved linearly till a base shear value of around 300 kN. At this point the flexural tension cracks at the base of the columns started to get generated and the structure displayed a reduced stiffness. After reaching a base shear value of approximately 500 kN, the cracks at the base of the columns opened wider and failures at other locations namely beams and beam-column joints started to show up. As a result the stiffness of the structure further went down, that can be seen from the pushover curves. After reaching the base shear values of 700 kN, the joints of the structure displayed rapid degradation and the inter-storey drift increased rapidly. On further increase in the lateral load, the structure displayed a brittle behaviour with large displacement increase for the same increase in the base shear. After reaching a base shear of 882.90 kN, i.e. 9t load at first floor, 18t at second floor, 27t at third floor and 36t at fourth floor, the structure started undergoing increasing displacement at constant load.

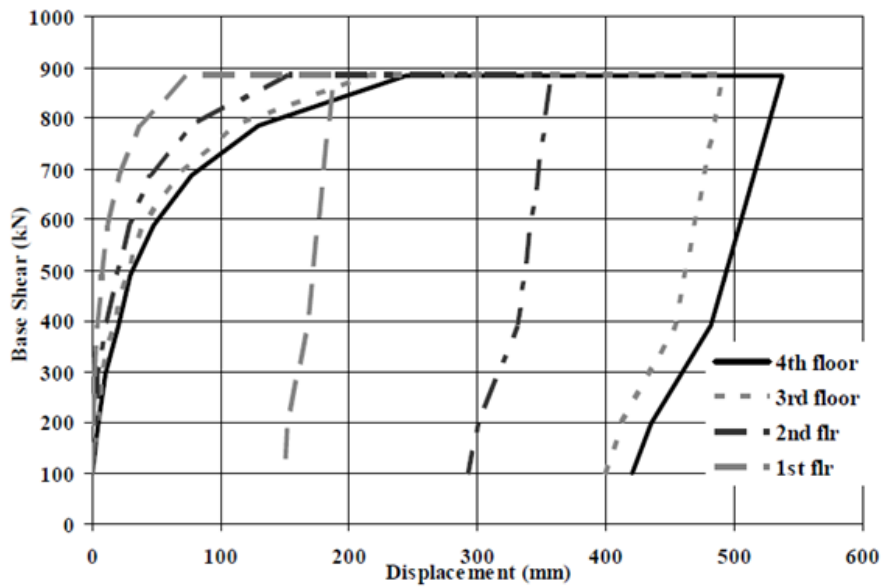


Figure 3.11 Pushover curve for CL 16 side (Akanshu Sharma et al., 2010)

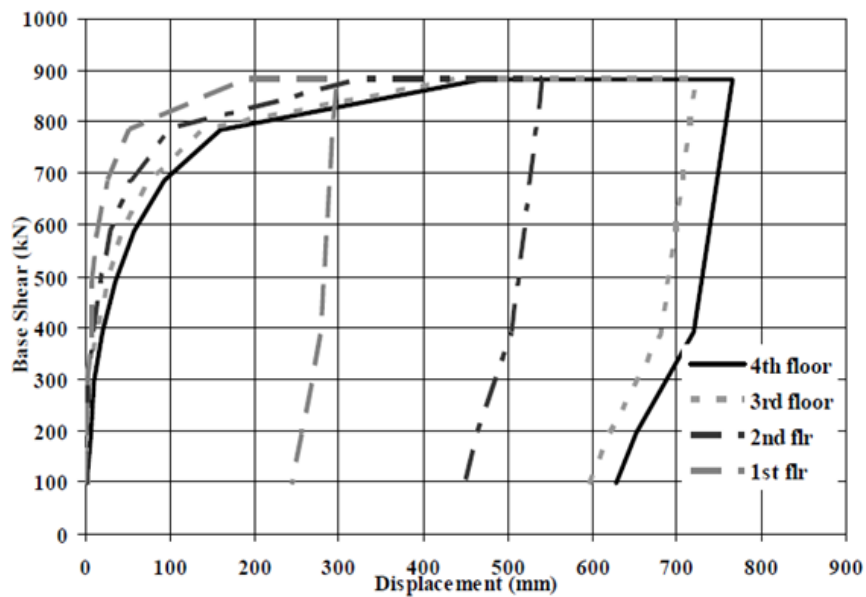


Figure 3.12 Pushover curve for CL 20 side (Akanshu Sharma et al., 2010)

3.11.2 Failure Patterns

Figs 3.13 to 3.26 show various failure modes and patterns observed during the experiment. Figs 3.13 and 3.14 show the failure of bottom storey columns on compression side, namely columns CL16 and CL20 respectively. As the lateral load was increased on the structure, columns CL 16 and CL20 underwent increasing

compressive forces combined with bending moment. Thus, due to this combined axial compression and bending, the column section started to show tension cracks on the rear face. On further increase in the loads, which resulted in increase in both bending moment as well as axial forces on the column, these tension cracks grew further along the depth of the section demonstrating the shifting of neutral axis towards the front face of the columns. Due to the shift of neutral axis, less area was available to resist higher compressive forces. Consequently, crushing of concrete on front face of the column commenced and the state of the columns at the failure is depicted in Figs 3.13 and 3.14. Also, the failure mode of column CL 15 and CL 19 is shown Figs, 3.15 and 3.16.



Fig 3.13 Failure mode of CL 16



Fig 3.14 Failure mode of CL 20



Fig 3.15 Failure mode of CL 15



Fig 3.16 Failure mode of CL 19

Fig 3.17 and 3.18 shows the failure modes of the beam in flexural and flexure-shear mode while testing and after the test with the loose concrete removed. These figures show the end of the beam BF 205 connected to CL 15 at 1st floor. Due to lateral loading, the bending moments were generated in the beam with hogging moments towards the end fixed with column CL16 and sagging moments towards the end fixed with column CL15. As a result, flexural tension cracks could be seen initiating from the soffit of the beam and propagating towards the slab as shown in Fig 3.17. Spalling of concrete was observed on the tension face of the beams. Fig 3.18 shows the status of the beam after all the loose concrete was removed and the clear beam hinging could be well appreciated with lot of spalling on compression and tension faces of the beams.



Fig 3.17 Failure mode of Beam BF 205 **Fig 3.18 Failure mode of Beam BF 205**

Figs 3.19 and 3.20 show the torsional failure of beam transverse to the direction of loading during the test and after the removal of loose concrete. As the lateral load increased, the beams transverse to the direction of loading in the front namely BF225 suffered large torsional moments. This is attributed to the design, loading arrangement and direction of loading. The design, as was provided in the original building, recommended beam dimensions of 230mm×1000mm and the slab depth was 130mm. Therefore, as the lateral load was applied on the slab, it pushed the beam laterally at the top, which induced high torsional stresses in these beams.



Fig 3.19 Torsional failure of Beam BF 225 while testing



Fig 3.20 Torsional failure of Beam BF 225 after removal of loose concrete

Figs 3.21, 3.22, 3.23 and 3.24 show typical joint failure patterns. Under the action of lateral forces, beam-column joints are subjected to large shear stresses in the core. Typically, high bond stress requirements are also imposed on reinforcement bars entering into the joint. The axial and joint shear stresses result in principal tension and compression that leads to diagonal cracking and/or crushing of concrete in the joint core. The flexural forces from the beams and columns cause tension or compression forces in the longitudinal reinforcements passing through the joint. During plastic hinge formation, relatively large tensile forces are transferred through bond. When the longitudinal bars at the joint face are stressed beyond yield, splitting cracks are initiated along the bar at the joint face. If the cover to the reinforcement bars is less and if the joint core is not confined by confining reinforcement in the form of stirrups, the cover concrete is spalled off due to the pressure exerted by the beam reinforcement bars.

Fig 3.21 (a) shows the failure of joint of CL 19 at first floor while testing and Fig 3.21 (b) shows the state of the joint after the removal of loose concrete. In this case, the column depth (400mm) was much smaller than beam depth (1000mm) and also the beam eccentricity was high since the beam of width 230mm was flushed with the face of the column with the width of 900 mm. High stresses in the joint resulted in diagonal cracks in the core followed by cover spalling due to the pressure exerted by the beam longitudinal reinforcement. From Fig 3.21 (b), which shows the state of the joint after removal of concrete, the joint details can be observed. As seen here, no joint confining reinforcement was provided but there were side face reinforcement in the form of 12 mm dia bars which were bent into the joint. Fig 3.22 shows the failure of joint of CL 19 at 2nd floor level, which shows the beam bar bursting out of the joint. Such a failure can, in general, be prevented if proper confining reinforcement is provided in the joint core.



Fig 3.21 (a) Joint failure of CL 19 at 1st floor during the test
(b) State of Joint of CL 19 at 1st floor after removal of loose concrete



Fig 3.22 State of Joint of CL 19 at 2nd floor after removal of loose concrete

Fig 3.23 shows the failure of the joint of CL16 at first floor level that exhibited bond failure along with beam flexural failure and spalling of side cover due to pressure exerted by the reinforcement. High tension force in the beam reinforcement resulted in bond deterioration and ultimately failure with splitting of concrete.



Fig 3.23 Joint failure of CL 16 due to bond at 1st floor level

Fig 3.24 shows a typical diagonal (shear) crack in the joint of CL16, 2nd floor along with beam flexural cracks. The diagonal cracks in the joints are formed due to principal tensile stresses generated as a result of axial and joint shear stresses. As the lateral forces were increased on the structure, the joint shear stress increased and in combination with the axial stresses, resulted in diagonal tension that was responsible for the development of diagonal tension cracks.



Fig 3.24 Joint failure of CL 16 due to bond at 2nd floor level

Fig 3.25 shows diagonal shear crack in the joint of CL20, 2nd floor during the test with flexural and flexure-shear cracks in the beam and bond failure of the tension reinforcement. Fig 3.26 shows the state of the joint after the removal of loose concrete. It can be observed that a clear diagonal shear crack appeared in the joint during the test but it was not further opened and the failure essentially got transferred through bond mechanism. Although, the beam longitudinal reinforcement was bent up to the required development length inside the column, as seen in Fig 3.21 (b), it is quite clear that such development by bending in the re-bars may not be good enough to prevent the bond failure.



Fig 3.25 Joint failure of CL 20 due to joint shear, beam flexure and bond at 2nd floor



Fig 3.26 State of Joint of CL 20 at 2nd floor after removal of loose concrete

CHAPTER 4

ANALYTICAL INVESTIGATION

4.1 INTRODUCTION

This chapter presents the methodology and analytical investigation for fragility estimates of reference RC building.

4.2 METHODOLOGY FOR SEISMIC FRAGILITY ESTIMATES

The thesis provide an analytical methodology to establish seismic fragility estimates of reference building as depicted in Figure 4.1 and Numerical simulation of 4-story reinforced concrete building is summarized as follows,

Step 1: Analytical Building Model

In general, the nonlinear behaviour is represented using the concentrated plasticity concept with rotational springs or distributed plasticity concept where the plastic behaviour occurs over a finite length. The rotational behaviour of the plastic regions in both cases follows a bilinear hysteretic response based on the Deterioration Model.

In this work, plastic hinge regions are provided at the supports and joints having plastic hinge length i.e., $l_{pl} = 0.5 d$ ($d =$ depth of the section)

Step 2: Non-Linear Static Analysis/ Pushover Analysis

Conventional pushover analysis is carried out as depicted in Figure 4.2 to determine the ground motion intensity the building must be subjected to for it to displace to a specified inter-story drift ratio using SAP-2000. The general procedure for the implementation of the Capacity Spectrum Method (CSM) with the consideration of variation in material strength for a reference building is as shown in Figure 4.3.

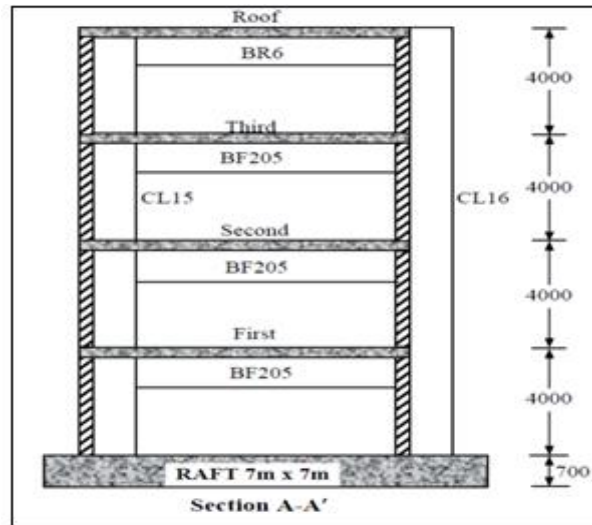


Figure 4.1 Overall geometry of the structure

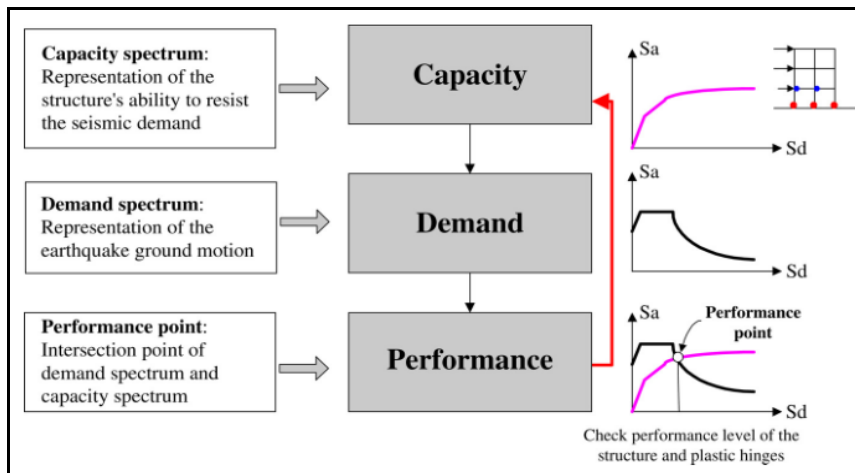


Figure 4.2 Nonlinear analysis procedures

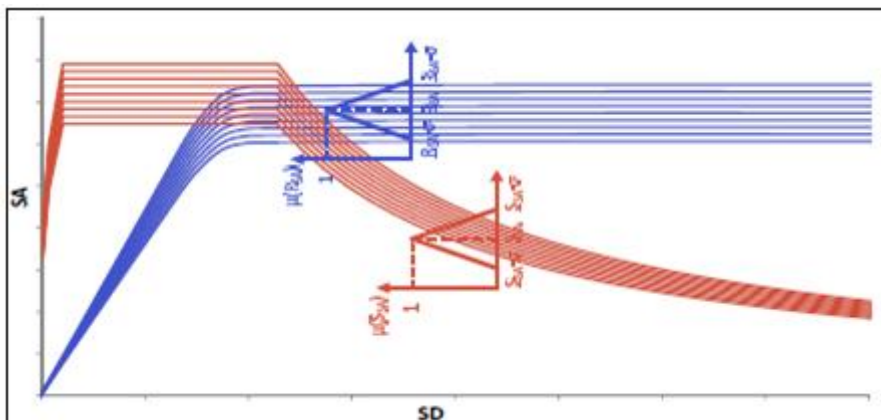


Figure 4.3 Capacity spectrum methods (Nikos D. Lagaros, 2012)

Step 3: Define Damage State Indicator Levels (Failure Criteria and Performance Limit States)

The top storey displacement is often used by many researchers as a failure criterion because of the simplicity and convenience associated with its estimation. The limit states (immediate occupancy, life safety, and collapse prevention) associated with various performance levels of reinforced concrete frames as mentioned in FEMA 356 and the damage state indicator levels are defined depending on progressive collapse starting from yielding and rotation to instability, which has been tabulated in Table 4.1.

One of the most challenging steps in fragility estimates for RC building is the determination of damage parameters and their corresponding limit states. These parameters are very essential for defining damage state as well as determining the performance of RC building under a seismic event. Therefore, realistic damage limit states are required in the development of reliable fragility curves.

Table 4.1: Damage state indicator levels

Slight Damage	Hinge yielding at one floor
Moderate Damage	Yielding of beams or joints at more than one floor
Extensive Damage	Hinge rotation exceeds plastic rotation capacity
Collapse	Structural Instability

Step 4: The non-linear analysis: a parametric study

Conduct a vulnerability analysis of reference RC building located in Zone-IV of IS: 1893-2002 with variation in material strength.

The capacity of a structure to withstand a load is a function of its geometry and material properties. These are fixed and can potentially be known, but it may be very difficult to evaluate them. If the strength of materials is also a function of environmental variables such as temperature, humidity, or moisture content, these are inherently variable.

Step 5: Building Fragility Curves

Develop an analytical fragility estimates to quantify the seismic vulnerability of RC frame building, which includes damage classification and quantification.

In general, damage states for both structural and non structural components of a building should be separately defined (Kircher et al., 1997b). Damage state thresholds are separately provided in terms of spectral displacement S_d and spectral acceleration S_a in order to address structural and non structural damage, respectively.

In addition to this empirical definition of damage state thresholds, two different sets of criteria are provided in HAZUS Advanced Engineering Module (FEMA, 2002; Table 4.2) where damage state medians are related to:

- a) The fraction of structural components reaching a certain control point (C, respectively E) on an idealized component load versus deformation curve (capacity curve; Figure 4.4), and
- b) The point where 50% of the structural components have reached their yield point (i.e., control point B) on the component load versus deformation curve (Figure 4.4).

Table 4.2: Relating component (i.e. element deformations to average inter-storey drift ratios of structural damage state medians (after FEMA, 2002))

Damage State	Criteria set no.1			Criteria set no.2		
	Fraction	Limit	Factor	Fraction	Limit	Factor
Slight	> 0%	C	1.0	50%	B	1.0
Moderate	≥ 5%	C	1.0	50%	B	1.5
Extensive	≥25%	C	1.0	50%	B	4.5
Complete	≥ 50%	E	1.0 - 1.5	50%	B	12

Other damage classifications characterize the thresholds of damage states in terms of capacity curve characteristics, i.e. yield and ultimate spectral displacement, S_{dy} and

S_{du} respectively. These classifications have been developed by Giovinazzi (2005), Barbat et al. (2006), Ioana, Olteanu et al., 2011 and Kappos et al. (2006). Their proposed damage classifications and damage state thresholds are listed in Table 4.3, respectively. Another attempt to define damage limit states (light damage, significant damage and collapse) to a point on the capacity curve has been suggested by Borzi et al. (2006) as shown in Figure 4.5.

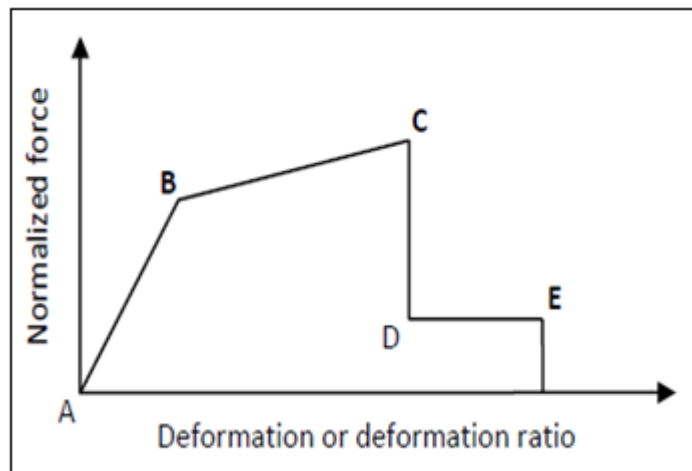


Figure 4.4 Idealized component load deformation curve with control points A to E (after NEHRP Guidelines for Seismic Rehabilitation of Buildings, FEMA 1997a)

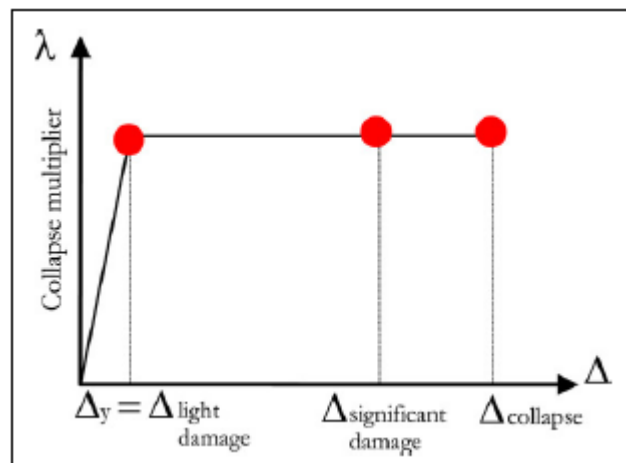


Figure 4.5 Capacity curve for elastic-perfectly-plastic structural behaviour (Borzi et al., 2006)

Table 4.3: Damage state thresholds dependent on capacity curve parameters S_{dy} and S_{du} (Giovinazzi, 2005, Barbat *et al.*, 2006, Ioana, Olteanu *et al.*, 2011, Kappos *et al.*, 2006)

Damage State	Median value of threshold spectral displacement S_{dk}					Damage State
	K	Giovinazzi (2005)	Barbat <i>et al.</i> (2006) and Ioana, Olteanu <i>et al.</i> (2011) (Figure 4.6)	Kappos <i>et al.</i> (2006)	k	
Slight	1	$0.7 \cdot S_{dy}$	$0.7 \cdot S_{dy}$	$0.7 \cdot S_{dy}$	1	Slight
Moderate	2	$1.5 \cdot S_{dy}$	$1.0 \cdot S_{dy}$	$1.0 \cdot S_{dy}$	2	Moderate
Extensive	3	$0.5 \cdot (S_{dy} + S_{du})$	$S_{dy} + 0.25 \cdot (S_{du} - S_{dy})$	$2.0 \cdot S_{dy}$	3	Substantial to heavy
Complete	4	S_{du}	S_{du}	$0.7 \cdot S_{du}$	4	Heavy to very heavy
				S_{du}	5	Collapse

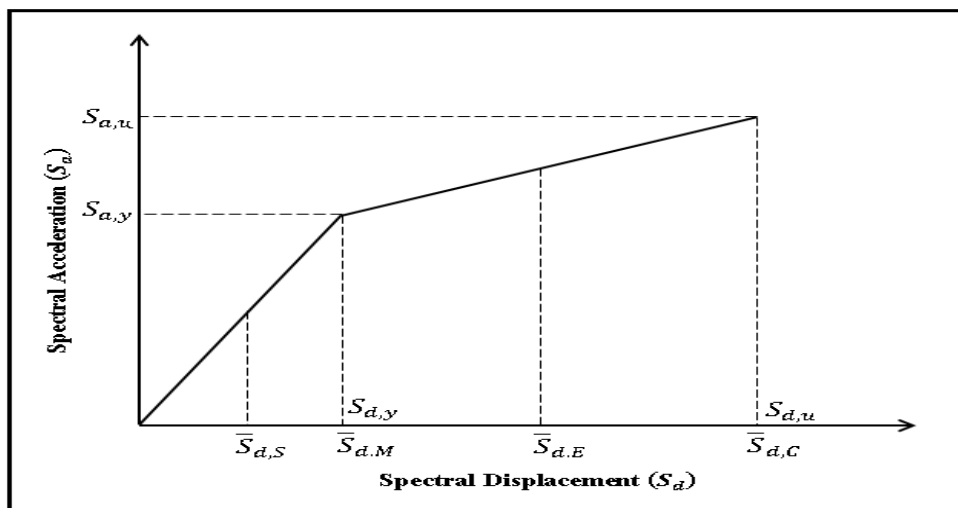


Figure 4.6 Damage state thresholds on bilinear capacity spectrum

(Barbat *et al.*, 2006 and Ioana, Olteanu *et al.*, 2011)

The methodology uses the data from the capacity curves, which have been used in this thesis. This curve distributes damages in terms of slight, moderate, severe and collapse damage states. For a particular spectral response or displacement, the discrete damage state probability is calculated as the difference between cumulative probabilities of damage states.

As known, fragility curves are defined by lognormal functions (common assumption in seismic fragility studies) that describe the conditional probability of reaching, or exceeding, a defined damage state, given deterministic (median) estimates of spectral response (for example the spectral displacement) is defined by the relationship (Eq.4.1); the variability associated with capacity curve properties, damage states, model errors and ground shaking should be properly taken into account.

$$P[d_s/S_d] = \Phi \left[\frac{1}{\beta_{ds}} \ln \left(\frac{S_d}{S_{d_{rds}}} \right) \right] \quad \text{--- (Eq. 4.1)}$$

Where, S_d is the spectral displacement defining the threshold of a particular damage state; $S_{d_{rds}}$ is the median value of spectral displacement at which the building reaches the threshold of damage states or damage state medians, can be calculated by various damage state models; β_{ds} is standard deviation of the natural logarithm of S_d for damage states; Φ is standard normal cumulative distribution function.

Fragility curves define various damage states. HAZUS defines two- criteria approach based on the performance levels of the individual members. The damage state thresholds are defined using the model proposed by Ioana, Olteanu et al. (2011) has been adopted. Damage state variability parameters considered for the buildings proposed by Giovinazzi and Lagomarsino (2006) (see Table 4.4) based on the capacity spectrum of the buildings, and the same approach has been used in the present study.

Step 6: Development of Damage state Variability

The lognormal beta or standard deviation describes the total variability of the damage states as shown in Table 4.4 . The variability associated with the capacity Curve, β_C , demand spectrum, β_D , and the variability associated with the discrete threshold of

each damage state, β_{Tds} are to be accounted while calculating the total variability. The demand spectrum is developed from 5% damped elastic response (input) spectrum in terms of Spectral Acceleration versus Spectral Displacement and the Capacity curve is the plot of force-deformation in terms of Spectral Acceleration versus Spectral Displacement. Thus, the demand spectrum and capacity curves are inter dependent, the variability accounted by both are combined by convolution process. The third component β_{Tds} is mutually independent from the first two variability components and its effect is considered by combing it with the results of CONV process using SRSS method (HAZUS, 2003).

$$\beta_{ds} = \sqrt{(CONV[\beta_C, \beta_D])^2 + (\beta_{Tds})^2} \quad \text{--- (Eq.4.2)}$$

Table 4.4 Damage state variability parameters considered for the buildings

Storey Number	Design levels	Post-yield degradation (<i>k</i>)	Damage state variability (β_{rds})	Capacity curve variability (β_C)	Damage state variability (β_{ds})
3 Storey	SMRF	Minor Degradation (0.9)	Moderate(0.4)	Moderate(0.3)	0.8
	OMRF	Major Degradation (0.1)	Moderate(0.4)	Moderate(0.3)	1.0
	Gravity-designed	Extreme Degradation (0.1)	Moderate(0.4)	Moderate(0.3)	1.05
6 Storey	SMRF	Minor Degradation (0.9)	Moderate(0.4)	Moderate(0.3)	0.75
	OMRF	Major Degradation (0.1)	Moderate(0.4)	Moderate(0.3)	0.85
	Gravity-designed	Extreme Degradation (0.1)	Moderate(0.4)	Moderate(0.3)	1

Where, β_{Tds} is the lognormal standard deviation parameter that describes total variability associated with the discrete threshold of each damage state, β_C is the lognormal standard deviation parameter that describes variability associated with the capacity curve, β_D is the lognormal standard deviation parameter that describes variability associated with demand spectrum, ($\beta_D = 0.45$ at short periods and $\beta_D = 0.5$ at long periods).

The median spectral displacements can be determined analytically. Estimation of variability is a difficult process requiring statistical data for local conditions. Therefore, variability parameters are directly used from HAZUS. For Indian buildings, such data is not available. The damage state thresholds presented by Ioana, Olteanu et al. (2011), as being on conservative side have used in the present study. As discussed earlier, in the case of ‘gravity-designed building’, extreme degradation has been considered as there is no conforming transverse reinforcement has been provided (Giovinazzi and Lagomarsino, 2006).

4.3 ANALYTICAL INVESTIGATION

4.3.1 Introduction

The building description and details of structural system and members are provided in section 3.2 (Chapter 3). Structural modelling and modelling approaches have been discussed herein.

4.3.2 Material Properties

The material properties considered for the analysis are given in Table 4.5.

Table 4.5: Material properties

Material	Characteristic Strength(MPa)	Modulus of Elasticity (MPa)
Concrete(M20)	$f_{ck} = 20$	$E_c = 22360$
Reinforcing steel (Fe415)	$f_y = 415$	$E_s = 2 \times 10^5$

4.3.3 The Nonlinear Analysis: A Parametric Study

Compatibly to the values of test samples extracted from existing building, whose mean value of compressive strength of concrete is approximately $f_{ck}=30.86$ MPa, the compressive strength of concrete, f_{ck} is considered to vary in the range (20-30) MPa. For the steel, whose mean tensile strength $f_y= 502$, the considered tensile strength values are $f_y= (520, 540, 560, 580 \& 600)$ MPa for Fe415 steel, that is the steel used in the studied building. Considering different combinations of f_{ck} and f_y a number of 35 analyses are performed.

4.4 STRUCTURAL MODELLING

The analytical model was created in such a way that the different structural components represent as accurately as possible the characteristics like mass, strength, stiffness and deformability of the structure. Non-structural components were not modelled. The various primary structural components that were modelled are as follows,

4.4.1 Beams and Columns

Beams and columns were modelled as 3D frame elements. The characteristics like strength, stiffness and deformability of the members were represented through the assignment of properties like cross sectional area, reinforcement details and the type of material used. The following values are adopted for effective flexural stiffness of cross-section: $I_{eff} = 0.5 I_g$ for beams, and $I_{eff} = 0.70 I_g$ for columns (I_g is the moment of inertia of the gross concrete section). In this way, the effects of stiffness reduction due to concrete cracking and bar yielding are taken into consideration.

4.4.2 Beam-Column Joints

The beam-column joints were assumed to be rigid and were modelled by giving end-offsets to the frame elements. This was intended to get the bending moments at the face of the beams and columns. A rigid zone factor of 1 was considered to ensure rigid connections of the beams and columns.

4.4.3 Slab

The slabs were not modelled physically, since modelling as plate elements would have induced complexity in the model. However the structural effects of the slabs i.e., the high in-plane stiffness giving a diaphragm action and the weight due to dead load were modelled separately.

4.5 MODELLING APPROACHES

4.5.1 Introduction

Analytical modelling of reinforced concrete members has gained the attention of many researchers in the past and present. Consequently, many models have been proposed to model reinforced concrete structures, considering various effects. However, most of the models are either too simple to predict the response accurately, or accurate but overly complex to incorporate in the analysis. Few models offer a good balance between simplicity and accuracy.

4.5.2 Stress-strain curve for concrete and steel

IS: 456-2000 specifies the limiting strain of concrete as 0.0035 (Figure 4.7 (a)). But for the strain of steel, only a lower bound value of $0.002 + f_y / 1.15E_s$ (Figure 4.7 (b)) is specified; the strain in reinforcement is permitted to reach any value more than this specified minimum.

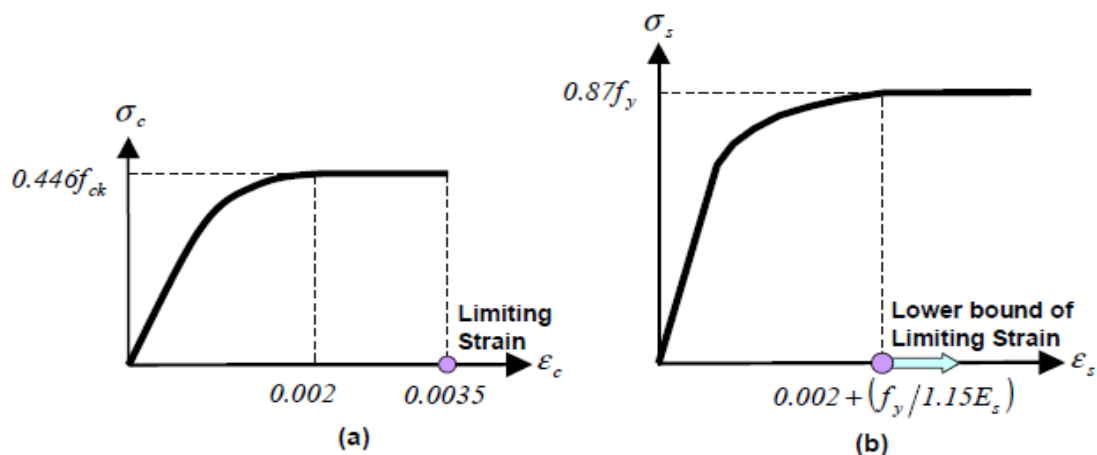


Figure 4.7: Stress-strain curve for (a) concrete, and (b) steel

4.5.3 Kent and Park Model and Modified Kent and Park Model

The original model as shown in Figure 4.8 was proposed by Kent and Park (1971) and modified by Park et al. (1982) as depicted in Figure 4.9. In the original model, the ascending part of the stress strain curve of concrete was considered to be unaffected by confinement. The slope of the descending part was a function of the amount of lateral steel and the ratio between core width and tie spacing. Park et al. (1982) modified the original model by making an allowance for the enhancement in the concrete strength and the peak strain due to confinement. The slope of the descending part of the curve remained the same as in the original model up to a stress of 20% of the maximum, beyond which a horizontal line represented the curve.

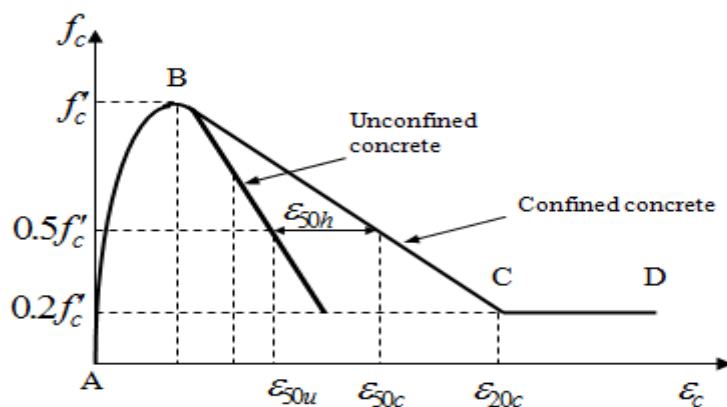


Figure 4.8: Kent and Park Stress-Strain Model

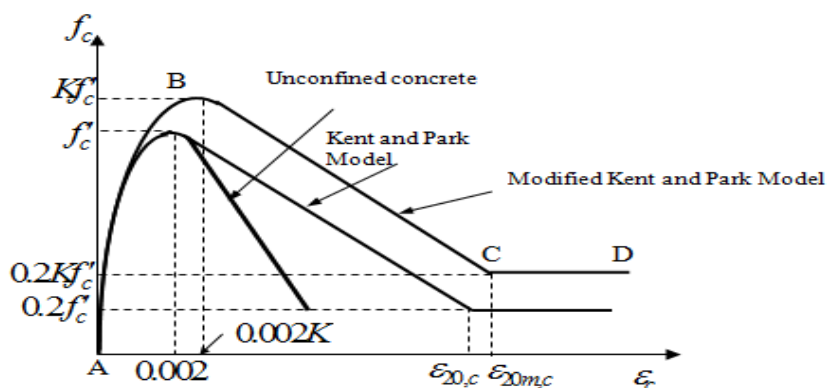


Figure 4.9: Modified Kent and Park Stress-strain Model

4.5.4 Unified Stress-Strain Approach Proposed by Mander

Mander et al. (1984) have proposed a unified stress-strain approach for confined concrete applicable to both circular and rectangular shaped transverse reinforcement. The stress-strain model is illustrated in Figure 4.10. This is proposed for a confined and unconfined concrete with monotonic loading at slow strain (quasi-static) rate.

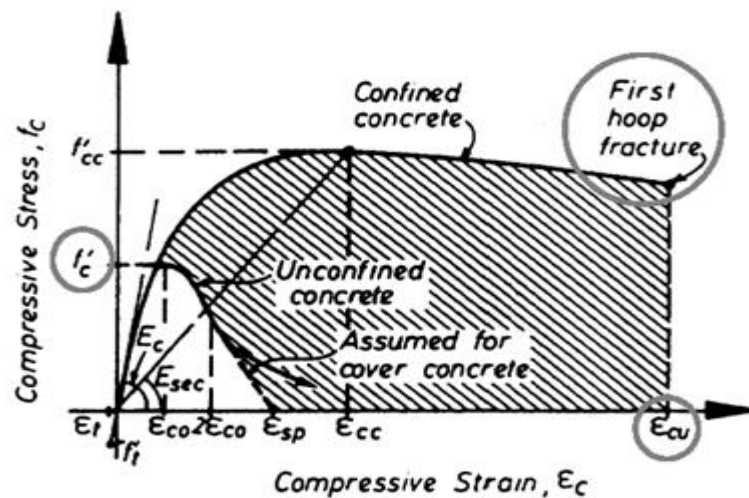


Figure 4.10: Mander Stress-Strain Model Proposed For Monotonic Loading

4.5.5 Stress-Strain Models Pertaining to Confined Concrete

Various modelling approaches pertaining to stress-strain relation of confined concrete are available. Such as,

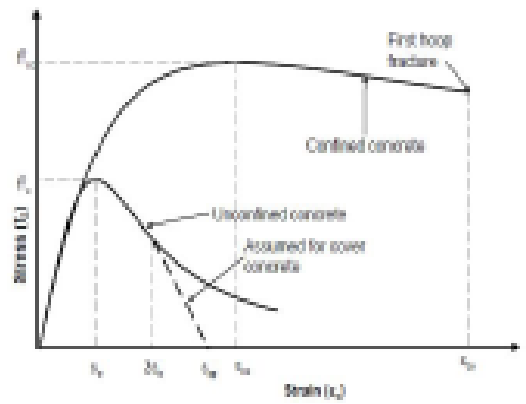
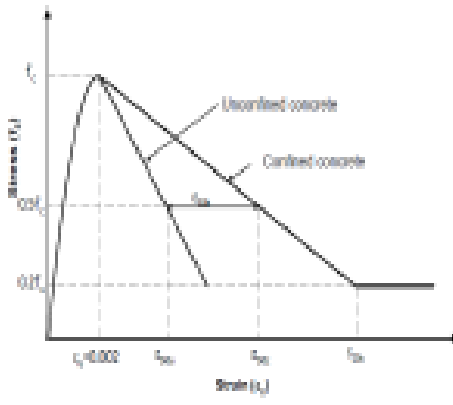
- Mander model
- Kent and Park model

Mander model is simple and the most used model since it is effective in considering the effect of confinement (Mander *et al.* 1998). Regardless of the arrangement of the confinement reinforcement used, the performance over the stress-strain range is similar and its peak stress and strain co-ordinates can be found.

In Kent and Park model, a second degree parabola represents the ascending part of curve and assumes that the confined steel has no effect on shape of this part of the curve or strain at maximum stress (Madhu 2009).

Brief descriptions of both models are represented in Table 4.6.

Table 4.6 Description for Mander model and Kent and Park model (Mander *et al.* 1998, Madhu 2009)

MANDER MODEL	KENT AND PARK MODEL
 <p>The Mander model diagram shows Stress (f) on the y-axis and Strain (ε) on the x-axis. It features three curves: 'Unconfined concrete' (a simple peak), 'Assumed for axially confined concrete' (a higher peak), and 'Confined concrete' (a curve that rises to a peak f_c at strain ε_{cu} and then descends to a residual stress f_r at strain ε_{cu}, labeled 'First loop fracture'). Key strain points on the x-axis are ε₁, ε₂, ε₃, ε_{cu}, and ε_u.</p>	 <p>The Kent and Park model diagram shows Stress (f) on the y-axis and Strain (ε) on the x-axis. It compares 'Unconfined concrete' (a linear elastic peak at ε_c = 0.002) and 'Confined concrete' (a curve that rises to a peak f_c at strain ε₂, then descends to a residual stress f_r at strain ε₃, and finally drops to zero at strain ε_u). Key strain points on the x-axis are ε_c = 0.002, ε₂, ε₃, and ε_u.</p>
$f_c = \frac{f'_{cu} x^r}{r - 1 + x^r}$ <p>where, $x = \frac{\epsilon_c}{\epsilon_{cu}}$</p> $\epsilon_c = 0.002 \left[1 + 5 \left(\frac{f'_{cu}}{f'_{cu}} - 1 \right) \right]$ $r = \frac{E_c}{E_c - E_{un}}$ $E_c = 5000 \sqrt{f'_{cu}}$ $E_{un} = \frac{f'_{cu}}{\epsilon_{cu}}$ $f'_{cu} = f'_{cu} \left(-1.254 + 2.254 \sqrt{1 + \frac{7.94 f'_c}{f'_{cu}}} - 2 \frac{f'_c}{f'_{cu}} \right)$ $k_r = \frac{\left(1 - \sum_{i=1}^n \frac{(w_i)^2}{6b_i d_i} \right) \left(1 - \frac{s'}{2b_c} \right) \left(1 - \frac{s'}{2d_c} \right)}{1 - \rho_{un}}$ $f'_{lx} = k_r \rho_x f_{yh}$ $f'_{ly} = k_r \rho_y f_{yh}$ $f'_l = f'_{lx} + f'_{ly}$	<p>If, $\epsilon_c \leq 0.002$</p> $f_c = f'_c \left[\frac{2\epsilon_c}{0.002} - \left(\frac{\epsilon_c}{0.002} \right)^2 \right]$ <p>If, $0.002 \leq \epsilon_c \leq \epsilon_{2bc}$</p> $f_c = f'_c [1 - Z(\epsilon_c - 0.002)]$ <p>where</p> $Z = \frac{0.5}{\epsilon_{2bc} + \epsilon_{3bc} - 0.002}$ $\epsilon_{2bc} = \frac{3 + 0.002 f'_c}{f'_c - 1000}, \epsilon_{3bc} = \frac{3}{4} \rho_x \sqrt{\frac{b'}{s_b}}$ $\rho_x = \frac{2(b' + d'') A_s}{b' d' s_b}, \epsilon_{3bc} = \epsilon_{2bc} + \epsilon_{3bc}$ <p>If, $\epsilon_c \geq \epsilon_{2bc}$</p> $f_c = 0.2 f'_c$ $\epsilon_{2bc} = \frac{0.8}{Z} + 0.002$

4.5.6 Procedure to develop moment-curvature relationship (M-φ)

Theoretical determination of moment-curvature characteristics for reinforced concrete section with flexure and axial load is based on the following assumptions.

1. Plane sections before bending remains plane after bending.
2. Stress-strain relationship for both concrete and steel is known.
3. Tension carrying capacity of concrete is ignored.

The curvatures associated with a range of bending moments and axial loads may be determined using these assumptions and from strain compatibility and equilibrium of forces. Programs are developed in language Matlab language version 7.1 is used to get moment-curvature relationship of beams and columns. The procedure used for developing programs for developing moment curvature relationship is explained below and flowchart is shown in figure 4.11.

1. The model is subjected to gravity load analysis to find out the axial load coming on the element. For beam, axial load is assumed to be zero.
2. The stress strain curves for concrete and steel are assumed. The assumed stress strain relation relationship is as per IS 456-2000. The typical stress-strain curve for concrete material for M20 grade is shown in figure 4.12. The stress-strain curve for rebar material for Fe415 grade is shown in figure 4.13.
3. Cross section of beam or column is divided into the number of elemental strips and the distance of each strip is measured from the surface corresponding to the extreme compression.
4. Assume extreme compression strain, the strain values of each strips are calculated from assumed neutral axis. From these strain profile, stresses are calculated from stress strain relationship. Force in each strip is obtained by multiplying corresponding stress with strip area.
5. The neutral axis for particular strain is located by equating axial load carrying capacity with load coming on it. The moment and curvature is found out for that particular extreme compression strain.
6. These steps are repeated for different values of strain from zero to ultimate strain. The moment curvature relation is plotted.

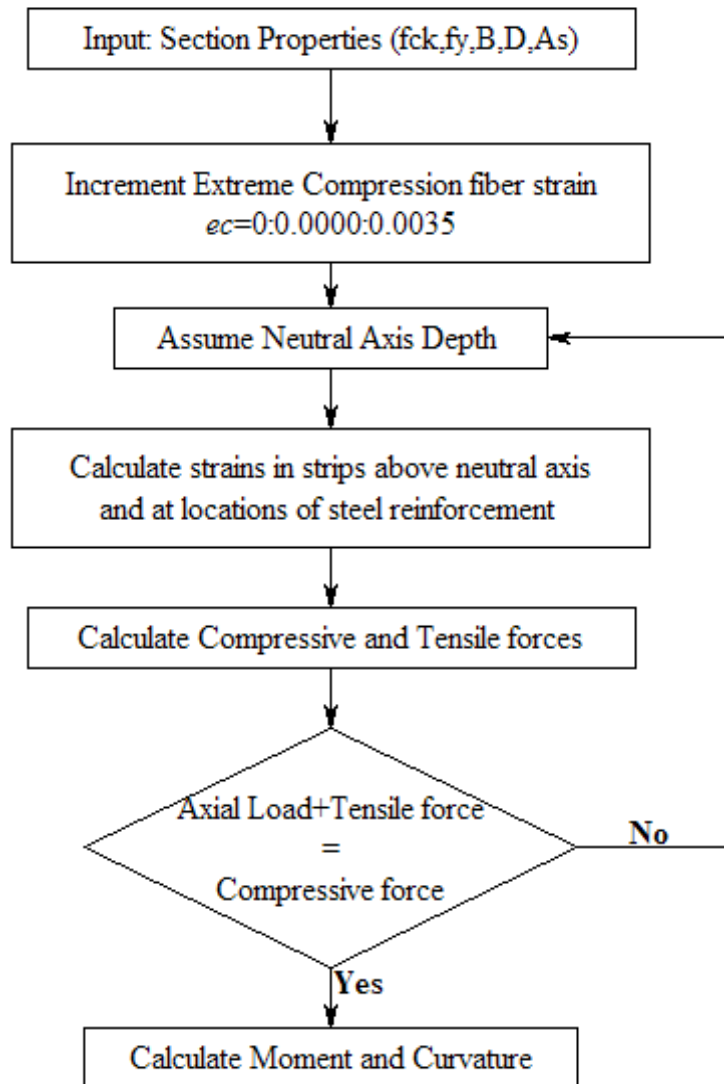


Figure 4.11 Flowchart to develop moment curvature relationship

4.5.6.1 M- ϕ characteristics considering IS: 456

The permissible compressive stress in concrete are considered as: $\sigma_{cu} = 0.67f_{ck}$. Under any loading condition, the section undergoes strains and consequent stresses. A linear strain distribution over the depth of cross-section is assumed for stress distribution in concrete and steel (Figs.4.12 and 4.13).

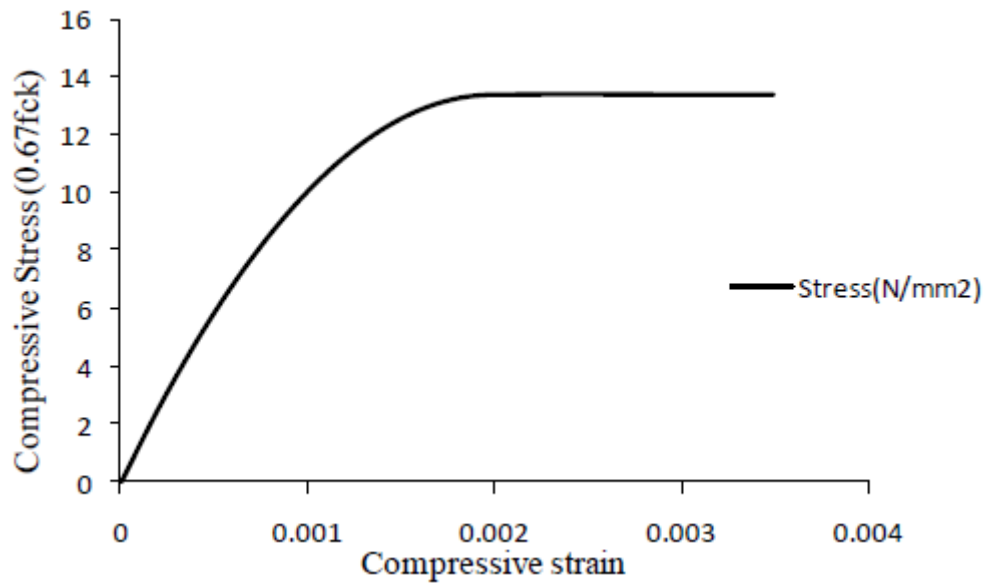


Figure 4.12 Stress-strain curve for concrete

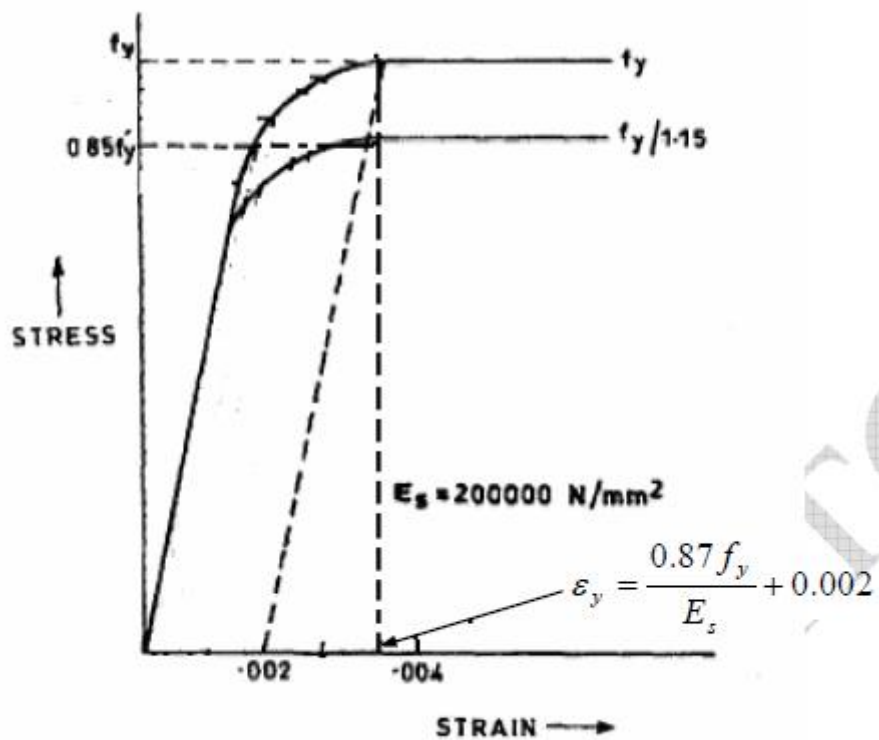


Fig 4.13 (a) Stress strain diagram of steel (Fe415) as per IS 456 (2000)

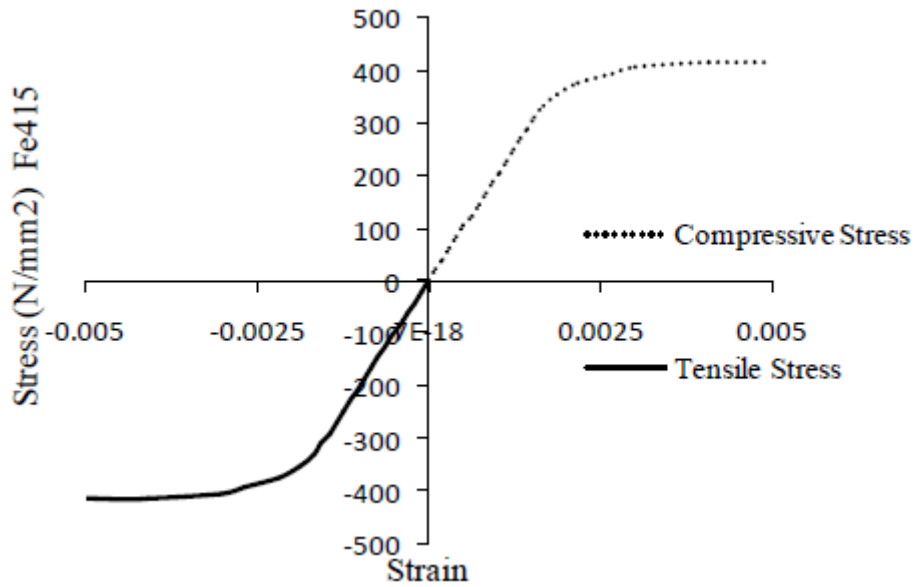


Figure 4.13 (b) Stress-strain curve for Fe415 grade steel

The stress strain curve for Fe415 grade steel till failure of steel and the strain at which steel ruptures/fails are tabulated in Table 4.7.

Table 4.7 Stress-strain values for Fe415 grade steel

ϵ	σ (MPa)
0.00000	0.0
0.00144	288.7
0.00163	306.7
0.00192	324.8
0.00241	342.8
0.00276	351.8
≥ 0.0038	360.9

CHAPTER 5

RESULTS AND DISCUSSIONS

5.1 INTRODUCTION

This chapter provides analytical results and discussions of fragility estimates for RC buildings with variation in material strength and usage of Indian ground motion data based on pushover analysis. The available experiment results have been compared with that of pushover analysis results (both for unconfined, confined concrete section and for the provisions of code specified as well as for user defined response spectra).

5.2 DYNAMIC PROPERTIES OF THE STRUCTURE.

Structure used for analysis is a four storied RCC structure with single bay 5m x 5m dimension. The structure is the part of an existing structure. Height of the storey is 4m. An analytical four storey building model is modeled using SAP 2000 software, version 17. Dynamic properties of the structure is obtained (Fig. 5.1) are as shown in Table 5.1.

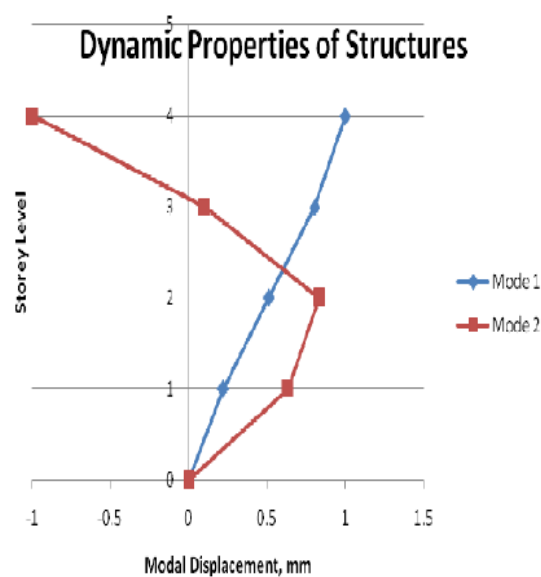


Fig. 5.1: Normalized Mode Shape of the Structure

Table 5.1 Dynamic properties of the structure

Dynamic Properties		Mode	
		1	2
Period (Sec)		0.297076	0.262477
Modal Participation Factor		229.906679	150.62003
Modal Mass Factor		55.936	24.0079
Mode Shapes	Roof	1	-1
	3 rd Floor	0.8049	0.1
	2 nd Floor	0.5122	0.8333
	1 st Floor	0.2195	0.6333

5.3 PARAMETRIC STUDY-I (UN-CONFINED CONCRETE SECTION)

5.3.1 Moment curvature characteristics

The following are the plots of moment curvature characteristics for unconfined concrete sections (beams and columns) of the considered frame as depicted in Figs.5.2 and 5.3.

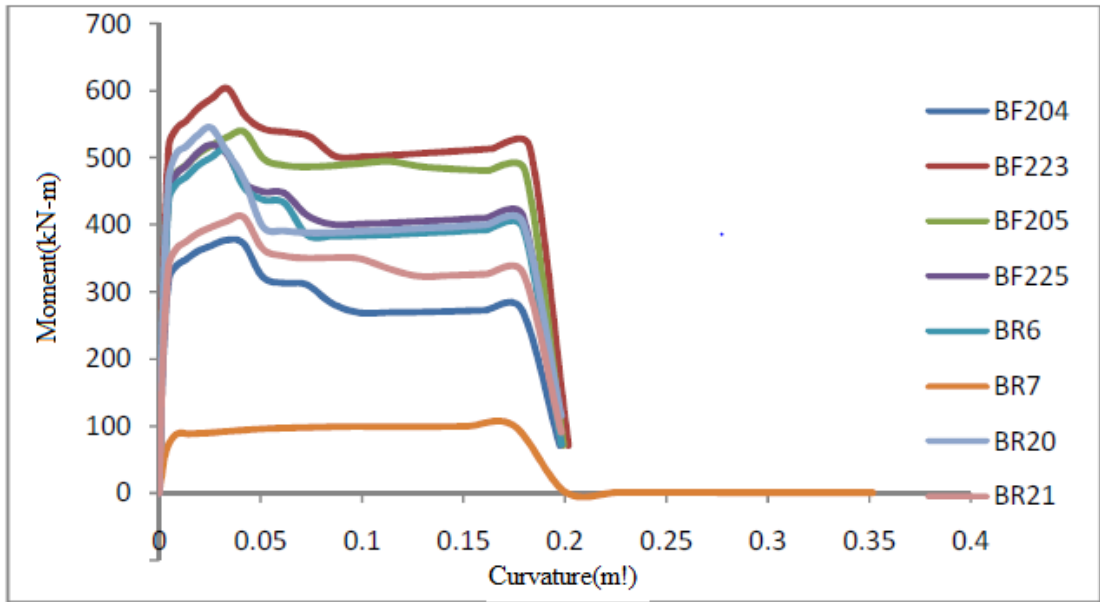


Fig. 5.2 Moment curvature relationships for beams (Unconfined model with $f_{ck}=20\text{MPa}$ and $f_y=520\text{ MPa}$)

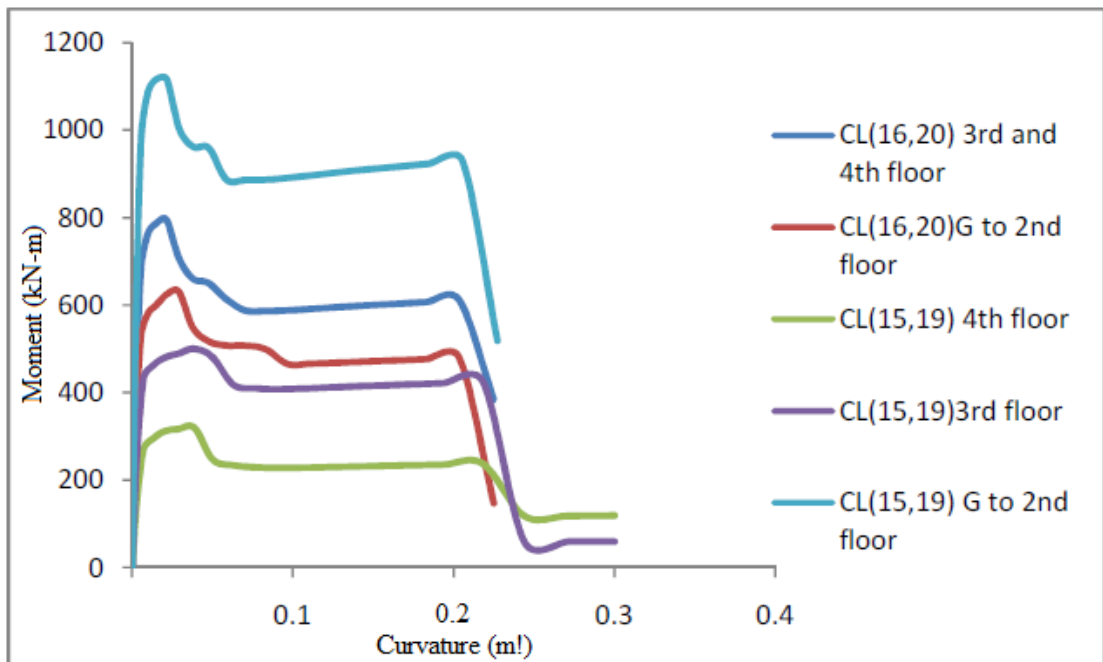


Fig. 5.3 Moment curvature relationships for columns (Unconfined model with $f_{ck}=20\text{MPa}$ and $f_y=520\text{ MPa}$)

5.3.2 Pushover Analysis Results for Buildings with Unconfined Concrete Section

The pushover analysis of a structure is a static non-linear analysis procedure in which the magnitude of the structural loading is monotonically increased in a certain predefined pattern (Inverted Triangular Pattern). Pushover analysis will provide adequate information on seismic demands imposed on the structure on which the ground motion is acting.

Pushover analysis of the reference structure was performed using SAP2000. The analysis results include variation of base shear and corresponding roof displacement for varying values of compressive strength of concrete and tensile strength of steel. From the capacity curve obtained from pushover analysis, fragility curves are plotted for the seismic loading along X direction.

The objective of this study is to see the variation of load-displacement graph and to check the maximum base shear and displacement of the frame. From nonlinear static pushover analysis conducted, base shear versus roof displacement was obtained from SAP2000. It can be seen that the maximum base shear obtained is almost comparable to that of the experimental result. The values of base shear versus roof displacement values for the variation in material strengths are obtained and the values are tabulated in the Table 5.2.

It is observed from the Table 5.2 that as the compressive strength of concrete increases, the base shear increases. It is also observed from the Table 5.2 that with the variation in tensile strength of steel, base shear remains same without any changes for a particular value of compressive strength. The following Figure 5.2 gives the base shear versus displacement graph for the variation of strength of concrete and tensile strength of steel (constant) in X directional loading.

The mechanical properties adopted respectively, for concrete 20-30 MPa as compression strength and, for the reinforcement, 520-600 MPa as yield strength. Figure 5.2 summarizes the results in terms of pushover curve (that is base shear versus displacement curve). Although the models provide a quite good agreement on

results with particular reference to maximum base shear reached and the collapse mechanism activated.

Table 5.2: Base shear versus roof displacement for the variation in material strength

Compressive Strength of Concrete in N/mm ²		Tensile Strength of Steel in N/mm ²				
		520	540	560	580	600
20	V _B (kN)	840.1	840.1	840.1	840.1	840.1
	Δ(m)	0.259	0.259	0.259	0.259	0.259
21.5	V _B (kN)	848.5	848.5	848.5	848.5	848.5
	Δ(m)	0.259	0.259	0.259	0.259	0.259
23	V _B (kN)	855.1	855.1	855.1	855.1	855.1
	Δ(m)	0.258	0.258	0.258	0.258	0.258
25	V _B (kN)	864.8	864.8	864.8	864.8	864.8
	Δ(m)	0.258	0.258	0.258	0.258	0.258
27	V _B (kN)	872.5	872.5	872.5	872.5	872.5
	Δ(m)	0.256	0.256	0.256	0.256	0.256
28.5	V _B (kN)	877.5	877.5	877.5	877.5	877.5
	Δ(m)	0.253	0.253	0.253	0.253	0.253
30	V _B (kN)	881.6	881.6	881.6	881.6	881.6
	Δ(m)	0.253	0.253	0.253	0.253	0.253

5.3.2.1 Comparison of Results in Terms of Pushover Curves

The summary of pushover results for various strength values as done, along with experimental results provided by BARC is shown in Figure 5.4 below.

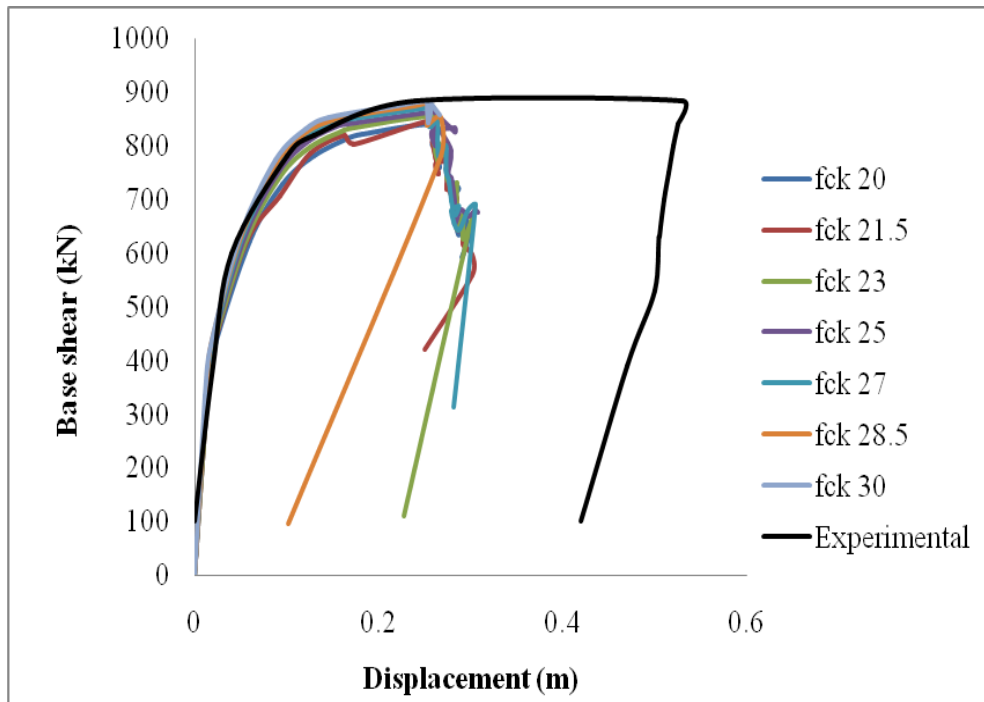


Figure 5.4 Comparison of results provided by SAP2000 with experimental pushover curve (X-direction)

Once geometrical features and mechanical parameters are shared, non-linear static analyses were performed for varying values of f_{ck} and keeping f_y constant. Paying attention to the analyses performed in X-direction, Figure 5.4 shows comparison of results in terms of pushover curves. In particular, the contribution to the global base shear distinguishing between that carried by varying f_{ck} and that by RC frame (experimental) as seen in Figure 5.4. It could be observed that all the seven curves follow the same path.

Nevertheless, the following issues have to be pointed out. There is some improvement in base shear values as the strength varies. There is no significant improvement in displacement values for varying values of f_{ck} and f_y . The results of all models are quite well agree in particular until reaching of the maximum base shear. Actually, differences in softening phase (more sudden in case of $f_{ck}=28.5$ MPa) and in computation of displacement (the parameter which governs the collapse elements) are similar to each other. Moreover, the models also agree in terms of global failure mode.

5.3.2.2 Performance evaluation of building

Table 5.3 shows performance point for different values of f_{ck} (MPa) and f_y (MPa) in X direction. Performance appears to be same with varying values of tensile strength.

Table 5.3: Performance point for different values of f_{ck} (MPa) and f_y (MPa) in X direction (Unconfined Model)

Compressive Strength of Concrete in MPa	Performance Details	Tensile strength of steel in MPa				
		$f_y = 520$	$f_y = 540$	$f_y = 560$	$f_y = 580$	$f_y = 600$
$f_{ck} = 20$	V_B (kN)	656.76	656.76	656.76	656.76	656.76
	Δ (m)	0.050	0.050	0.050	0.050	0.050
	S_a	0.585	0.585	0.585	0.585	0.585
	S_d	0.041	0.041	0.041	0.041	0.041
$f_{ck} = 21.5$	V_B (kN)	661.49	661.49	661.49	661.49	661.49
	Δ (m)	0.058	0.058	0.058	0.058	0.058
	S_a	0.590	0.590	0.590	0.590	0.590
	S_d	0.040	0.040	0.040	0.040	0.040
$f_{ck} = 23$	V_B (kN)	664.35	664.35	664.35	664.35	664.35
	Δ (m)	0.056	0.056	0.056	0.056	0.056
	S_a	0.593	0.593	0.593	0.593	0.593
	S_d	0.040	0.040	0.040	0.040	0.040
$f_{ck} = 25$	V_B (kN)	669.57	669.57	669.57	669.57	669.57
	Δ (m)	0.055	0.055	0.055	0.055	0.055
	S_a	0.597	0.597	0.597	0.597	0.597
	S_d	0.039	0.039	0.039	0.039	0.039
$f_{ck} = 27$	V_B (kN)	671.70	671.70	671.70	671.70	671.70
	Δ (m)	0.054	0.054	0.054	0.054	0.054
	S_a	0.597	0.597	0.597	0.597	0.597
	S_d	0.038	0.038	0.038	0.038	0.038
$f_{ck} = 28.5$	V_B (kN)	676.05	676.05	676.05	676.05	676.05

	Δ (m)	0.053	0.053	0.053	0.053	0.053
	S_a	0.601	0.601	0.601	0.601	0.601
	S_d	0.037	0.037	0.037	0.037	0.037
$f_{ck}=30$	V_B (kN)	678.40	678.40	678.40	678.40	678.40
	Δ (m)	0.053	0.053	0.053	0.053	0.053
	S_a	0.603	0.603	0.603	0.603	0.603
	S_d	0.037	0.037	0.037	0.037	0.037

5.4 PARAMETRIC STUDY-II (CONFINED CONCRETE SECTION)

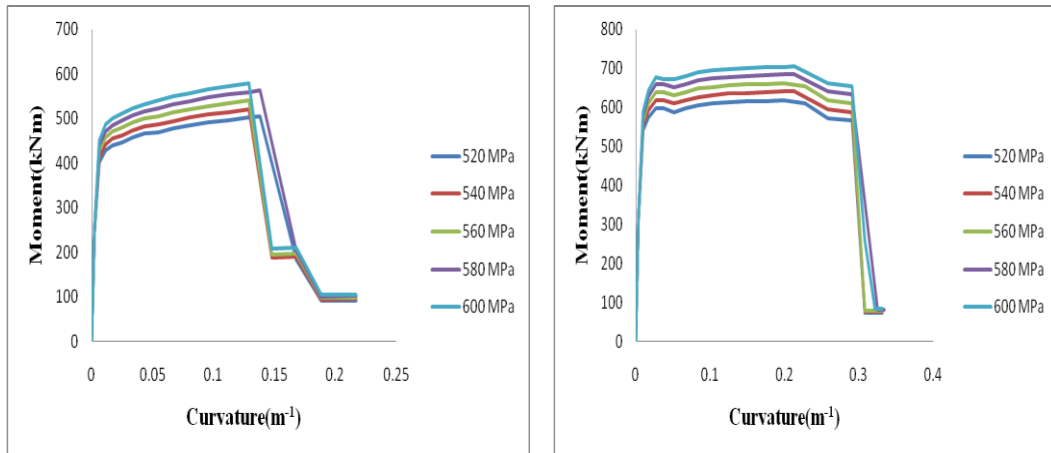
5.4.1 Moment Curvature Relationship

Moment curvature analysis is a method to accurately determine the load deformation behaviour of a concrete section using nonlinear material stress-strain relationship. It is the representation of strength and deformation of the section in terms of moment and corresponding curvature of the section. In order to obtain moment characteristics for structural elements, two modelling approaches have been preferred (Mander Model & Kent and Park Model).

Figures 5.5 represents moment-curvature plots of beam BF204 and column CL15 by Mander model respectively for compressive strength of concrete = 20 MPa and varying values of tensile strength of steel. Similarly, Figures 5.6 represents moment-curvature plots by Kent and Park model.

For the pushover analyses, flexural and shear hinges were assigned at the ends of beams and columns. Axial hinges were assigned at the middle of the members. The moment versus rotation property of a flexural hinge was developed from the calculated non-linear moment versus curvature curve for the section of the beam or column. For a column, the curve was calculated in presence of the axial force due to gravity loads. The curvature at each step was multiplied by the length of plastic hinge (assumed to be 0.5 times the depth of the member) to get rotation. Each flexural hinge property was approximated as a bilinear curve (up to the moment capacity) with the transition at yielding of the reinforcing bars. The shear force versus deformation

property of a shear hinge was considered to be linear till the shear capacity of a beam or column section.

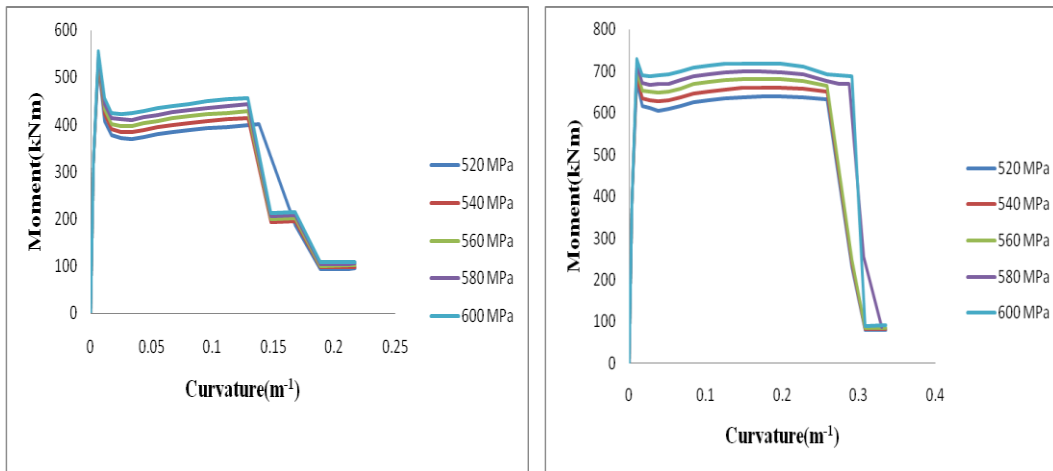


a) BF204

b) CL-15

Figure 5.5: Moment curvature relation for Beam BF204 and Column CL-15 for $f_{ck}=20\text{MPa}$ and varying tensile strength of steel (Mander Model)

The present investigation was aimed at an analytical study of the behavior of loaded structural members as the applied load was increased monotonically from zero load until failure. The moment-curvature (or moment-rotation) characteristics derived can be found useful in the limit analysis studies of two or three dimensional reinforced concrete frames. The analytical models adopted to simulate the moment-curvature behavior of reinforced concrete members. Based on the control of load increments, the algorithm enables deformation of moment-curvature-strain relationship with any geometry and material properties up to the maximum moment capacity of the section.



a) BF204

b) CL-15

Figure 5.6 Moment curvature relation for BF204 and CL 15 for $f_{ck}=20\text{MPa}$ and varying tensile strength of steel (Kent & Park Model)

The moment curvature relations is observed from its inelastic behavior in all the models. The beams and columns are modelled as fibre discretised elements considering flexural, shear and axial deformations, wherein the flexural and shear deformations for beams are coupled. Spread plasticity and effect of confinement on the hysteretic behaviour of the elements are included. Inelastic action was monitored in terms of crack initiation, steel yielding and concrete ultimate strain exceedence rather than by defining bi-linear moment curvature relationships. The inelasticity propagates into the upper floors due to redistribution of the load within the structure. So that with successive cycles of lateral loading, stiffness and degradation occurs within the elements leading to a declining lateral capacity. M20 and Fe415 reinforcing steel were assumed in the model.

5.4.2 Pushover Analysis Results (Confined Concrete Section)

The pushover curve obtained from two approaches are displayed below for varying values compressive strength of concrete and tensile strength of steel=520 MPa.

5.4.2.1 Mander's Model

Base shear (kN) versus roof displacement (m) for different values of f_{ck} (MPa) and f_y (MPa) by Mander's Model are tabulated in Table 5.4. Figures 5.7 shows pushover

curves for varying values compressive strength of concrete and tensile strength of steel=520 MPa along with that of experimental pushover curve.

Table 5.4: Base shear (kN) versus roof displacement (m) for different values of f_{ck} (MPa) and f_y (MPa) in X direction (Mander Model)

Compressive Strength of Concrete in MPa	Base Shear	Tensile strength of steel in MPa				
	Displacement	$f_y = 520$	$f_y = 540$	$f_y = 560$	$f_y = 580$	$f_y = 600$
$f_{ck} = 20$	V_B (kN)	955.3	981.8	998.12	998.12	998.12
	Δ (m)	0.342	0.289	0.328	0.328	0.328
$f_{ck} = 21.5$	V_B (kN)	961.6	1014.74	1019.61	1019.61	1019.61
	Δ (m)	0.240	0.347	0.288	0.288	0.288
$f_{ck} = 23$	V_B (kN)	979.5	1022.0	1000.8	1000.8	1000.8
	Δ (m)	0.247	0.367	0.243	0.243	0.243
$f_{ck} = 25$	V_B (kN)	1006.6	1019.7	1029.5	1029.5	1029.5
	Δ (m)	0.274	0.249	0.254	0.254	0.254
$f_{ck} = 27$	V_B (kN)	1072.8	1038.8	1057.6	1057.6	1057.6
	Δ (m)	0.268	0.259	0.260	0.260	0.260
$f_{ck} = 28.5$	V_B (kN)	1100.1	1054.4	1081.2	1081.2	1081.2
	Δ (m)	0.299	0.260	0.267	0.267	0.267
$f_{ck} = 30$	V_B (kN)	1118.0	1130.9	1114.3	1114.3	1114.3
	Δ (m)	0.293	0.271	0.293	0.293	0.293

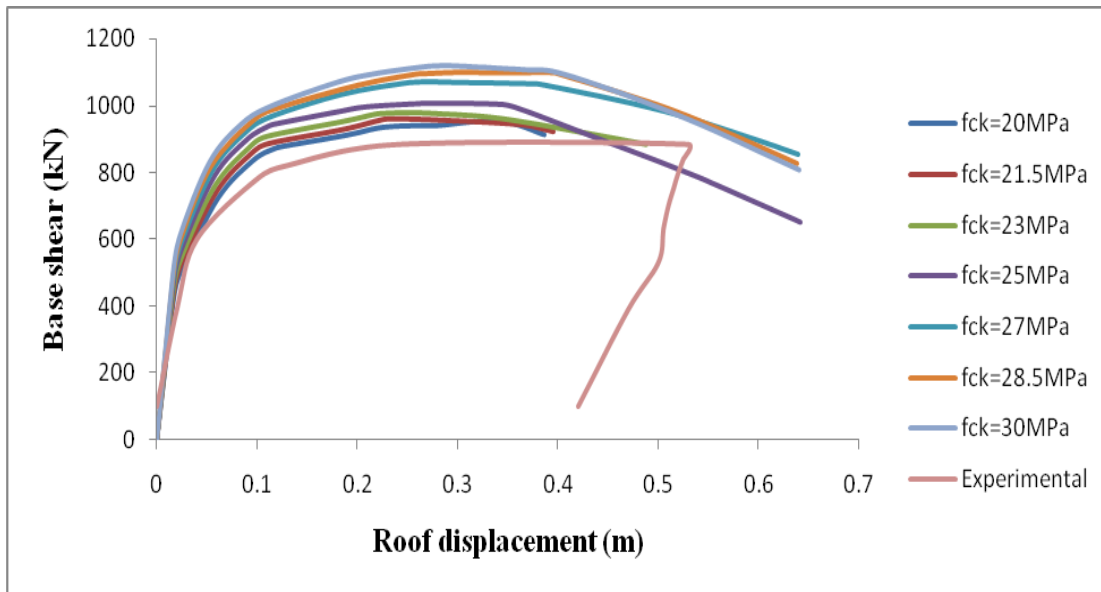


Figure 5.7: Comparison of analytical results for varying values f_{ck} and $f_y=520\text{MPa}$ with experimental pushover curve

5.4.2.2 Kent and Park Model

Base shear (kN) versus roof displacement (m) for different values of f_{ck} (MPa) and f_y (MPa) by Kent and Park are tabulated in Table 5.5. Figures 5.8 shows pushover curves for varying values compressive strength of concrete and tensile strength of steel=520 MPa along with with that of experimental pushover curve.

From pushover curves, it can be observed that, the base shear increases with the increase in compressive strength of concrete. However, the models showed no change in the value of base shear or the roof displacement with the increase in tensile strength of steel for a particular compressive strength of concrete. Therefore, pushover curve is independent of tensile strength of steel, but shows a positive increment with respect to variation of compressive strength of concrete.

It can be seen that the maximum base shear obtained from SAP2000 is almost comparable to that of experimental result as shown in 5.8 for all the cases. The base shear obtained from experiment was found to be nearly 882kN. Whereas, it is ranged from 955 kN to 1118 kN for varying values of compressive strength of concrete from Mander's model. It is ranged from 1009 to 1180 kN from Kent and Park model for varying values of compressive strength of concrete in X direction. Such variations in

base shear with respect to X direction can be attributed to the orientation of column, unsymmetrical section at each floor level.

Table 5.5: Base shear (kN) versus roof displacement (m) for different values of f_{ck} (MPa) and f_y (MPa) in X direction (Kent & Park model)

Compressive Strength of Concrete in MPa	Base Shear	Tensile strength of steel in MPa				
	Displacement	$f_y = 520$	$f_y = 540$	$f_y = 560$	$f_y = 580$	$f_y = 600$
$f_{ck} = 20$	V_B (kN)	1009.4	1061.9	1110.5	1110.5	1110.5
	Δ (m)	0.222	0.230	0.267	0.267	0.267
$f_{ck} = 21.5$	V_B (kN)	1030.8	1042.9	1051.2	1051.2	1051.2
	Δ (m)	0.215	0.223	0.226	0.226	0.226
$f_{ck} = 23$	V_B (kN)	1049.4	1065.2	1075.7	1075.7	1075.7
	Δ (m)	0.227	0.217	0.215	0.215	0.215
$f_{ck} = 25$	V_B (kN)	1074.6	1091.5	1100.0	1100.0	1100.0
	Δ (m)	0.218	0.226	0.196	0.196	0.196
$f_{ck} = 27$	V_B (kN)	1113.1	1114.3	1123.3	1123.3	1123.3
	Δ (m)	0.205	0.191	0.193	0.193	0.193
$f_{ck} = 28.5$	V_B (kN)	1126.6	1135.3	1142.1	1142.1	1142.1
	Δ (m)	0.206	0.214	0.202	0.202	0.202
$f_{ck} = 30$	V_B (kN)	1179.8	1142.3	1164.0	1164.0	1164.0
	Δ (m)	0.216	0.183	0.213	0.213	0.213

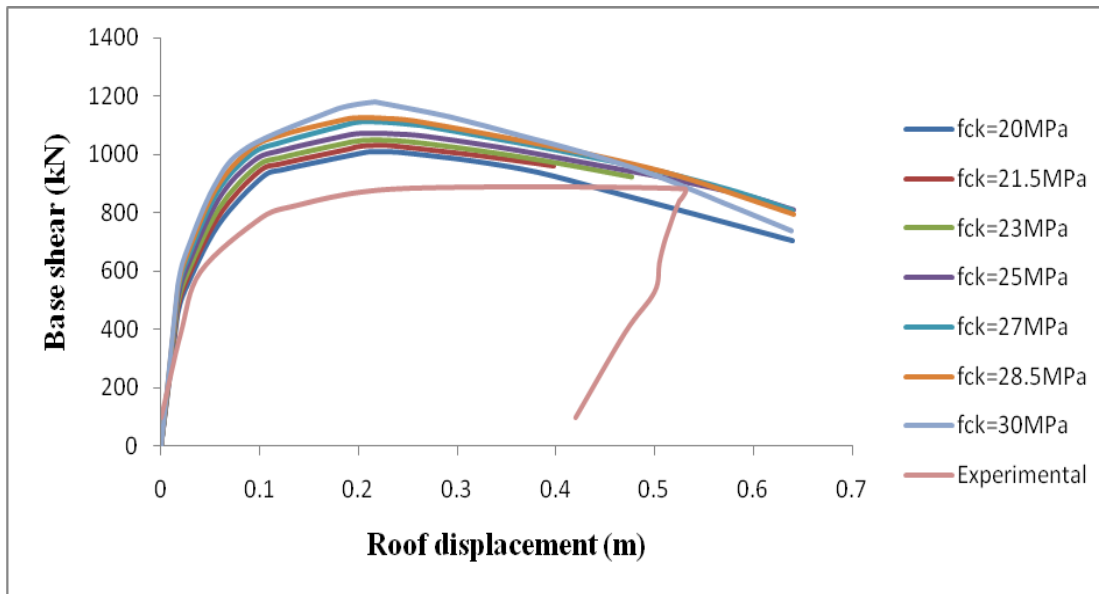


Figure 5.8: Comparison of analytical results for varying values f_{ck} and $f_y=520\text{MPa}$ with experimental pushover curve

Figure 5.8 shows the comparison between the analyses performed with pseudo-triangular load pattern in terms of base shear versus displacement; this represents a kind of normalized pushover curve aimed to standardize the different f_{ck} examined. The pseudo-triangular load pattern has been adopted as reference to discuss in a qualitative way the different behaviours occurred. Pushover analyses were stopped till the maximum displacement reached.

Comparison of pushover curves of both the models is given in Figure-5.8. It could be observed that all the seven curves follow the same path. Maximum displacement is observed at a base shear of 1118.0 kN. The corresponding lateral roof displacement is 0.293 mm, when $f_{ck}=30\text{ N/mm}^2$ and $f_y=520\text{ Mpa}$ for Mander's model. Maximum displacement is observed at a base shear of 1180 kN. The corresponding lateral roof displacement is 0.216 mm, when $f_{ck}=30\text{ N/mm}^2$ and $f_y=520\text{ Mpa}$ for Kent and Park model. For all the cases a mechanism is formed at a maximum base shear with a maximum roof displacement.

5.4.2.3 Performance evaluation of building

Using capacity spectrum method the seismic performance of the building is evaluated. Table 5.6 and Table 5.7 represents the performance point of the structure for Mander

and Kent and Park model respectively in X-direction in terms of base shear(V_B) and roof displacement(Δ) from FEMA 356 and spectral acceleration(S_a) and spectral displacement(S_d) from ATC40. Different modelling technique for confined model shows only slight change in the performance point.

Table 5.6: Performance point for different values of f_{ck} (MPa) and f_y (MPa) in X direction (Mander Model)

Compressive Strength of Concrete in MPa	Performance Details	Tensile Strength of Steel in MPa				
		$f_y= 520$	$f_y= 540$	$f_y= 560$	$f_y= 580$	$f_y= 600$
$f_{ck}= 20$	V_B (kN)	738.79	743.31	744.94	744.94	744.94
	Δ (m)	0.065	0.066	0.066	0.066	0.066
	S_a	0.349	0.351	0.352	0.352	0.352
	S_d	0.051	0.051	0.051	0.051	0.051
$f_{ck}= 21.5$	V_B (kN)	757.80	762.59	764.20	764.20	764.20
	Δ (m)	0.064	0.064	0.064	0.064	0.064
	S_a	0.358	0.360	0.361	0.361	0.361
	S_d	0.050	0.050	0.050	0.050	0.050
$f_{ck}= 23$	V_B (kN)	775.15	781.06	782.77	782.77	782.77
	Δ (m)	0.062	0.062	0.063	0.063	0.063
	S_a	0.366	0.368	0.369	0.369	0.369
	S_d	0.049	0.049	0.049	0.049	0.049
$f_{ck}= 25$	V_B (kN)	799.41	803.51	805.07	805.07	805.07
	Δ (m)	0.060	0.061	0.061	0.061	0.061
	S_a	0.377	0.378	0.379	0.379	0.379
	S_d	0.047	0.047	0.047	0.047	0.047
$f_{ck}= 27$	V_B (kN)	819.46	825.34	829.48	829.48	829.48
	Δ (m)	0.059	0.059	0.059	0.059	0.059
	S_a	0.386	0.389	0.390	0.390	0.390
	S_d	0.046	0.046	0.046	0.046	0.046
$f_{ck}= 28.5$	V_B (kN)	832.14	841.06	845.09	845.09	845.09
	Δ (m)	0.058	0.058	0.058	0.058	0.058
	S_a	0.392	0.396	0.398	0.398	0.398
	S_d	0.045	0.045	0.046	0.046	0.046
$f_{ck}= 30$	V_B (kN)	846.47	854.01	858.17	858.17	858.17
	Δ (m)	0.057	0.057	0.057	0.057	0.057
	S_a	0.399	0.402	0.404	0.404	0.404
	S_d	0.045	0.045	0.045	0.045	0.045

Table 5.7: Performance point for different values of f_{ck} (MPa) and f_y (MPa) in X direction (Kent and Park Model)

Compressive Strength of Concrete in MPa	Performance Details	Tensile Strength of Steel in MPa				
		$f_y= 520$	$f_y= 540$	$f_y= 560$	$f_y= 580$	$f_y= 600$
$f_{ck}= 20$	V_B (kN)	773.54	773.52	773.50	773.50	773.50
	Δ (m)	0.062	0.062	0.062	0.062	0.062
	S_a	0.377	0.377	0.377	0.377	0.377
	S_d	0.047	0.047	0.047	0.047	0.047
$f_{ck}= 21.5$	V_B (kN)	796.33	796.43	796.45	796.45	796.45
	Δ (m)	0.061	0.061	0.061	0.061	0.061
	S_a	0.387	0.387	0.387	0.387	0.387
	S_d	0.045	0.045	0.045	0.045	0.045
$f_{ck}= 23$	V_B (kN)	818.32	818.44	818.51	818.51	818.51
	Δ (m)	0.059	0.059	0.059	0.059	0.059
	S_a	0.398	0.398	0.398	0.398	0.398
	S_d	0.045	0.045	0.045	0.045	0.045
$f_{ck}= 25$	V_B (kN)	846.14	846.14	846.14	846.14	846.14
	Δ (m)	0.058	0.058	0.058	0.058	0.058
	S_a	0.411	0.411	0.411	0.411	0.411
	S_d	0.043	0.043	0.043	0.043	0.043
$f_{ck}= 27$	V_B (kN)	866.14	868.98	868.98	868.98	868.98
	Δ (m)	0.056	0.056	0.056	0.056	0.056
	S_a	0.420	0.421	0.421	0.421	0.421
	S_d	0.042	0.042	0.042	0.042	0.042
$f_{ck}= 28.5$	V_B (kN)	881.22	884.52	884.25	884.25	884.25
	Δ (m)	0.055	0.055	0.055	0.055	0.055
	S_a	0.428	0.429	0.429	0.429	0.429
	S_d	0.042	0.042	0.042	0.042	0.042
$f_{ck}= 30$	V_B (kN)	894.58	899.56	899.09	899.09	899.09
	Δ (m)	0.054	0.054	0.054	0.054	0.054
	S_a	0.434	0.436	0.436	0.436	0.436
	S_d	0.041	0.041	0.041	0.041	0.041

5.5 PARAMETRIC STUDY-III (CODE PROPOSED AND USER DEFINED RESPONSE SPECTRA)

5.5.1 Moment Curvature Relationships for Code proposed and user defined property

Moment curvature analysis is a technique utilized to precisely focus on the load deformation conduct of a concrete segment by nonlinear material stress-strain relationship. It is the representation of strength and deformation of a component relating moment and corresponding curvature of the section. The essential key prerequisite in foreseeing the Moment Curvature behavior of a flexural member is the information on the conduct of its components. With the increasing use of the high grade concrete, the ductility of which is significantly less than the normal concrete it is essential to confine the concrete.

Below tables presents the moment curvature of a beam element BF 204 and a column element CL15 and 19 (third floor) with varying f_{ck} and f_y values obtained from the thirty five models.

5.5.1.1 Code proposed property

From the above figures 5.9 through 5.12 it can be observed that as the tensile strength of the steel increases in beams as well as columns, the moment also increases. Provision of high tensile steel increases the ductile capacity of the frame which results in the increased moment carrying capacity of the structure. It can also be noticed that moment carrying ability of the frame increases with the increase in compressive strength of concrete.

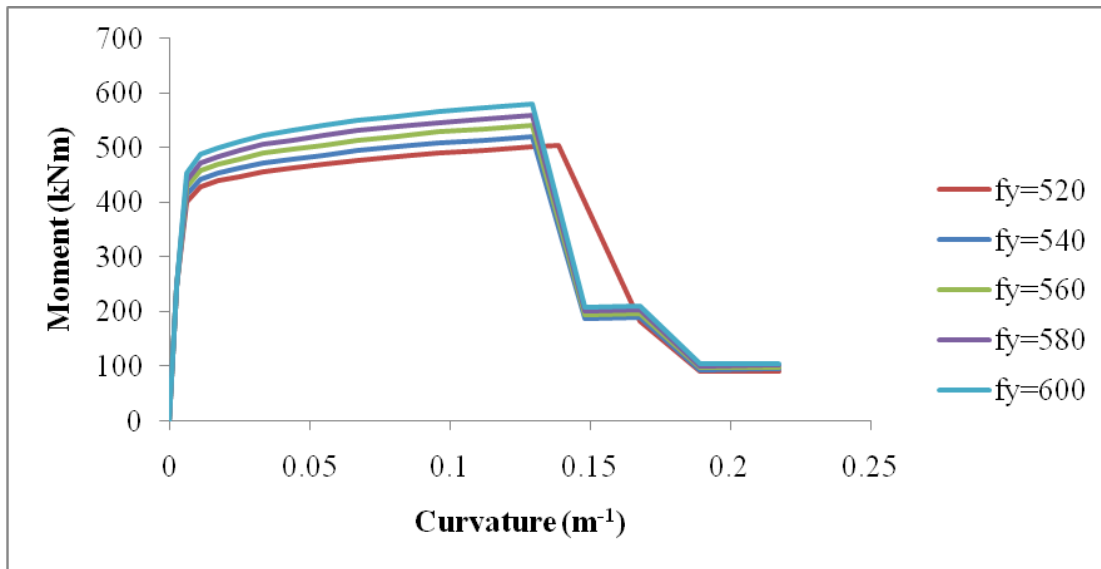


Fig.5.9: Moment curvature relation for BF204 for $f_{ck}= 20$ MPa and varying f_y values

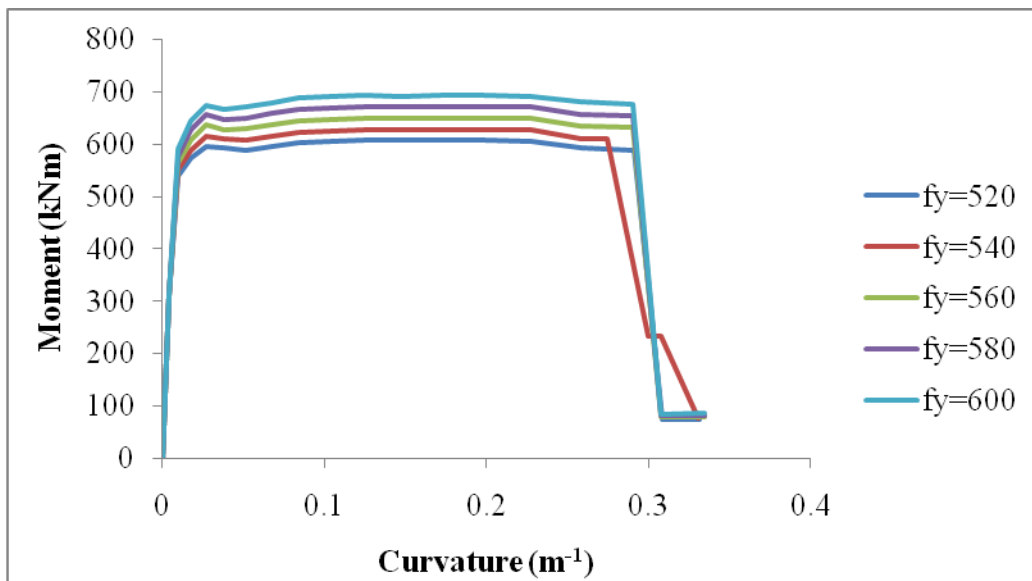


Fig.5.10: Moment curvature relation for CL 15 and 19 for $f_{ck}= 20$ MPa and varying f_y values

5.5.1.2 User defined property models

The moment carrying ability of the structure in case of user defined case model is found out to be slightly higher than that of code proposed case as seen in Fig. 5.11 and Fig. 5.12. It can also be noticed that moment carrying ability of the frame increases with the increase in compressive strength of concrete.

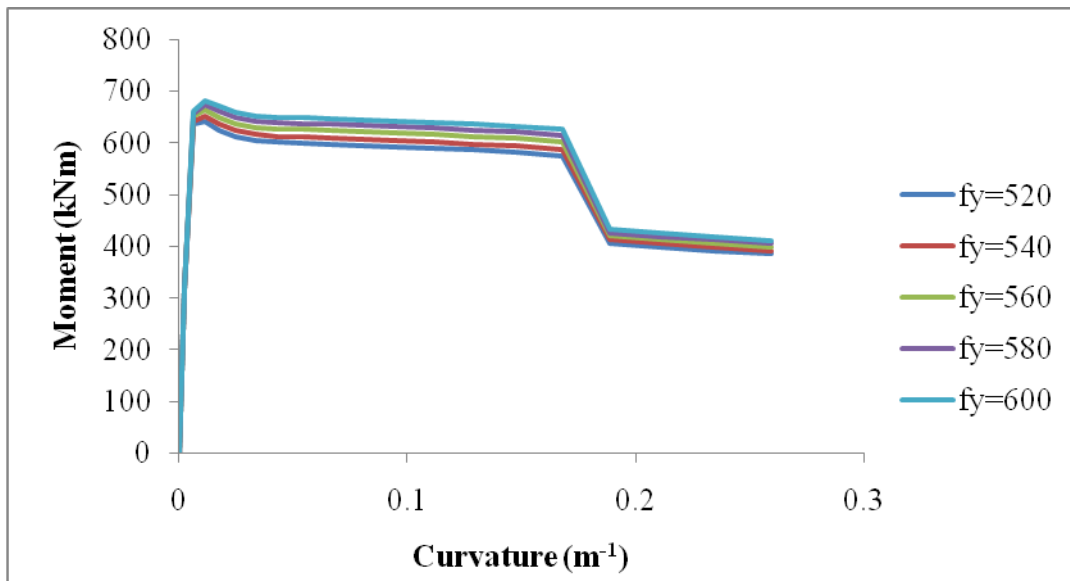


Fig.5.11: Moment curvature relation for BF204 for $f_{ck}= 20$ MPa and varying f_y values

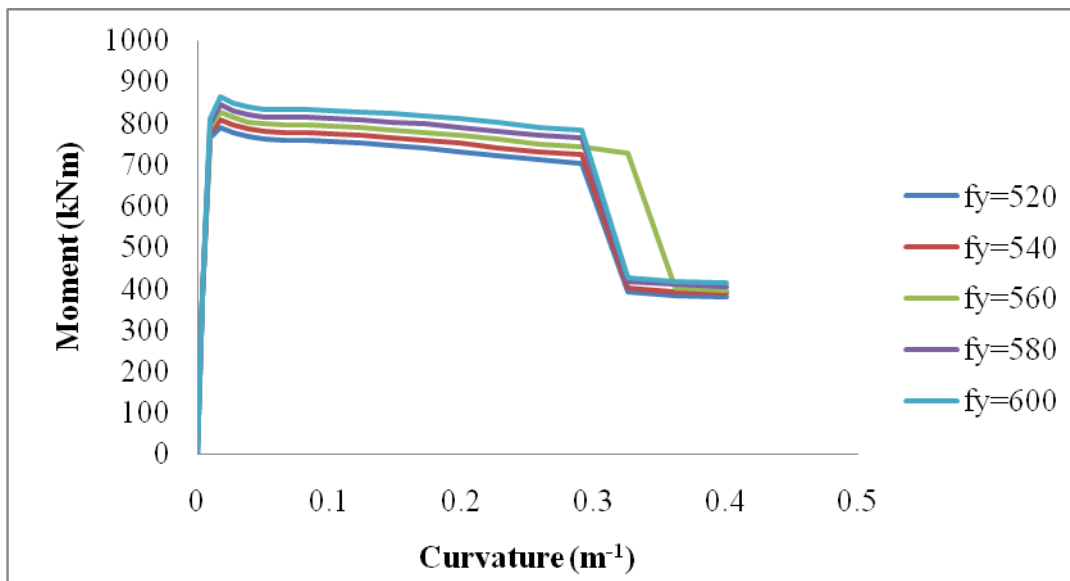


Fig.5.12: Moment curvature relation for CL 15 and 19 for $f_{ck}= 20$ MPa and varying f_y values

5.5.2 Pushover Analysis Results for Code Proposed and User Defined Response Spectra

5.5.2.1 Code Proposed Response Spectra

The pushover analysis is carried out for the frame for the requirements of IS: 1893-2002 code proposed response spectra using SAP 2000 software. Table 5.8 shows base shear (kN) versus displacement (m) for different values of f_{ck} (MPa) and f_y (MPa) in X direction. Figure 5.13 shows analytical pushover curves with that of experimental pushover curve.

Pushover analyses were conducted on the computational model for the X-directional loading. This is denoted as Push-X, respectively. For the analysis in X-direction, the distribution of the lateral loads at each step was in the parabolic pattern as given in IS1893:2002(Part 1). The load at each floor level was applied at a design eccentricity from the centre of rigidity. In each pushover analysis, a “lateral push” was applied in the X-direction. The pushover curves and the hinge distributions (at the instance of reaching the performance points) for frame with variation in material strength, are shown in Figure 5.13 respectively. It can be observed that the inelastic part is stretched more, which indicates that the hinges are well distributed throughout the levels. Apart from the hinges in the status, hinges have formed in the beams near their left supports, due to inadequate sagging moment capacities. A few hinges have formed in the columns. After the analysis, the damage thresholds were calculated and fragility status was obtained.

Table 5.8: Base shear (kN) versus Displacement (m) for different values of fck(MPa) and fy (MPa) in X direction

Compressive Strength of Concrete in MPa	Base Shear	Tensile strength of steel in MPa				
	Displacement	fy=520	fy=540	fy=560	fy=580	fy=600
fck =20	V _B (kN)	915.6	912.0	994.1	994.1	994.1
	Δ(m)	0.189	0.187	0.247	0.247	0.247
fck =21.5	V _B (kN)	952.6	948.4	996.4	996.4	996.4
	Δ(m)	0.259	0.188	0.206	0.206	0.206
fck=23	V _B (kN)	967.2	985.4	955.8	955.8	955.8
	Δ(m)	0.282	0.265	0.197	0.197	0.197
fck =25	V _B (kN)	986.9	970.6	988.9	988.9	988.9
	Δ(m)	0.187	0.181	0.176	0.176	0.176
fck =27	V _B (kN)	1032.7	1016.9	1001.4	1001.4	1001.4
	Δ(m)	0.255	0.204	0.179	0.184	0.184
fck =28.5	V _B (kN)	1048.9	1047.7	1019.9	1019.9	1020.5
	Δ(m)	0.240	0.262	0.193	0.193	0.188
fck =30	V _B (kN)	1070.1	1082.3	1033.9	1033.9	1034.0
	Δ(m)	0.235	0.246	0.194	0.194	0.185

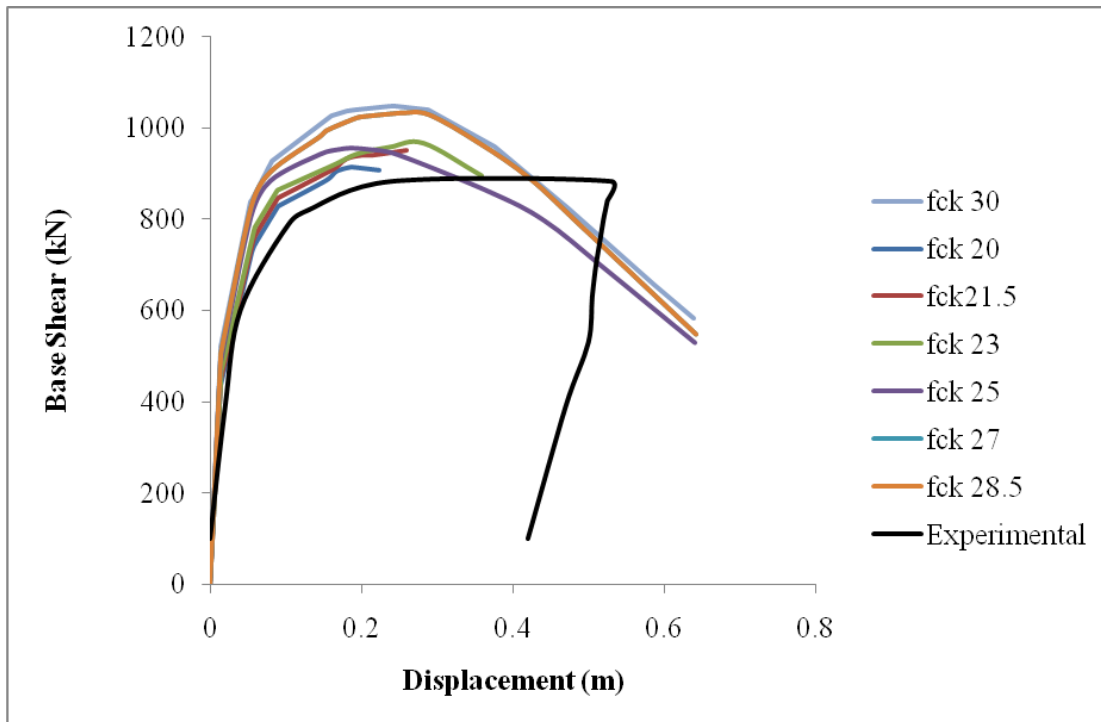


Fig.5.13: Comparison of analytical pushover curves with experimental pushover curve

From the above Table 5.8, it is very clear that base shear increases with increase in compressive strength of concrete. The base shear remains same for the increase in tensile strength of steel. It can be seen that the maximum base shear obtained from SAP2000 is almost comparable to that of experimental result as shown in Fig 5.13. The base shear obtained from experiment was found to be nearly 882kN. Whereas, it is ranged from 915.6 kN for $f_{ck} = 20$ MPa to 1070.1 kN for $f_{ck} = 30$ MPa and $f_y = 520$ MPa. The values remain same for variations in material strength especially for $f_y = 560, 580$ and 600 MPa. Such variations in base shear with respect to X direction can be attributed to the orientation of column, unsymmetrical cross section at each floor level.

5.5.2.2 User Defined Response Spectra

Here, 20 different ground motions are taken to study the response of the building. In order to match the Indian code design spectrum; these records were scaled as a set. Mean spectra has been established from a set of 20 Indian ground motions as shown

in Figure 5.14. Code proposed spectra along with mean spectra of selected ground motions as shown in Figure 5.15.

As seismic design continues to move toward the adoption of performance-based concepts, the need to predict the response of structure to earthquake shaking requires POA. Because nonlinear static analyses operate in the time domain, they require ground motions as inputs. As a result, procedures for the identification and selection of appropriate ground motions are required. An attempt has been made for the selection of ground motions and modification, and development of mean response spectra as a user defined property in SAP2000.

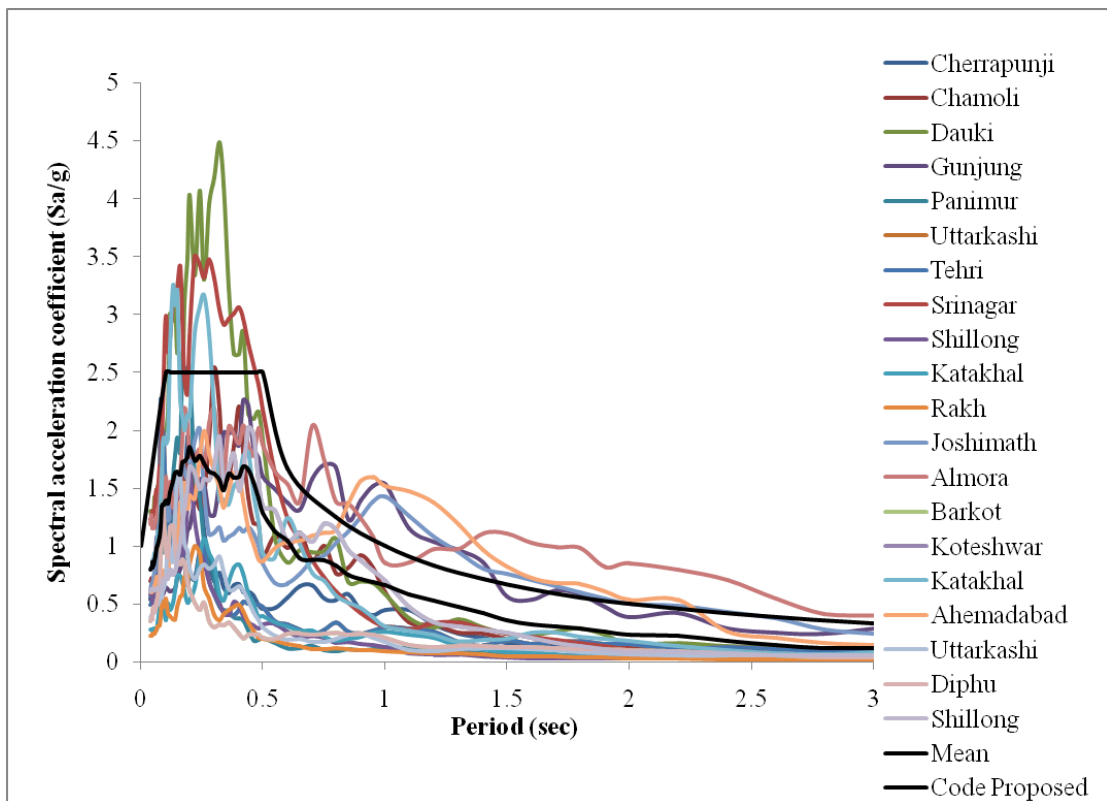


Figure 5.14 Response spectra for selected ground motions

Base shear (kN) versus displacement (m) for different values of f_{ck} (MPa) and f_y (MPa) are tabulated in Table 5.8. Figure 5.16 shows the analytical pushover plots along with that of experimental pushover curve.

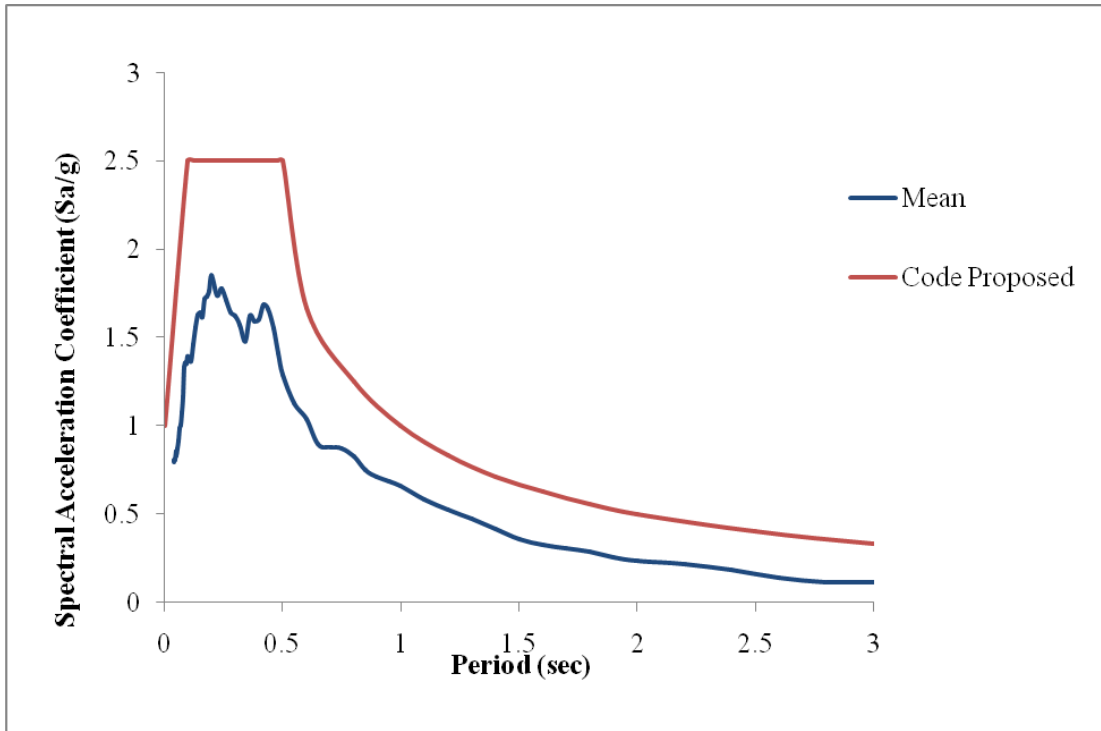


Figure 5.15 Code proposed spectra along with mean spectra of selected ground motions

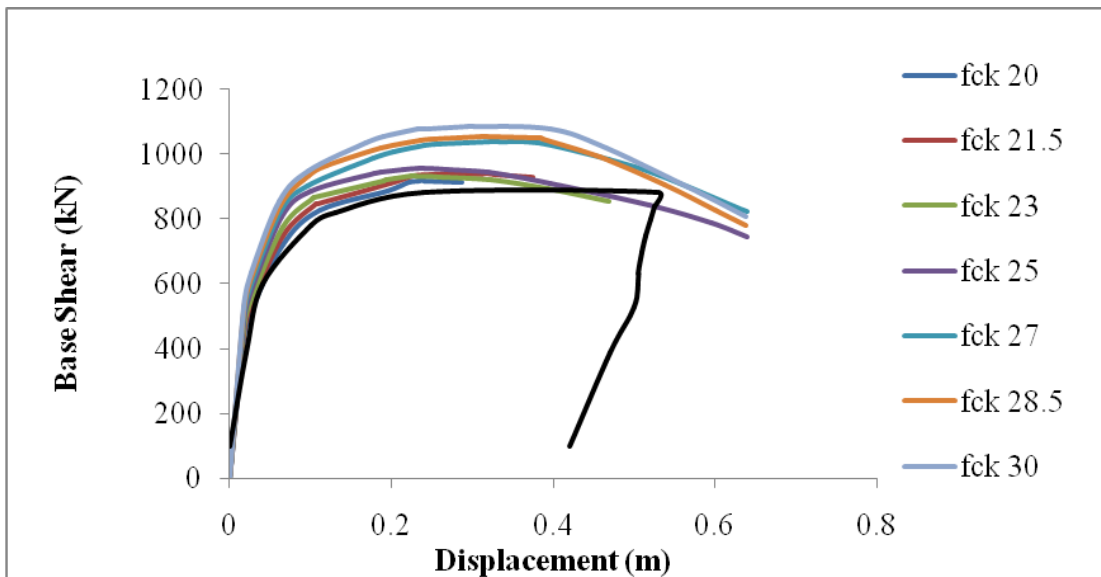


Fig.5.16: Analytical pushover curves with experimental pushover curve

From the below Table 5.8 it can be observed that, the base shear increases with the increase in the value of compressive strength of concrete. The value of base shear also increases with the increase in the tensile strength of the steel up to a certain extent, later it becomes constant as seen in the below Table 5.9.

Table 5.9: Base shear (kN) versus displacement (m) for different values of fck(MPa) and fy (MPa) in X direction

Compressive Strength of Concrete in MPa	Base Shear	Tensile strength of steel in MPa				
	Displacement	fy=520	fy=540	fy=560	fy=580	fy=600
fck =20	V _B (kN)	912.2	953.5	994.8	994.8	994.8
	Δ(m)	0.287	0.249	0.338	0.338	0.338
fck =21.5	V _B (kN)	938.9	949.0	969.5	969.5	969.5
	Δ(m)	0.311	0.240	0.283	0.283	0.283
fck=23	V _B (kN)	941.6	961.5	960.0	960.0	960.0
	Δ(m)	0.231	0.251	0.246	0.246	0.246
fck =25	V _B (kN)	957.0	970.7	989.0	989.0	989.0
	Δ(m)	0.269	0.232	0.225	0.225	0.225
fck =27	V _B (kN)	1037.9	1017.1	1001.5	1001.5	1001.5
	Δ(m)	0.329	0.264	0.235	0.235	0.235
fck =28.5	V _B (kN)	1055.0	1047.9	1020.6	1020.6	1020.6
	Δ(m)	0.317	0.345	0.241	0.241	0.241
fck =30	V _B (kN)	1085.4	1082.4	1034.5	1034.5	1034.5
	Δ(m)	0.302	0.325	0.236	0.236	0.236

The value of base shear obtained from the analysis using SAP 2000 is almost comparable to the results obtained from experiment as seen in 5.16. The value of base shear obtained from experiment was around 882kN. The analytical results obtained varied from 912kN to 1085kN for user defined spectra for fck=20MPa and

$f_{ck}=30\text{MPa}$, where as $f_y =520\text{MPa}$ kept constant respectively. This slight change in the base shear value occurs due to the column orientations and unsymmetrical sections at different floor levels. From the Table 5.8, it can be observed that displacement value remains same for varying values of tensile strength of steel and the displacement of the building decreases with the increase in the compressive strength of concrete.

5.5.2.3 Comparison of Code Proposed and User Defined Response Spectra

A comparison of pushover curves for the code proposed and user defined property of RC building is as shown in Figure 5.17 to Figure 5.23. The pushover analysis involved the application of monotonically increasing lateral load pattern and monitoring the inelastic behavior within the structure. It can be observed that the pushover curve for the RC building with code proposed response spectra has a capacity approximately equal to that of user defined response spectra for the variation in material strength.

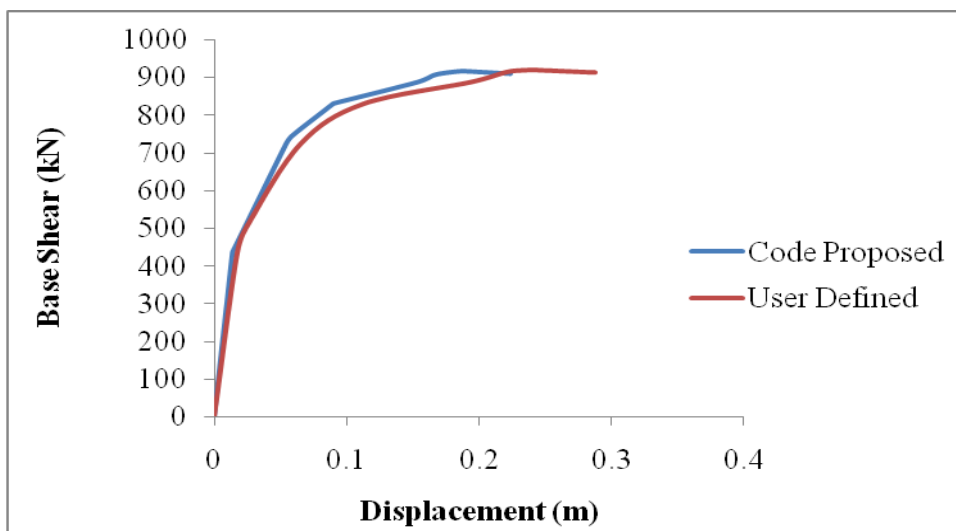


Figure 5.17 Pushover curve for $f_{ck} = 20\text{MPa}$, $f_y = 520\text{MPa}$

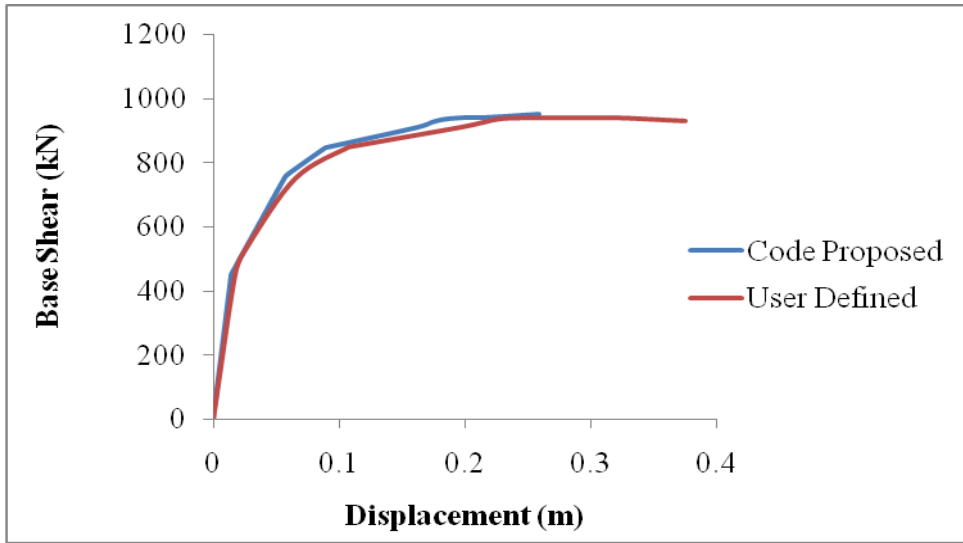


Figure 5.18 Pushover curve for $f_{ck} = 21.5\text{MPa}$, $f_y = 520\text{MPa}$

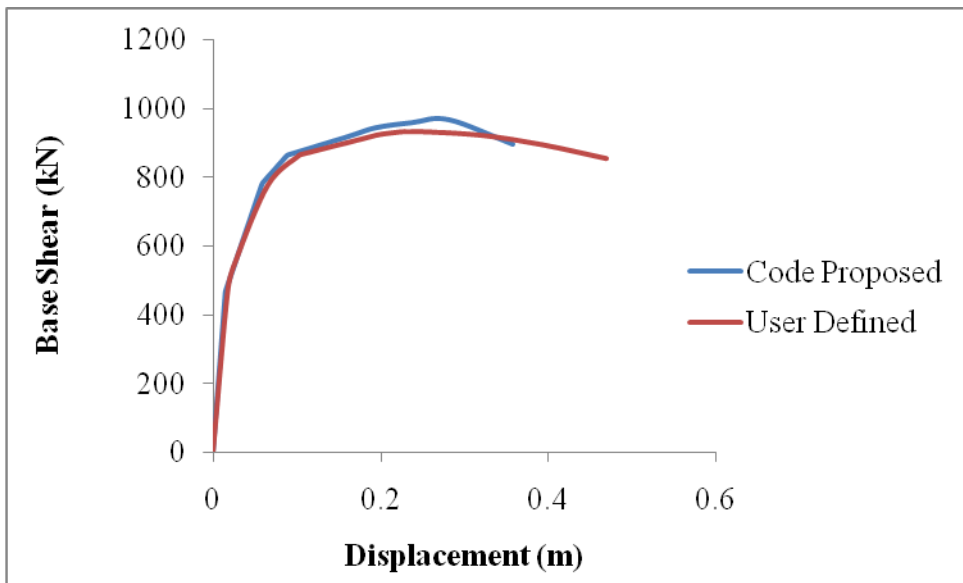


Figure 5.19 Pushover curve for $f_{ck} = 23\text{MPa}$, $f_y = 520\text{MPa}$

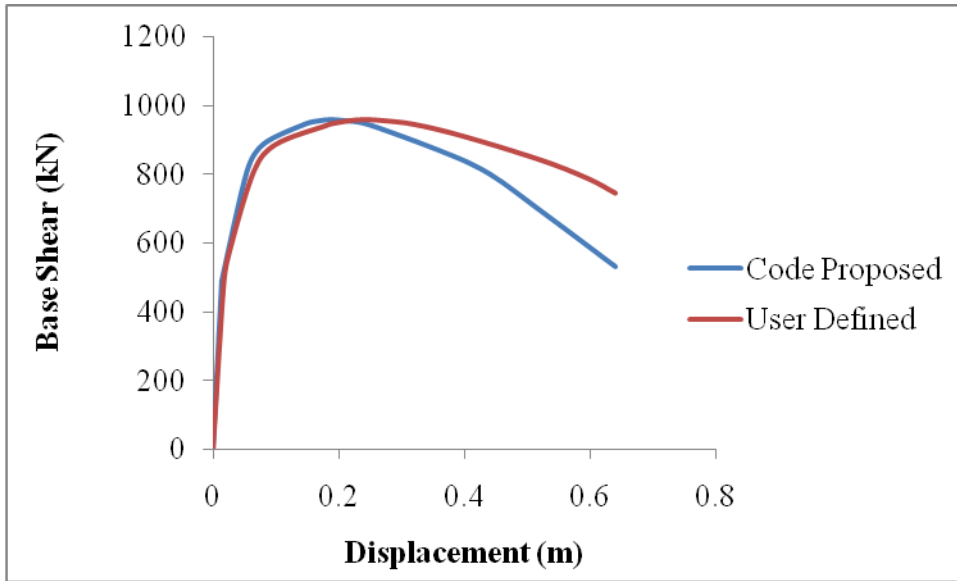


Figure 5.20 Pushover curve for $f_{ck} = 25\text{MPa}$, $f_y = 520\text{MPa}$

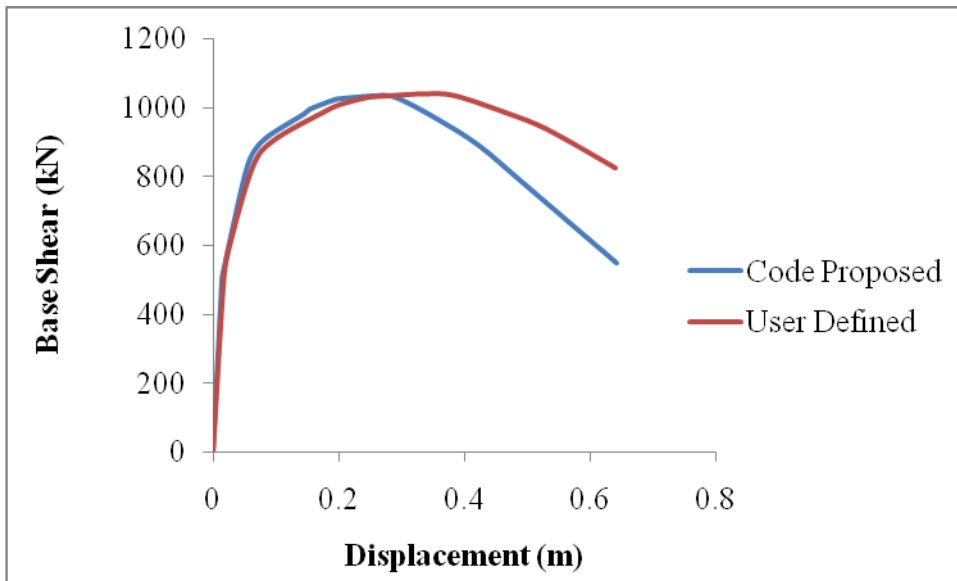


Figure 5.21 Pushover curve for $f_{ck} = 27\text{MPa}$, $f_y = 520\text{MPa}$

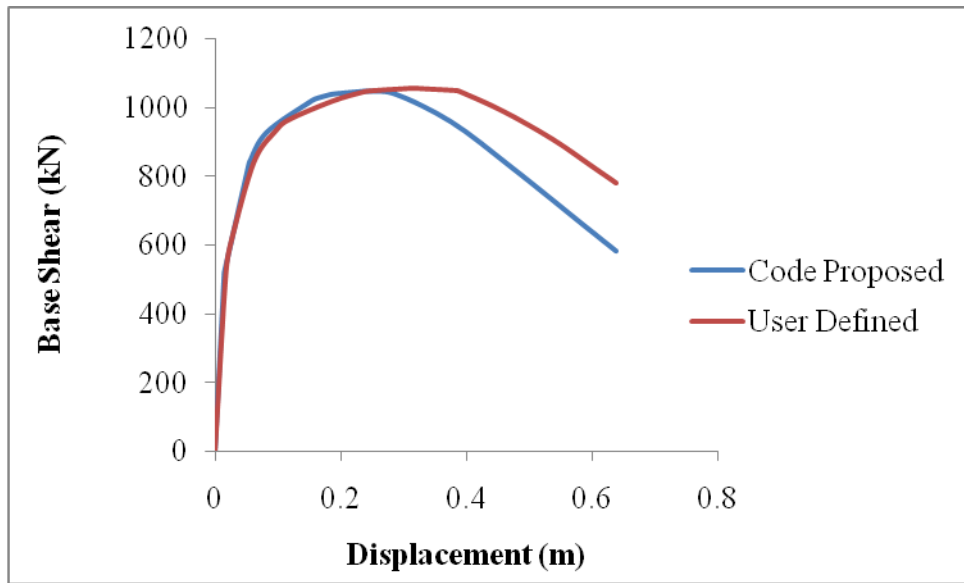


Figure 5.22 Pushover curve for $f_{ck} = 28.5\text{MPa}$, $f_y = 520\text{MPa}$

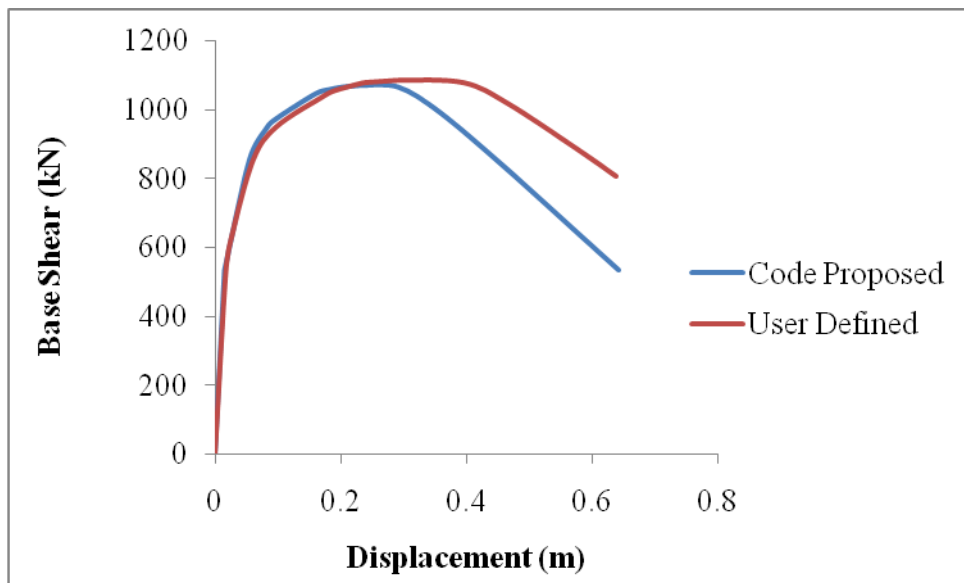


Figure 5.23 Pushover curve for $f_{ck} = 30\text{MPa}$, $f_y = 520\text{MPa}$

5.5.3 Performance Point Results

The seismic performance of building is usually assessed utilizing capacity spectrum method. The performance point which represents the rate of maximum inelastic capacity of the structure is found through the intersection of the capacity spectrum and demand spectrum for a given damping ratio. SAP 2000 calculates the performance point of the structure using this capacity spectrum method. The results

are in terms of base shear and roof displacement obtained from FEMA 356 and spectral displacement and spectral acceleration obtained from ATC 40. These obtained results can be later utilized for accessing the damage evaluation of the structure.

5.5.3. 1 Code proposed response spectra

Table 5.10: Performance point evaluation for varying values of f_{ck} (MPa) and f_y (MPa)

Compressive Strength of Concrete in MPa	Performance Details	Tensile Strength of Steel in MPa				
		$f_y=520$	$f_y=540$	$f_y=560$	$f_y=580$	$f_y=600$
$f_{ck}=20$	V_B (kN)	730.62	730.63	728.41	728.41	728.41
	Δ (m)	0.056	0.056	0.056	0.056	0.056
	Sa	0.343	0.343	0.341	0.341	0.341
	Sd	0.051	0.051	0.051	0.051	0.051
$f_{ck}=21.5$	V_B (kN)	746.42	746.42	746.42	746.42	746.42
	Δ (m)	0.056	0.056	0.056	0.056	0.056
	Sa	0.350	0.350	0.350	0.350	0.350
	Sd	0.051	0.051	0.051	0.051	0.051
$f_{ck}=23$	V_B (kN)	758.70	758.70	758.70	758.70	758.70
	Δ (m)	0.056	0.056	0.056	0.056	0.056
	Sa	0.355	0.355	0.355	0.355	0.355
	Sd	0.051	0.051	0.051	0.051	0.051
$f_{ck}=25$	V_B (kN)	795.09	795.46	795.463	795.46	795.46
	Δ (m)	0.053	0.053	0.053	0.053	0.053
	Sa	0.372	0.373	0.373	0.373	0.373
	Sd	0.048	0.048	0.048	0.048	0.048
$f_{ck}=27$	V_B (kN)	808.27	817.88	818.11	818.11	818.11
	Δ (m)	0.052	0.052	0.052	0.052	0.052
	Sa	0.378	0.383	0.383	0.383	0.383
	Sd	0.048	0.047	0.047	0.047	0.047
$f_{ck}=28.5$	V_B (kN)	817.82	832.81	828.56	828.56	833.92
	Δ (m)	0.052	0.051	0.051	0.051	0.051

	Sa	0.382	0.390	0.388	0.388	0.391
	Sd	0.047	0.046	0.047	0.047	0.046
f _{ck} =30	V _B (kN)	826.41	847.03	837.64	837.64	842.93
	Δ(m)	0.051	0.050	0.051	0.051	0.050
	Sa	0.386	0.396	0.392	0.392	0.394
	Sd	0.047	0.045	0.047	0.047	0.046

5.5.3. 2 User defined response spectra

Table 5.11: Performance point evaluation for varying values of f_{ck} (MPa) and f_y (MPa)

Compressive Strength of Concrete in MPa	Performance Details	Tensile Strength of Steel in MPa				
		f _y =520	f _y =540	f _y =560	f _y =580	f _y =600
f _{ck} =20	V _B (kN)	725.78	725.83	725.87	725.87	725.87
	Δ(m)	0.066	0.066	0.066	0.066	0.066
	Sa	0.340	0.340	0.340	0.340	0.340
	Sd	0.050	0.050	0.050	0.050	0.050
f _{ck} =21.5	V _B (kN)	747.45	747.45	747.45	747.45	747.45
	Δ(m)	0.065	0.065	0.065	0.065	0.065
	Sa	0.350	0.350	0.350	0.350	0.350
	Sd	0.049	0.049	0.049	0.049	0.049
f _{ck} =23	V _B (kN)	765.02	765.02	765.02	765.02	765.02
	Δ(m)	0.063	0.063	0.063	0.063	0.063
	Sa	0.358	0.358	0.358	0.358	0.358
	Sd	0.048	0.048	0.048	0.048	0.048
f _{ck} =25	V _B (kN)	787.40	787.51	787.51	787.51	787.51
	Δ(m)	0.062	0.062	0.062	0.062	0.062
	Sa	0.368	0.368	0.368	0.368	0.368
	Sd	0.047	0.047	0.047	0.047	0.047
f _{ck} =27	V _B (kN)	808.29	808.97	809.04	809.04	809.04
	Δ(m)	0.060	0.060	0.060	0.060	0.060
	Sa	0.378	0.378	0.378	0.378	0.378
	Sd	0.046	0.046	0.046	0.046	0.046

$f_{ck}=28.5$	$V_B(kN)$	821.95	824.13	824.46	824.46	824.46
	$\Delta(m)$	0.059	0.059	0.059	0.059	0.059
	Sa	0.384	0.385	0.385	0.385	0.385
	Sd	0.045	0.045	0.045	0.045	0.045
$f_{ck}=30$	$V_B(kN)$	836.48	838.75	839.06	839.06	839.06
	$\Delta(m)$	0.058	0.058	0.058	0.058	0.058
	Sa	0.391	0.392	0.392	0.392	0.392
	Sd	0.044	0.044	0.044	0.044	0.044

It can be observed from the above tables 5.10 and 5.11 that the value of base shear increases with the increase in the compressive strength of concrete for both the properties. However, the value of base shear does not show any variation with the change in tensile strength of the steel. Therefore, it can be concluded that the values of base shear and roof displacement are independent of tensile strength of steel during performance point evaluation. Roof displacement decreases with the increase in the base shear which can be observed from the above tables.

The values of spectral displacement and spectral acceleration increases along with the increase in the compressive strength of concrete. For code specified spectra and user defined spectra performance appears to be very close. This is due to the close similarity between the load patterns.

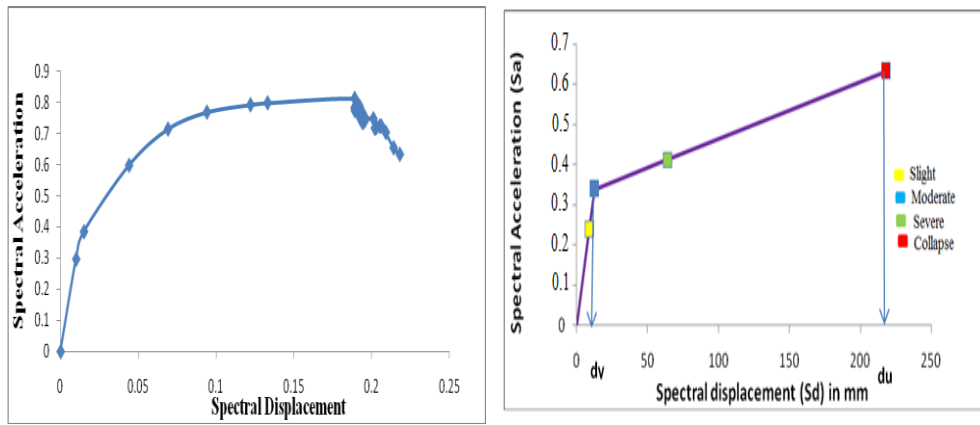
5.6 FRAGILITY CURVES OF INVESTIGATED RC BUILDINGS

5.6.1 Fragility Curves in terms of Spectral Displacement: Unconfined Concrete Section

Since the capacity determined from the pushover analysis is for a multi-degree-of – freedom system, in order to compare with the demand curves, capacity curves is converted to A-D (Acceleration-Deformation) format for an equivalent single-degree-of-freedom system. The capacity curve thus obtained is superimposed with the demand curve in order to obtain performance point. The capacity curves do not intersect the demand curves, implying that the building will be damaged due to worst earthquake scenario. The seven cases of cube strength are in the range of 20-30 MPa.

Figure illustrates the resulting fragility curves in case of the evaluation on pushover curves obtained by applying a pseudo-triangular distribution in X-direction. Capacity spectrum method is a method used to determine the performance point in Acceleration-Displacement Response Spectra (ADRS) format. In this method both the capacity curve and the demand curve should be represented in response spectral ordinates. As the displacement of the structure increase, the period of the structure lengthens. This is reflected directly in the capacity curve. The Capacity Spectrum Method reduces the demand to find an intersection with the capacity, where the displacement is consistent with the implied damping. The Figures 5.24 (a) shows the capacity curve for variation in material strength values say $f_{ck}=20$ Mpa and $f_y = 520$ Mpa. The Figure 5.24 (b) shows bilinear representation of capacity curve for say $f_{ck}=20$ N/mm² and $f_y = 520$ Mpa.

The damage state index is calculated from the bilinear capacity curve. Table 5.12 below shows a sample of summary of the used parameters for the damage state thresholds as functions of the yielding displacement, d_y , and the ultimate displacement, d_u , of the structure for the values of compressive strength of concrete = 20 N/mm² and tensile strength of steel= 520 N/mm² in X directional loading. Similarly damage state index can be computed for varying values of f_{ck} and f_y . It is also observed that by varying both compressive strength of concrete and tensile strength of steel the values remained unchanged in X direction.



a) Capacity spectrum curve

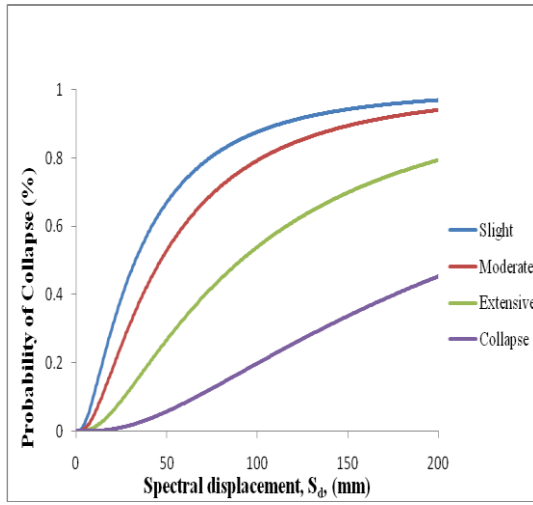
b) Bilinear capacity curve

Figure 5.24 Capacity curve and bilinear representation of capacity curve for $f_{ck} = 20$ MPa and tensile strength = 520 MPa

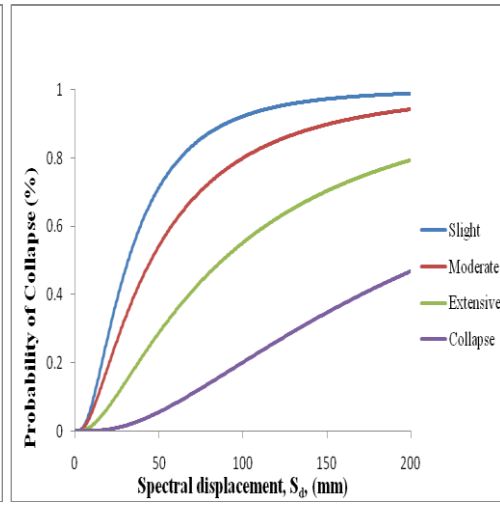
Table 5.12: Damage state thresholds in X direction

Damage State	Median value of threshold spectral displacement S_{rds} in 'mm'	
Slight	$0.7d_y$	8.6
Moderate	d_y	12.5
Severe	$d_y + 0.25(d_u - d_y)$	63.9
Collapse	d_u	218

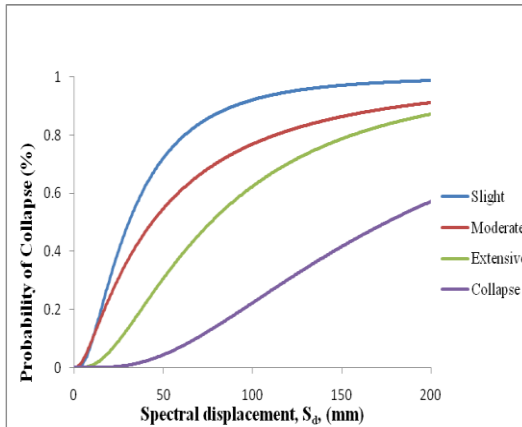
Graphical representation of the damage thresholds in the bilinear capacity spectrum for compressive strength of concrete =20 MPa and tensile strength of steel =520 MPa is as shown in the Figure 5.24 (b). Figures 5.25 (a) to 5.25 (g) represents fragility curves for varying values of compressive strength of concrete and tensile strength of steel =520 MPa.



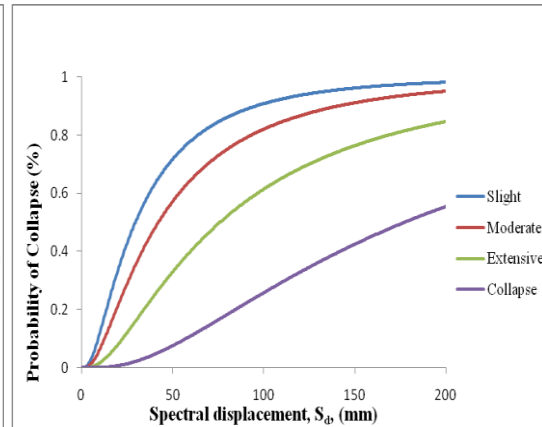
a) $f_{ck} = 20$ MPa



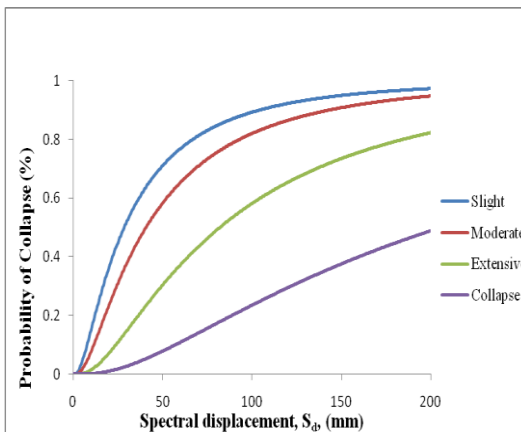
b) $f_{ck} = 21.5$ MPa



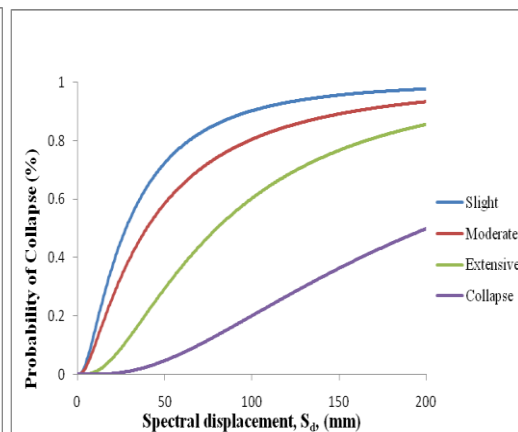
c) $f_{ck} = 23$ MPa



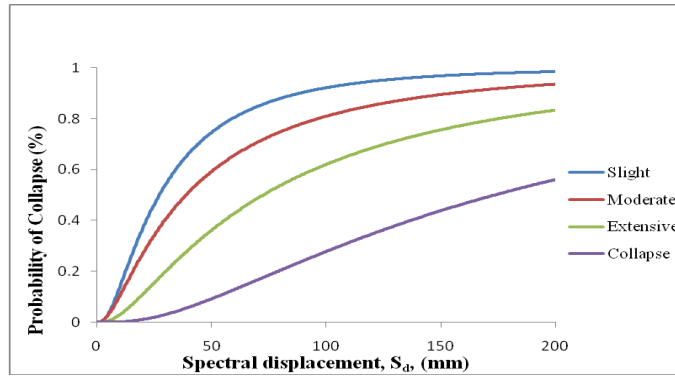
d) $f_{ck} = 25$ MPa



e) $f_{ck} = 27$ MPa



f) $f_{ck} = 28.5$ MPa

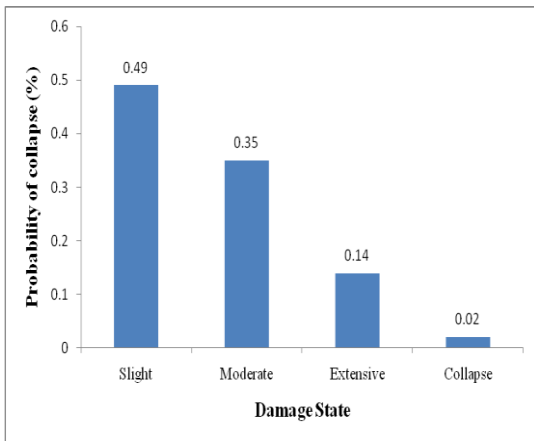


g) fck= 30 MPa

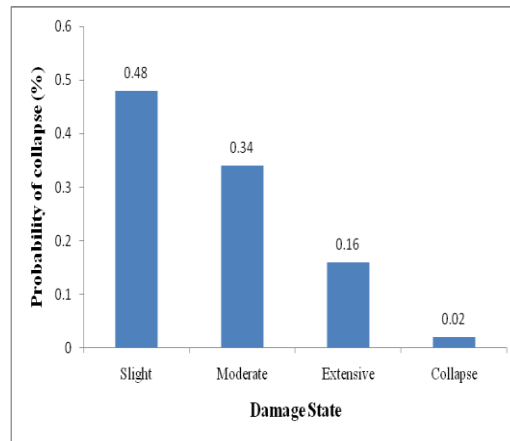
Figure 5.25 Fragility curve for varying values of compressive strength and tensile strength = 520 MPa

5.6.1.1 Damage State Thresholds for Unconfined Concrete Section

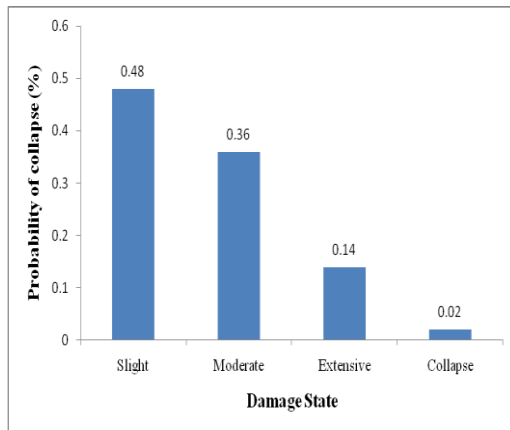
Damage state thresholds for varying values of compressive strength of concrete and tensile strength of steel =520 MPa have been shown in Figures 5.26 (a) to 5.26 (g).



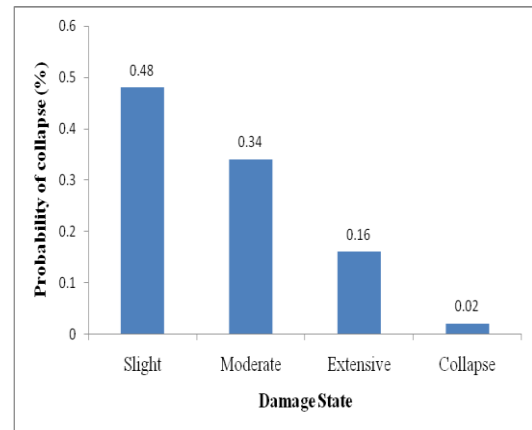
a) fck= 20 MPa



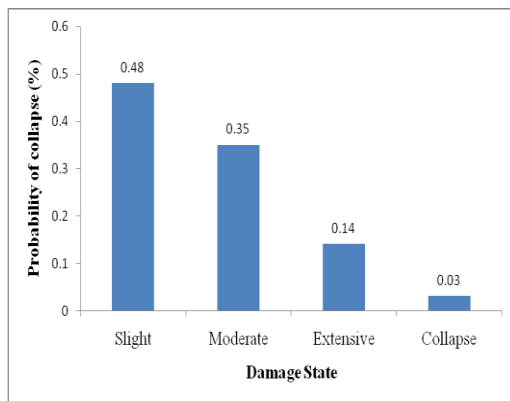
b) fck= 21.5 MPa



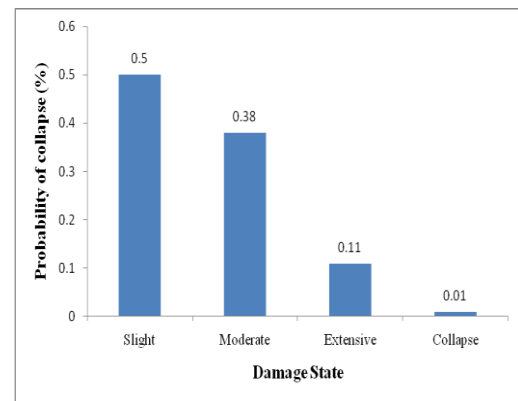
c) $f_{ck} = 23$ MPa



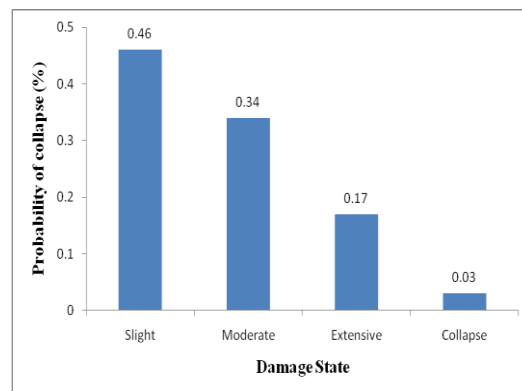
d) $f_{ck} = 25$ MPa



e) $f_{ck} = 27$ MPa



f) $f_{ck} = 28.5$ MPa



g) $f_{ck} = 30$ MPa

Figure 5.26 Damage state thresholds for varying values of f_{ck} and tensile strength of steel = 520 MPa

From the fragility analysis for the considered building, the results showed that, 49 %, 35%, 14% and 2% higher probability of slight, moderate, severe and collapse damage

respectively in RC building having unconfined concrete section, when $f_{ck}=20\text{MPa}$ and $f_y=520\text{MPa}$ as shown in Fig.26(a).

Building will suffer 48 %, 34%, 16% and 2% higher probability of slight, moderate, severe and collapse damage respectively, when $f_{ck}=21.5\text{ MPa}$ and $f_y=520\text{MPa}$ as shown in Fig.26(b).

Also, building showed that 48 %, 36%, 14% and 2% higher probability of slight, moderate, severe and collapse damage respectively, when $f_{ck}=23\text{ MPa}$ and $f_y=520\text{MPa}$ as shown in Fig.26(c).

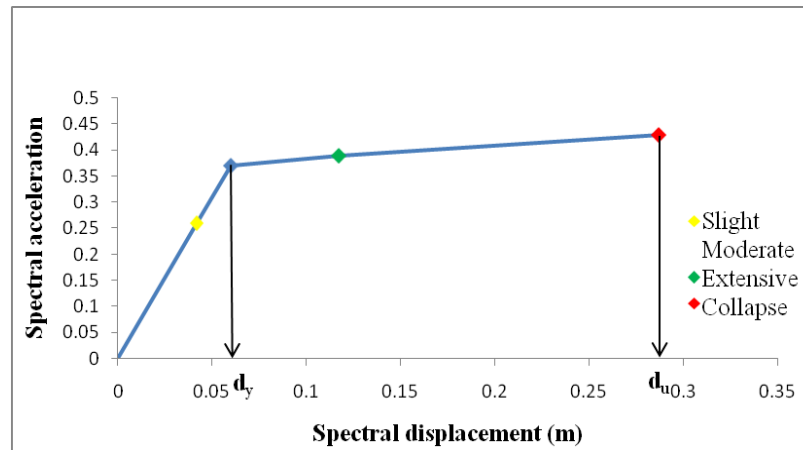
Similarly, Fig.26(d) shows that building will suffer 48 %, 34%, 16% and 2% higher probability of slight, moderate, severe and collapse damage respectively, when $f_{ck}=25\text{ MPa}$ and $f_y=520\text{MPa}$. Fig.26(e) shows that building will suffer 48 %, 35%, 14% and 3% higher probability of slight, moderate, severe and collapse damage respectively, when $f_{ck}=27\text{ MPa}$ and $f_y=520\text{MPa}$. Fig.26(f) shows that building will suffer 50 %, 38%, 11% and 1% higher probability of slight, moderate, severe and collapse damage respectively, when $f_{ck}=28.5\text{ MPa}$ and $f_y=520\text{MPa}$. Lastly, Fig.26(g) showed that building will suffer 46 %, 34%, 17% and 3% higher probability of slight, moderate, severe and collapse damage respectively, when $f_{ck}=30\text{MPa}$ and $f_y=520\text{MPa}$.

5.6.2 Fragility Curves in terms of Spectral Displacement: Confined Concrete Section

5.6.2.1 For Mander's Model

In order to establish the fragility curves of the studied frame, the model is characterized with compressive strength of concrete = 20 MPa and tensile strength of steel = 520 MPa has been taken into consideration. The bilinear representation of capacity curves obtained as a result of pushover analysis corresponding to earthquake is shown below in Figure 5.27 (Mander's model). Below Table 5.13 summarizes the used parameters for the damage state thresholds as functions of the yielding displacement, d_y , and the ultimate displacement, d_u , of the structure. The seismic

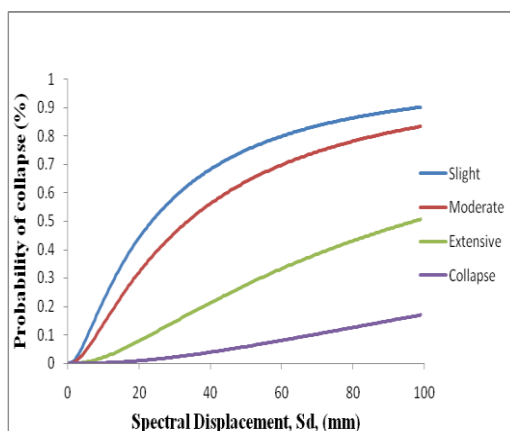
fragility curves in terms of spectral displacement are displayed for all the models in Figure 5.28(a) to Figure 5.28(g).



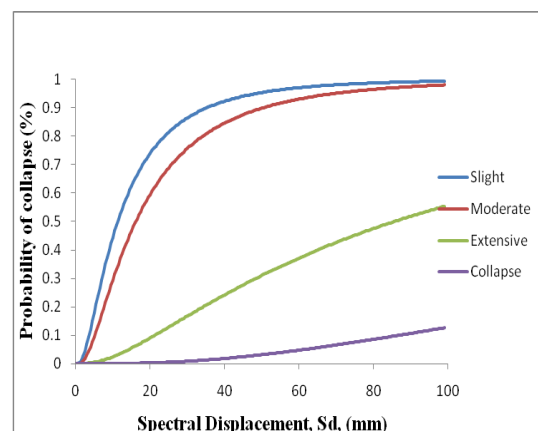
5.27 Bilinear Capacity Curve for Mander Model ($f_{ck} = 20\text{MPa}$; $f_y = 520\text{MPa}$)

Table 5.13: Damage state thresholds in X direction (Mander's Model)

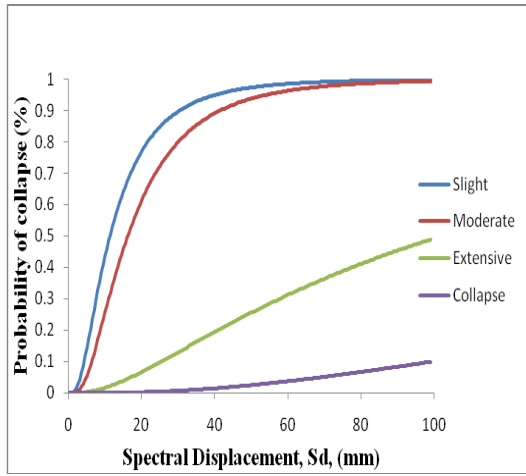
Damage state	Median value of threshold spectral displacement S_{rds} in 'mm'	
Slight	$0.7d_y$	42
Moderate	d_y	60
Extensive	$d_y + 0.25(d_u - d_y)$	117
Collapse	d_u	287



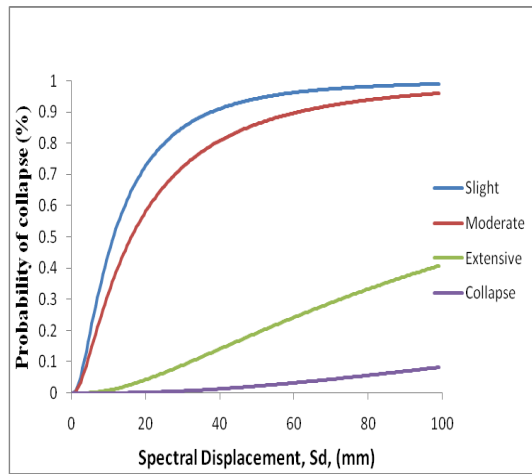
a) $f_{ck} = 20\text{ MPa}$



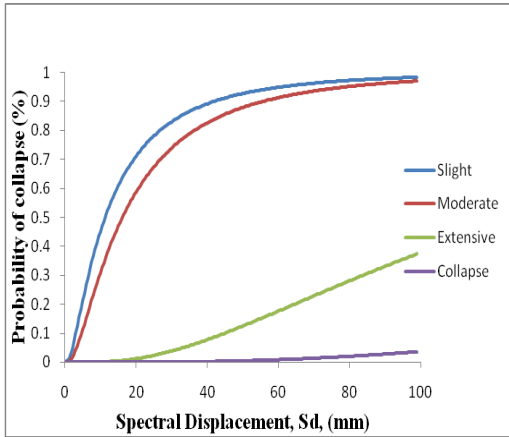
b) $f_{ck} = 21.5\text{ MPa}$



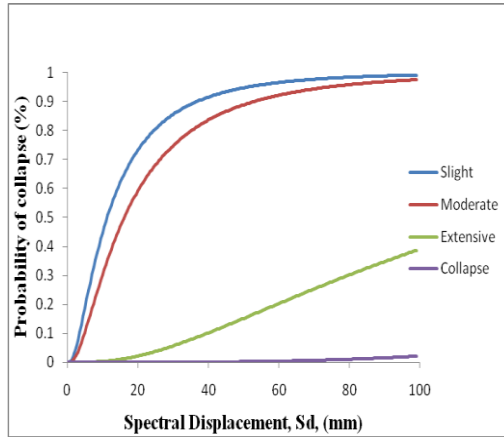
c) $f_{ck} = 23$ MPa



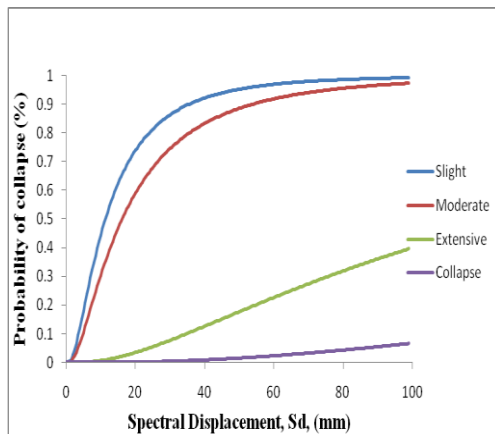
d) $f_{ck} = 25$ MPa



e) $f_{ck} = 27$ MPa



f) $f_{ck} = 28.5$ MPa



g) $f_{ck} = 30$ MPa

Figure 5.28 Fragility curve for varying values of compressive strength and tensile strength = 520 MPa

5.6.2.2 Kent and Park Model

Figure 5.29 represents bilinear curve for Kent and Park model for $f_{ck}= 20 \text{ MPa}$ and $f_y=520 \text{ MPa}$. Below Table 5.14 summarizes the used parameters for the damage state thresholds as functions of the yielding displacement, d_y , and the ultimate displacement, d_u , of the structure for Kent and Park model. The fragility curves in X-directional loading for all the models are as shown in Figure 5.30(a) to Figure 5.30(g).

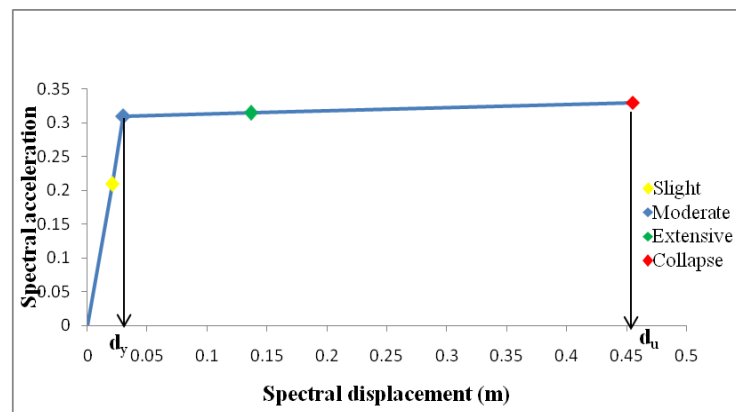
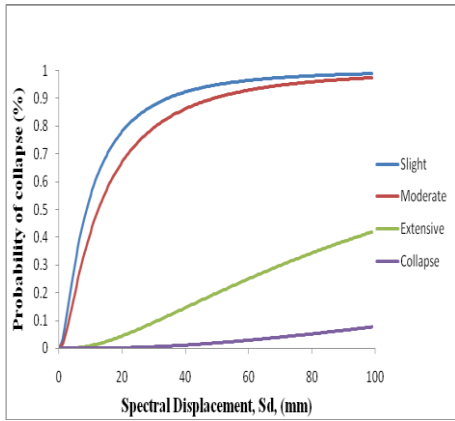


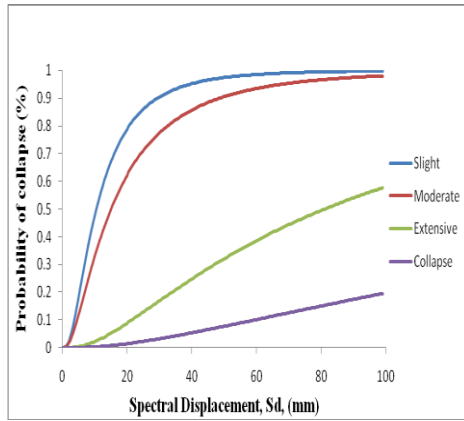
Figure 5.29: Bilinear Capacity Curve for Kent and Park Model ($f_{ck} = 20 \text{ MPa}$; $f_y = 520 \text{ MPa}$)

Table 5.14: Damage state thresholds in X direction (Kent and Park Model)

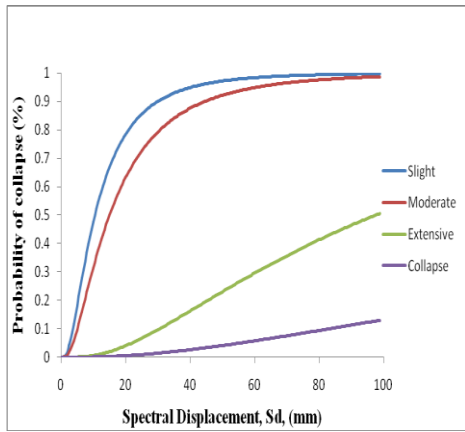
Damage state	Median value of threshold spectral displacement S_{rds} in 'mm'	
Slight	$0.7d_y$	21
Moderate	d_y	30
Extensive	$d_y + 0.25(d_u - d_y)$	137
Collapse	d_u	455



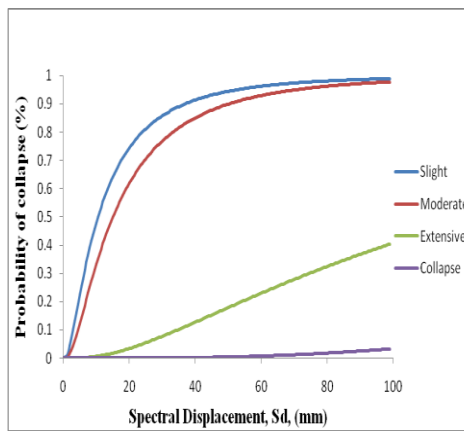
a) fck= 20 MPa



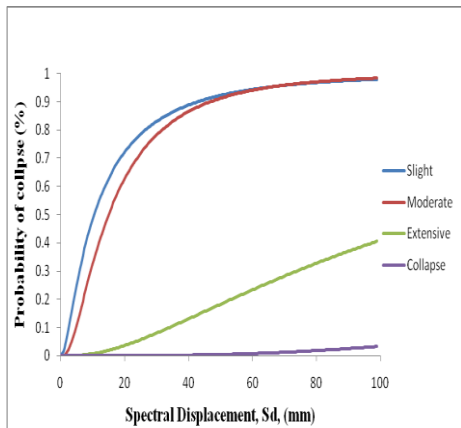
b) fck= 21.5 MPa



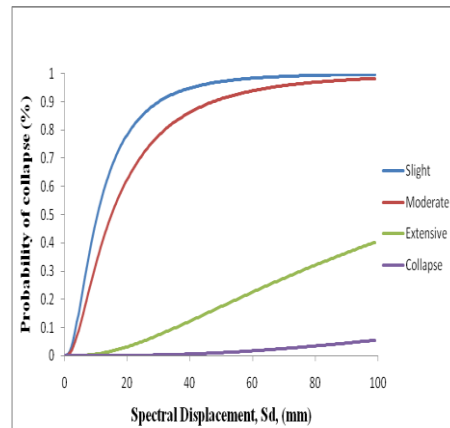
c) fck= 23 MPa



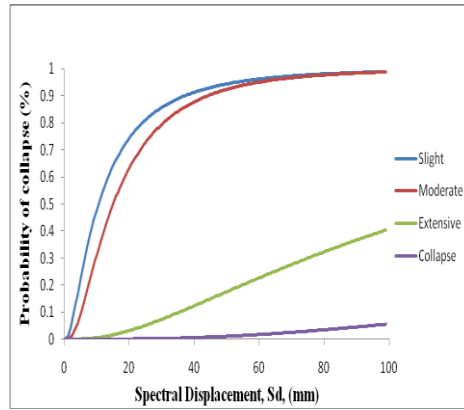
d) fck= 25 MPa



e) fck= 27 MPa



f) fck= 28.5 MPa

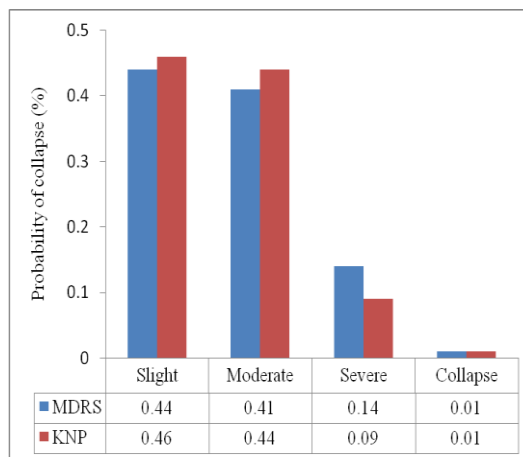


g) $f_{ck}= 30 \text{ MPa}$

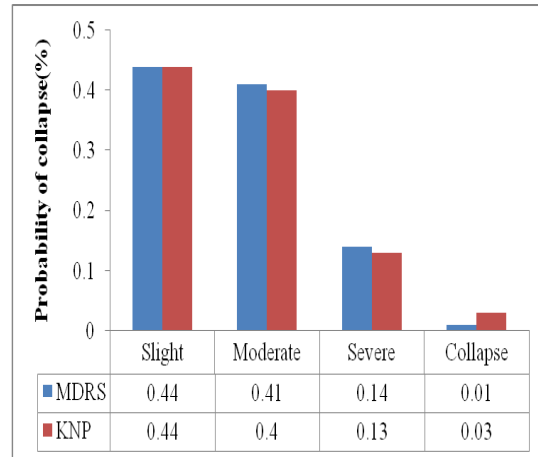
Figure 5.30: Fragility curve for varying values of compressive strength and tensile strength = 520 MPa

5.6.2.3 Comparison of Damage State Thresholds for Confined Concrete Section

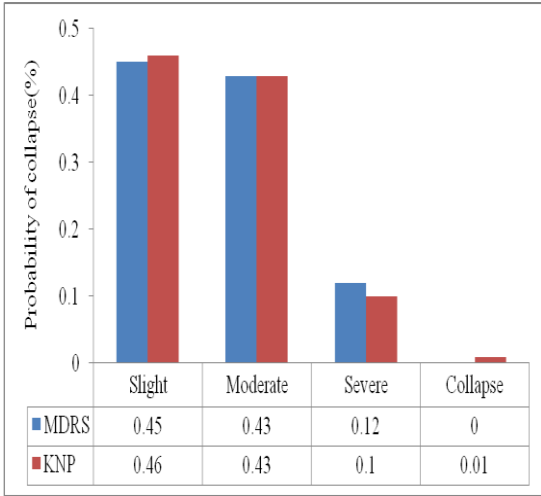
The comparisons of damage state thresholds by both the approaches are shown in Figure 5.31 (a) to Figure 5.31 (g).



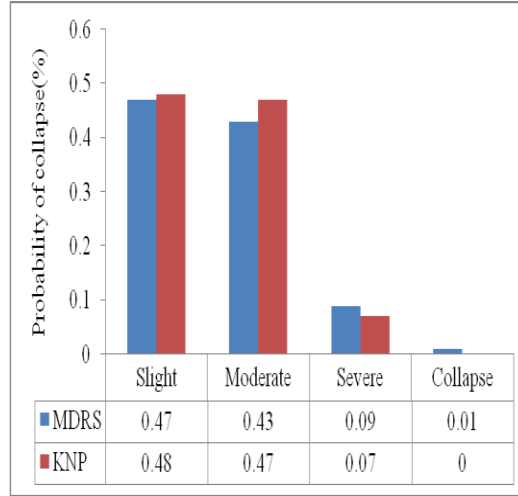
a) $f_{ck}=20\text{MPa}$; $f_y=520\text{MPa}$



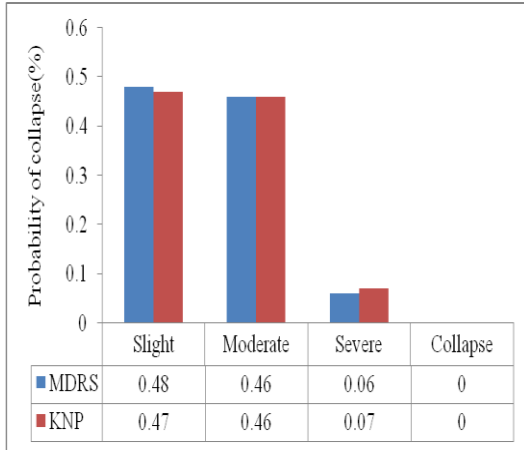
b) $f_{ck}=21.5\text{MPa}$; $f_y=520\text{MPa}$



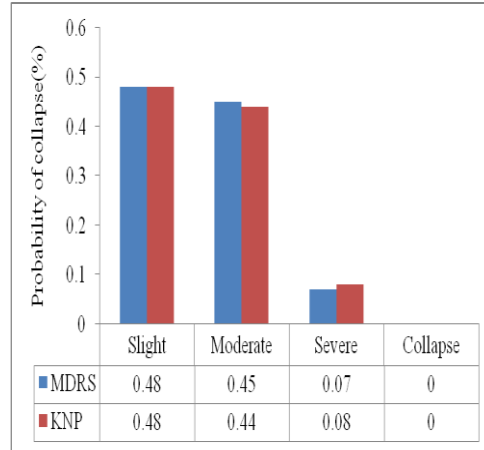
c) $f_{ck}=23\text{MPa}$; $f_y=520\text{MPa}$



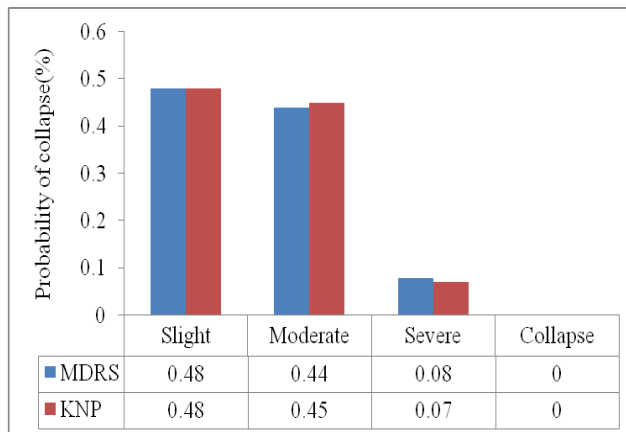
d) $f_{ck}=25\text{MPa}$; $f_y=520\text{MPa}$



e) $f_{ck}=27\text{MPa}$; $f_y=520\text{MPa}$



f) $f_{ck}=28.5\text{MPa}$; $f_y=520\text{MPa}$



g) $f_{ck}=30\text{MPa}$; $f_y=520\text{MPa}$

Figure 5.31: Damage state thresholds by both the models

From the fragility analysis for the considered building, the results showed that, 44 %, 41%, 14% and 1% higher probability of slight, moderate, severe and collapse damage in building for Mandar's model. Whereas building will suffer 46 %, 44%, 9% and 1% higher probability of slight, moderate, severe and collapse damage in building for Kent and Park model, when $f_{ck}=20\text{MPa}$ and $f_y=520\text{MPa}$ as shown in Fig.5.31 (a).

Also, the fragility analysis results showed that, 44 %, 41%, 14% and 1% higher probability of slight, moderate, severe and collapse damage in building for Mandar's model. Whereas building will suffer 44 %, 40%, 13% and 3% higher probability of slight, moderate, severe and collapse damage in building for Kent and Park model, when $f_{ck}=21.5\text{MPa}$ and $f_y=520\text{MPa}$ as shown in 5.31 (b).

The fragility analysis for the considered building, the results showed that, the building will suffer 45 %, 43%, 12% and 0% higher probability of slight, moderate, severe and no collapse damage in building for Mandar's model. Whereas building will suffer 46 %, 43%, 10% and 1% higher probability of slight, moderate, severe and collapse damages in building for Kent and Park model, when $f_{ck}=23\text{MPa}$ and $f_y=520\text{MPa}$ as shown in 5.31 (c).

The results showed that, 47 %, 43%, 9% and 1% higher probability of slight, moderate, severe and collapse damage in building for Mandar's model. Whereas building will suffer 48 %, 47%, 7% and 0% higher probability of slight, moderate, severe and no collapse damage in building for Kent and Park model, when $f_{ck}=25\text{MPa}$ and $f_y=520\text{MPa}$ as shown in 5.31 (d).

Fragility analysis results showed that, 48%, 46%, 6% and 0% higher probability of slight, moderate, severe and no collapse damage in building for Mandar's model. Whereas building will suffer 47 %, 46%, 7% and 0% higher probability of slight, moderate, severe and no collapse damage in building for Kent and Park model, when $f_{ck}=27\text{MPa}$ and $f_y=520\text{MPa}$ as shown in 5.31 (e).

Fragility analysis results showed that, 48 %, 45%, 7% and 0% higher probability of slight, moderate, severe and no collapse damage in building for Mandar's model. Whereas building will suffer 48 %, 44%, 8% and 0% higher probability of slight,

moderate, severe and no collapse damage in building for Kent and Park model, when $f_{ck}=28.5\text{MPa}$ and $f_y=520\text{MPa}$ as shown in 5.31 (f).

Lastly, the results showed that, 48 %, 44%, 8% and 0% higher probability of slight, moderate, severe and no collapse damage in building for code proposed response spectra. Whereas building will suffer 48 %, 45%, 7% and 0% higher probability of slight, moderate, severe and no collapse damage in building for Kent and Park model, when $f_{ck}=30\text{MPa}$ and $f_y=520\text{MPa}$ as shown in 5.31 (g).

5.6.3 Fragility Curves in terms of Spectral Displacement: Code Proposed and User Defined Response Spectra

The fragility curve defines the state of damage. For each damage state the corresponding fragility curve is obtained by plotting probabilities of collapse in ordinate and spectral displacement in abscissa. The capacity curve for $f_{ck}=20\text{MPa}$ and $f_y=520\text{MPa}$ is shown in Figure 5.30 for code proposed response spectra. Figure 5.33 represents bilinear curve for code proposed response spectra. The damage state index is tabulated in Table 5.15. The capacity curve for $f_{ck}=20\text{MPa}$ and $f_y=520\text{MPa}$ is shown in Figure 5.34 for user defined response spectra. Fig.5.35 shows Bilinear capacity curve for $f_{ck}=20\text{MPa}$ and $f_y=520\text{MPa}$ for user defined property. The damage state index is tabulated in Table 5.16.

Specific seismic fragility curves have been developed for RC building according to the seismic code proposed spectra and user defined response spectra (taking into account of Indian ground motion). Figure 5.36(a) to Figure 5.36(g) and Figure 5.37(a) to Figure 5.37(g) shows these seismic fragility curves for the code specified and user defined response spectra. It is apparent that the non-seismically designed RC building show high expected slight and moderate damage for the code proposed than user defined response spectra and are the most vulnerable in case of future earthquakes. It is clearly seen in the Figures that, in general, the building with code specified spectra for variation in material strength are more vulnerable than building with user defined response spectra for variation in material strength.

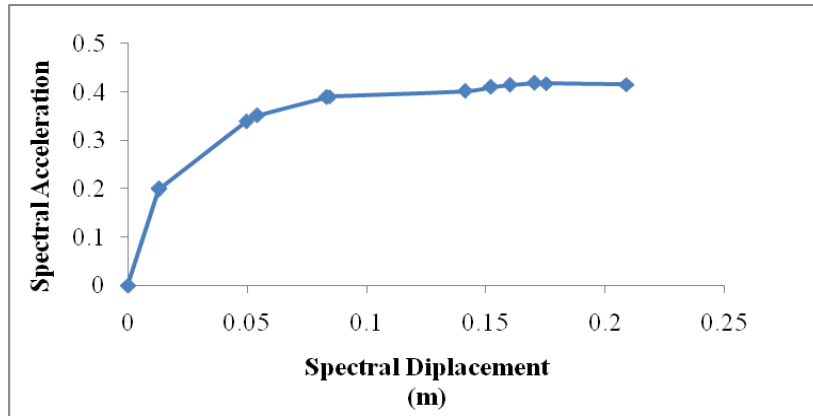


Fig.5.32 Capacity curve for $f_{ck}=20\text{MPa}$ and $f_y=520\text{MPa}$ for code proposed response spectra

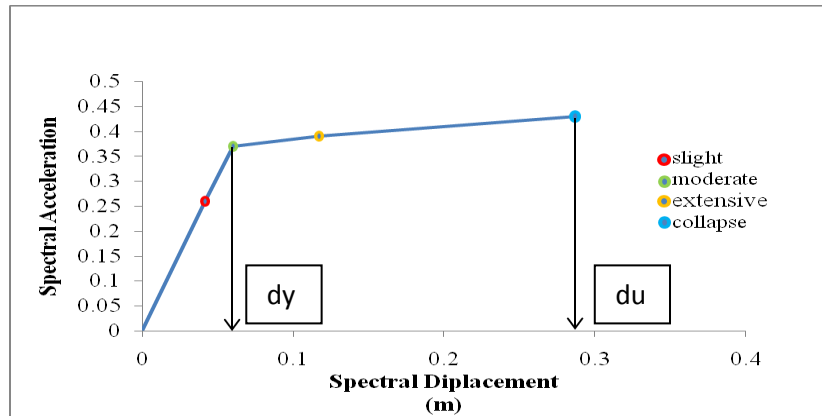


Fig.5.33 Bilinear capacity spectrum for $f_{ck}=20\text{MPa}$ and $f_y=520\text{MPa}$ for code proposed response spectra

Table 5.15: Damage state thresholds in X direction

Damage state	Median value of threshold spectral displacement S_{rds} in 'mm'	
Slight	$0.7dy$	36.33
Moderate	dy	51.9
Severe	$dy + 0.25(dy-du)$	91.13
Collapse	du	208.85

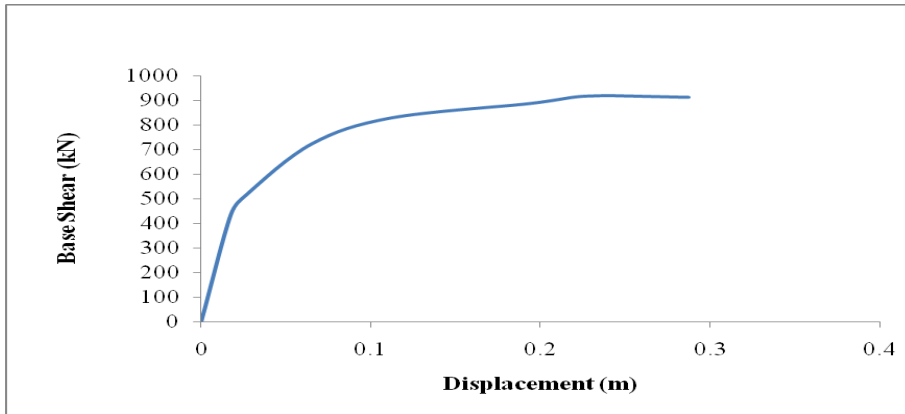


Fig.5.34: Pushover curve for $f_{ck} = 20\text{MPa}$, $f_y = 520\text{MPa}$ for user defined response spectra

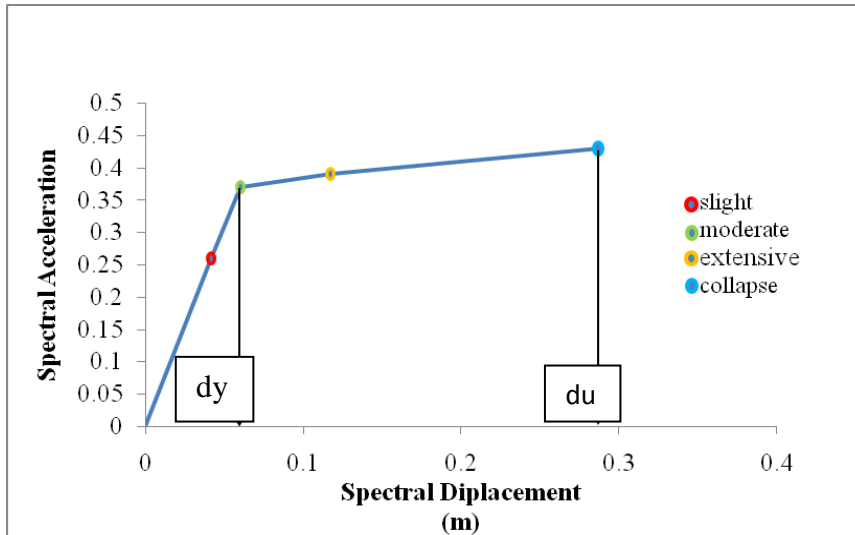
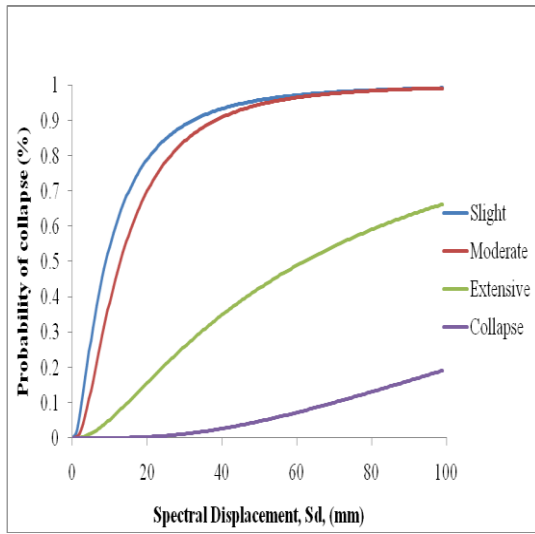


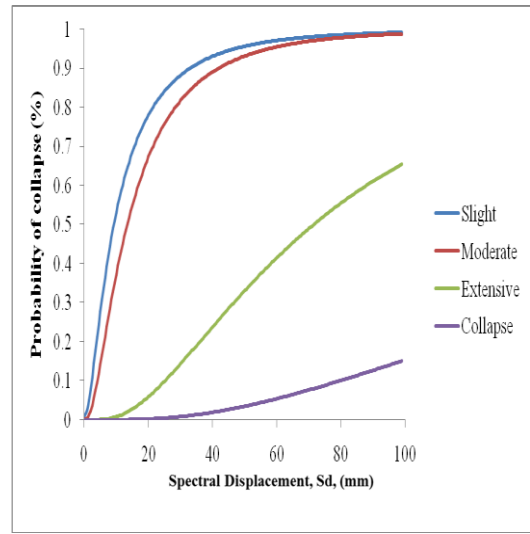
Fig.5.35 Bilinear capacity spectrum for $f_{ck}=20\text{MPa}$ and $f_y=520\text{MPa}$ for user defined response spectra

Table 5.16: Damage state thresholds in X direction

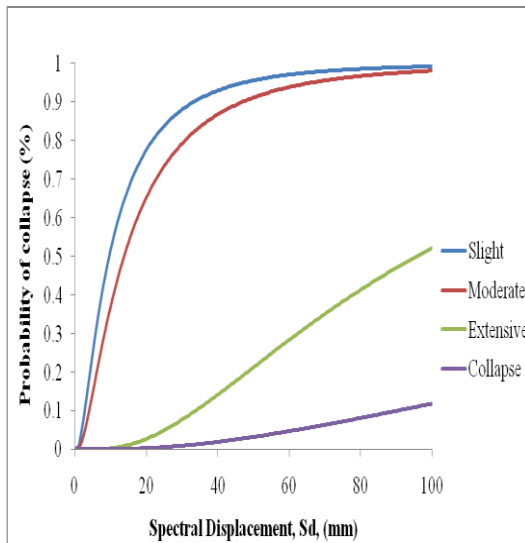
Damage state	Median value of threshold spectral displacement S_{rds} in 'mm'	
Slight	$0.7d_y$	39.9
Moderate	d_y	57.0
Severe	$d_y + 0.25(d_u - d_y)$	96.25
Collapse	d_u	214.0



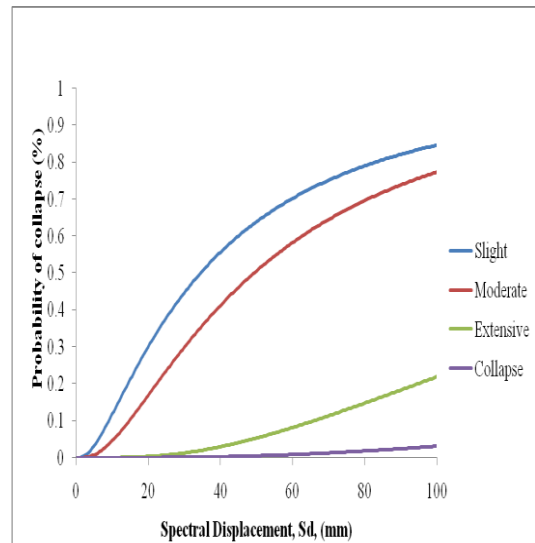
a) fck=20MPa and fy=520MPa



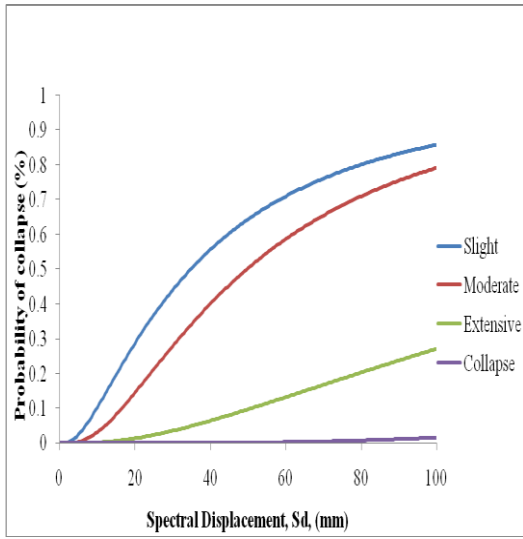
b) fck=21.5MPa and fy=520MPa



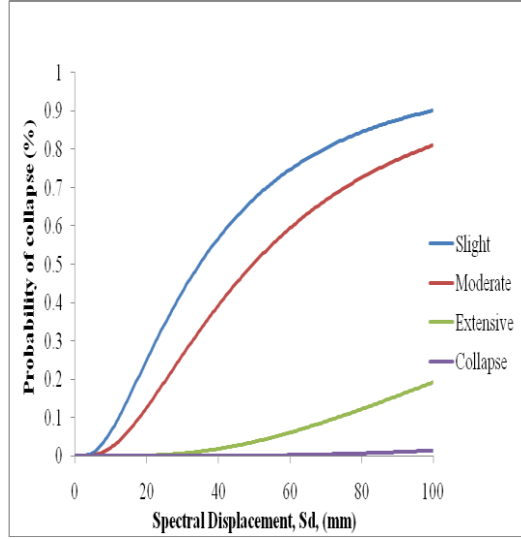
c) fck=23MPa and fy=520MPa



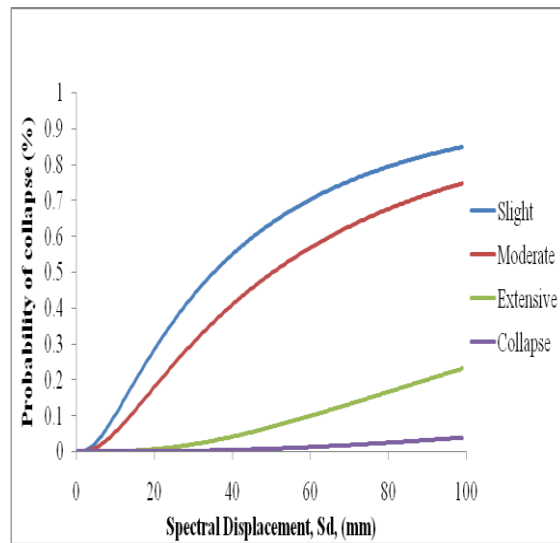
d) fck=25 MPa and fy=520MPa



e) $f_{ck}=27$ MPa and $f_y=520$ MPa

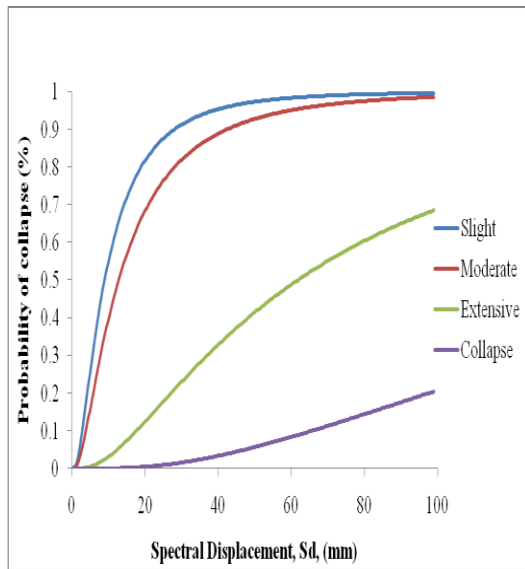


f) $f_{ck}=28.5$ MPa and $f_y=520$ MPa

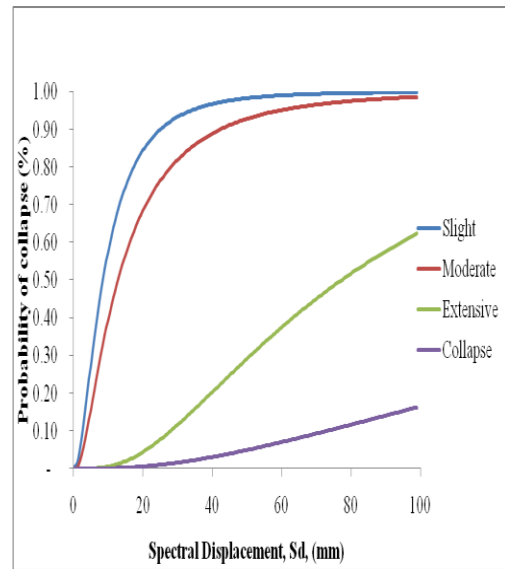


g) $f_{ck}=30$ MPa and $f_y=520$ MPa

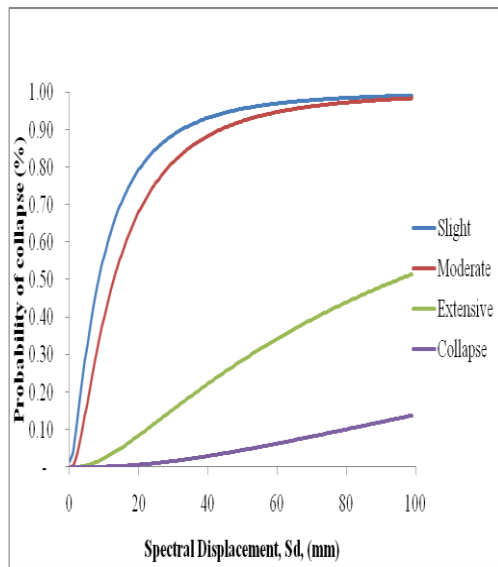
Figure 5.36 Fragility curves for Code Proposed Response Spectra



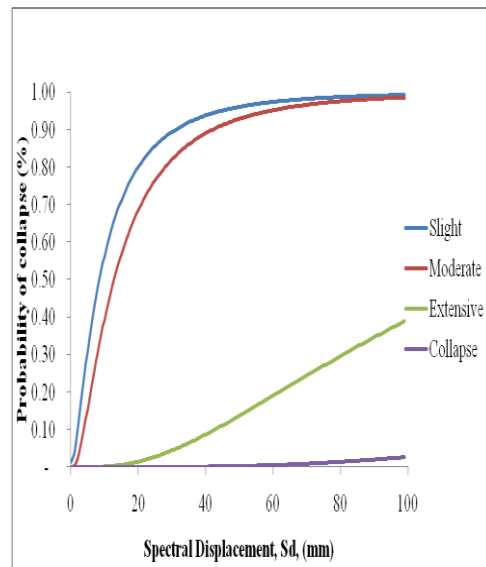
a) fck=20MPa and fy=520MPa



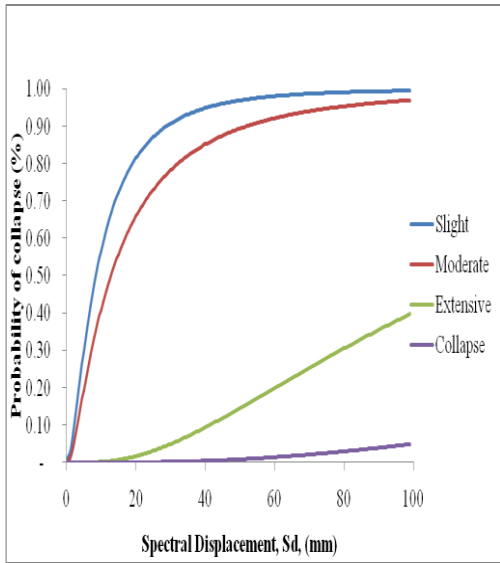
b) fck=21.5 MPa and fy=520MPa



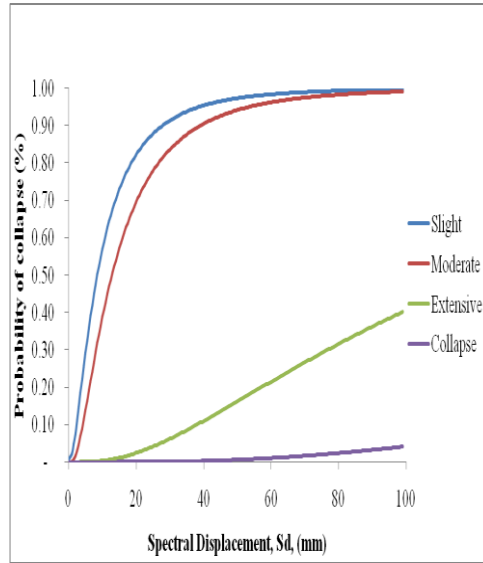
c) fck=23 MPa and fy=520MPa



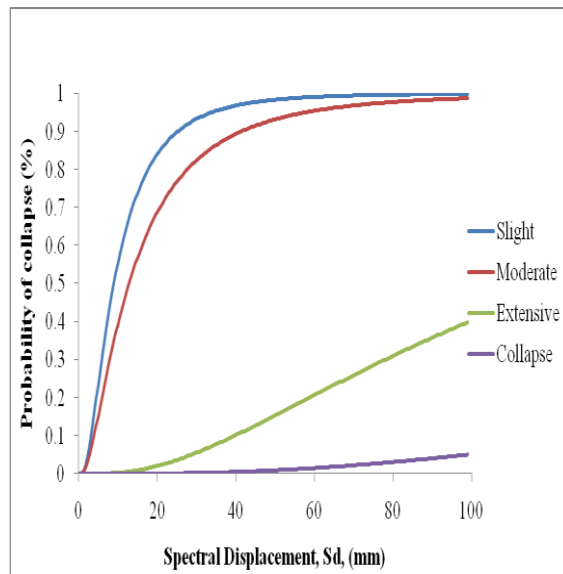
d) fck=25 MPa and fy=520MPa



e) $f_{ck}=27$ MPa and $f_y=520$ MPa



f) $f_{ck}=28.5$ MPa and $f_y=520$ MPa



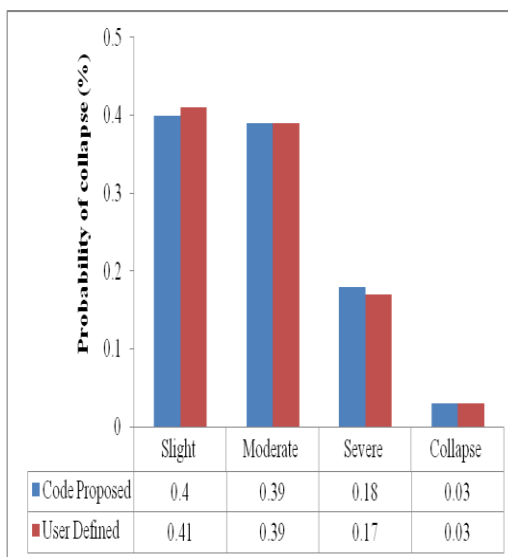
g) $f_{ck}=30$ MPa and $f_y=520$ MPa

Figure 5.37 Fragility curves for User Defined Response Spectra

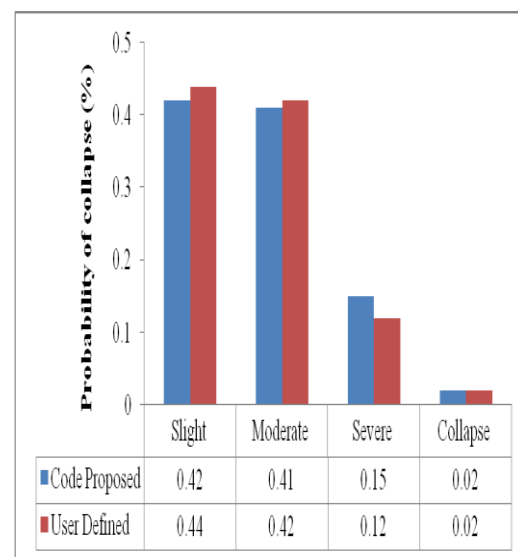
From the above figures it is observed that both for code defined and user defined property fragile states are almost similar with the variation in the compressive strength of the concrete.

5.6.3.1 Comparison of Damage State Thresholds for Code Proposed and Used Defined Response Spectra

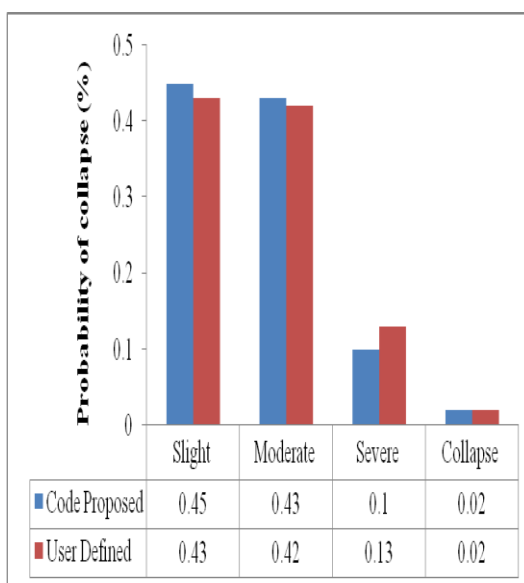
Comparisons of damage states for code defined as well as user defined property are shown in Figure 5.38 (a) to Figure 5.38 (g). It can be seen from the plots that the slight and moderate structural damage are higher for the lower compressive strength of the concrete and the probabilities of structure lying in the severe and collapse damage state decreases for the higher compressive strength of the concrete.



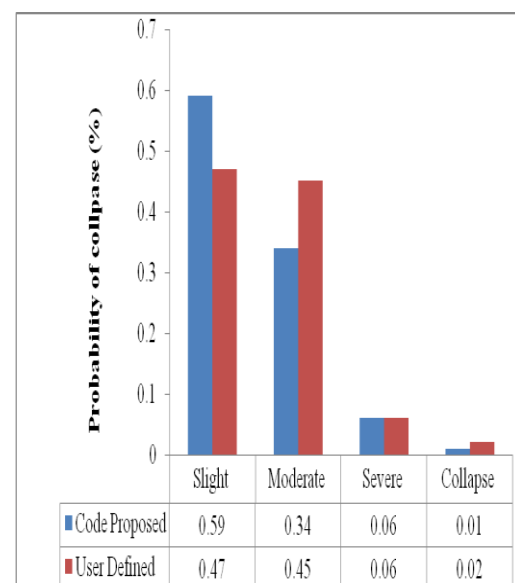
a) $f_{ck}=20\text{MPa}$ and $f_y=520\text{MPa}$



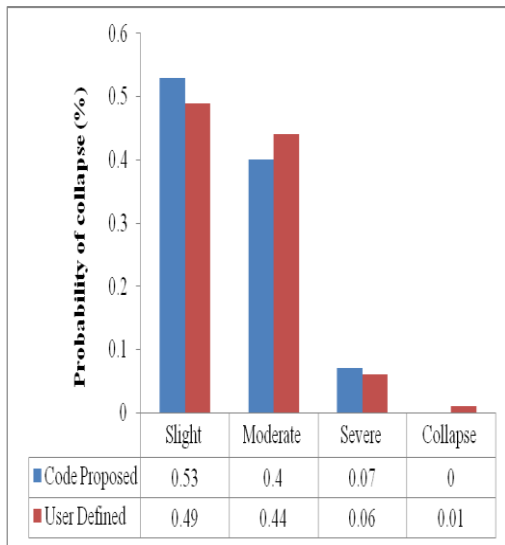
b) $f_{ck}=21.5\text{MPa}$ and $f_y=520\text{MPa}$



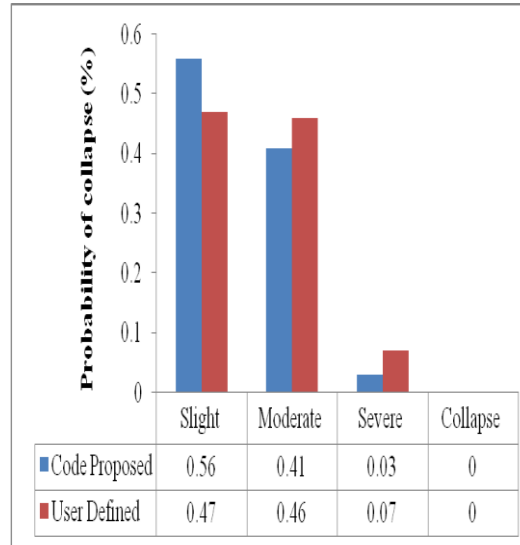
c) $f_{ck}=23\text{MPa}$ and $f_y=520\text{MPa}$



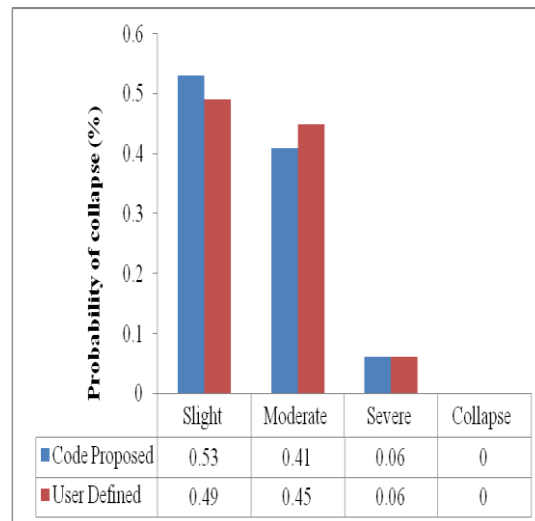
d) $f_{ck}=25\text{MPa}$ and $f_y=520\text{MPa}$



e) $f_{ck}=27\text{MPa}$ and $f_y=520\text{MPa}$



f) $f_{ck}=28.5\text{MPa}$ and $f_y=520\text{MPa}$



g) $f_{ck}=30\text{MPa}$ and $f_y=520\text{MPa}$

Figure 5.38 Damage state thresholds for both the properties

From the fragility analysis for the considered building, the results showed that, 40 %, 39%, 18% and 3% higher probability of slight, moderate, severe and collapse damage in building for code proposed response spectra. Whereas building will suffer 41 %, 39%, 17% and 3% higher probability of slight, moderate, severe and collapse damage respectively in building for user defined response spectra, when $f_{ck}=20\text{MPa}$ and $f_y=520\text{MPa}$ as shown in Fig.5.38 (a).

The fragility analysis results showed that, 42 %, 41%, 15% and 2% higher probability of slight, moderate, severe and collapse damage in building for code proposed

response spectra. Whereas building will suffer 44 %, 42%, 12% and 2% higher probability of slight, moderate, severe and collapse damage in building respectively for user defined response spectra, when $f_{ck}=21.5$ MPa and $f_y=520$ MPa as shown in 5.38 (b).

The results showed that, 45 %, 43%, 10% and 2% higher probability of slight, moderate, severe and collapse damage in building for code proposed response spectra. Whereas building will suffer 43 %, 42%, 13% and 2% higher probability of slight, moderate, severe and collapse damages in building respectively for user defined response spectra, when $f_{ck}=23$ MPa and $f_y=520$ MPa as shown in 5.38 (c).

Fragility analysis for the considered building, the results showed that, 59 %, 34%, 6% and 1% higher probability of slight, moderate, severe and collapse damage in building for code proposed response spectra. Whereas building will suffer 47 %, 45%, 6% and 2% higher probability of slight, moderate, severe and collapse damage in building respectively for user defined response spectra, when $f_{ck}=25$ MPa and $f_y=520$ MPa as shown in 5.38 (d).

Fragility analysis results showed that, 53%, 40%, 7% and 0% higher probability of slight, moderate, severe and no collapse damage in building for code proposed response spectra. Whereas building will suffer 49 %, 44%, 6% and 1% higher probability of slight, moderate, severe and collapse damage in building respectively for user defined response spectra, when $f_{ck}=27$ MPa and $f_y=520$ MPa as shown in 5.38 (e).

The results showed that, 56 %, 41%, 3% and 0% higher probability of slight, moderate, severe and no collapse damage in building for code proposed response spectra. Whereas building will suffer 47 %, 46%, 7% and 0% higher probability of slight, moderate, severe and no collapse damage in building respectively for user defined response spectra, when $f_{ck}=28.5$ MPa and $f_y=520$ MPa as shown in 5.38 (f).

Also, the fragility analysis for the considered building, the results showed that, 53 %, 41%, 6% and 0% higher probability of slight, moderate, severe and no collapse damage in building for code proposed response spectra. Whereas building will suffer

49 %, 45%, 6% and 0% higher probability of slight, moderate, severe and collapse damage in building for user defined response spectra, when $f_{ck}=30\text{MPa}$ and $f_y=520\text{MPa}$ as shown in 5.38 (g).

CHAPTER 6

CONCLUSIONS AND SCOPE FOR FUTURE WORK

6.1 CONCLUSIONS

The structure behaved linearly till a base shear value of around 300 kN. At this point the flexural tension cracks at the base of the columns started to get generated and the structure displayed a reduced stiffness. After reaching a base shear value of approximately 500 kN, the cracks at the base of the columns opened wider and failures at other locations namely beams and beam-column joints started to show up. As a result the stiffness of the structure further went down, that can be seen from the pushover curves. After reaching the base shear values of 700 kN, the joints of the structure displayed rapid degradation. On further increase in the lateral load, the structure displayed a brittle behaviour with large displacement increase for the same increase in the base shear. After reaching a base shear of 882.90 kN, i.e. 9t load at first floor, 18t at second floor, 27t at third floor and 36t at fourth floor, the structure started undergoing increasing displacement at constant load as reported by Akanshu Sharma et al., 2010.

Pushover analysis by applying inverted triangular load distribution along floors for the four storeyed building has been carried out considering design material properties.

In this research work following were considered:

- Strength properties of material.
- Effect of confinement in structural members by making use of modelling approaches.
- Possibility of hinge formation in beams and columns
- Some of the ground motions of India.

The mechanical properties adopted respectively, for concrete 20-30 MPa as compressive strength and, for the reinforcement, 520-600 MPa as tensile strength. Although the models provide a quite good agreement on results with particular reference to maximum base shear reached and the collapse mechanism activated.

Nevertheless, the following issues have to be pointed out. In case of the comparison of pushover analysis curves of all cases, it could be observed that all the seven curves follow the same path. Maximum base shear of 840.1 kN, 848.5 kN, 855.1 kN, 864.8 kN, 872.5 kN, 877.5 kN and 881.6 kN for $f_{ck} = 20, 21.5, 23, 25, 27, 28.5$ and 30 N/mm^2 respectively and for varying values of f_y . The corresponding lateral roof displacement are 0.259, 0.259, 0.258, 0.258, 0.256, 0.253 and 0.253m. This clearly demonstrates that there is some improvement in base shear values and there is no significant improvement in displacement values for varying values of f_{ck} and f_y for unconfined concrete section.

Once geometrical features and mechanical parameters are shared, non-linear static analyses were performed for main X-direction varying f_{ck} . Paying attention to the analyses performed in X-direction for the frame with unconfined concrete section, results in terms of pushover curves shows the contribution to the global base shear distinguishing between that carried by varying f_{ck} and that by RC frame (experimental). The results of all models quite well agree in particular until the reaching of the maximum base shear. Actually, differences in softening phase (more sudden in case of $f_{ck}=28.5 \text{ MPa}$) and in computation of displacement (the parameter which governs the collapse elements) are similar to each other. Moreover, all the models also agree in terms of global failure mode.

Comparison of pushover analysis curves of seven cases of both the models, it could be observed that all the seven curves follow the same path. The moment curvature relations is observed from its inelastic behavior in all the cases. Maximum displacement is observed at a base shear of 1118.0 kN. The corresponding lateral roof displacement is 0.293 m, when $f_{ck} = 30 \text{ N/mm}^2$ and $f_y = 520 \text{ Mpa}$ for Mander's model. Maximum displacement is observed at a base shear of 1180 kN. The corresponding lateral roof displacement is 0.216 m, when $f_{ck} = 30 \text{ N/mm}^2$ and $f_y = 520 \text{ Mpa}$ for Kent and Park model. For all the cases a mechanism is formed at a maximum base shear with a maximum roof displacement.

It is very clear that base shear increases with increase in compressive strength of concrete. The base shear remains same for the increase in tensile strength of steel. It

can be seen that the maximum base shear obtained from SAP2000 is almost comparable to that of experimental result. The base shear obtained from experiment was found to be nearly 882kN. Whereas, it is ranged from 915.6 kN for $f_{ck} = 20$ MPa to 1070.1 kN for $f_{ck} = 30$ MPa and tensile strength of steel = 520 MPa. The values remain same for variations in material strength especially for $f_y = 560, 580$ and 600 MPa. Such variations in base shear with respect to X direction can be attributed to the orientation of column, unsymmetrical cross section at each floor level.

The value of base shear obtained from the analysis using SAP 2000 is almost comparable to the results obtained from experiment. The value of base shear obtained from experiment was around 882kN. The analytical results obtained varied from 912kN to 1085kN for user defined spectra for $f_{ck} = 20$ MPa and $f_{ck} = 30$ MPa, where as $f_y = 520$ MPa kept constant respectively. This slight change in the base shear value occurs due to the column orientations and unsymmetrical sections at different floor levels. It can be observed that displacement value remains same for varying tensile strength of steel values and the displacement of the building decreases with the increase in the compressive strength of concrete.

The pushover analysis involved the application of monotonically increasing lateral load pattern and monitoring the inelastic behavior within the structure. It can be observed that the pushover curve for the RC building with code proposed response spectra has a capacity approximately equal to that of user defined response spectra for the variation in material strength.

Buildings under monotonic pushover loading clearly manifest the yielding and fracturing of reinforcement exhibiting the ductile pattern failure. Therefore, it can be concluded that the overall or final performance of a well designed reinforced concrete member depends upon its reinforcement used in the member while the other constituent material influences the behavior initially.

For unconfined and confined models base shears vary, but the pushover curves for confined concrete models indicate that confinement enhances the base shear capacity. With confinement displacement decreases and also from curves it is evident that

energy absorption capacity is enhanced. Comparison with the experimental pushover curve, suggests that frame modelled as confined gives results in close agreement.

For all the parametric study the performance points are very close. Different modelling technique for confined model shows only slight change in performance point. For code specified spectra and user defined spectra performance appears to be very close. This is due to the close similarity between the load patterns.

The seismic fragility curves were expressed by the damage probabilities of structures according to the code specified spectra and user defined spectra (taking into account of Indian ground motions). In order to characterize the damage state of RC buildings, the damage index proposed by Ioana, Olteanu et al. (2011) was applied as the damage characterization measure.

The present seismic fragility curves must be used with careful by the users since in our case these curves were derived for the requirements of zone-IV of RC building. The methodology is still applicable for other regions by considering the specificities of the seismic hazard and building characteristics of the studied zone. The obtained seismic fragility curves constitute excellent information sources and tools for risk managements, emergency planning and also useful for civil protection, prevention and preparedness for the Zone-IV of IS: 1893-2002.

From the fragility analysis for the considered building with unconfined concrete section, the results showed that, 49 %, 35%, 14% and 2% higher probability of slight, moderate, severe and collapse damage respectively in RC building, when $f_{ck}=20\text{MPa}$ and $f_y=520\text{MPa}$. Building will suffer 48 %, 34%, 16% and 2% higher probability of slight, moderate, severe and collapse damage respectively, when $f_{ck}=21.5\text{ MPa}$ and $f_y=520\text{MPa}$. Also, building showed that 48 %, 36%, 14% and 2% higher probability of slight, moderate, severe and collapse damage respectively, when $f_{ck}=23\text{ MPa}$ and $f_y=520\text{MPa}$.

Similarly, building will suffer 48 %, 34%, 16% and 2% higher probability of slight, moderate, severe and collapse damage respectively, when $f_{ck}=25\text{ MPa}$ and

$f_y=520\text{MPa}$. Building will showed that 48 %, 35%, 14% and 3% higher probability of slight, moderate, severe and collapse damage respectively, when $f_{ck}=27\text{ MPa}$ and $f_y=520\text{MPa}$. Building will suffer 50 %, 38%, 11% and 1% higher probability of slight, moderate, severe and collapse damage respectively, when $f_{ck}=28.5\text{ MPa}$ and $f_y=520\text{MPa}$. Lastly, building will suffer 46 %, 34%, 17% and 3% higher probability of slight, moderate, severe and collapse damage respectively, when $f_{ck}=30\text{MPa}$ and $f_y=520\text{MPa}$.

From the fragility analysis for the considered building with confined concrete section by two modelling approaches, the results showed that, 44 %, 41%, 14% and 1% higher probability of slight, moderate, severe and collapse damage in building for Mandar's model. Whereas building will suffer 46 %, 44%, 9% and 1% higher probability of slight, moderate, severe and collapse damage in building for Kent and Park model, when $f_{ck}=20\text{MPa}$ and $f_y=520\text{MPa}$. Also, the fragility analysis results showed that, 44 %, 41%, 14% and 1% higher probability of slight, moderate, severe and collapse damage in building for Mandar's model. Whereas building will suffer 44 %, 40%, 13% and 3% higher probability of slight, moderate, severe and collapse damage in building for Kent and Park model, when $f_{ck}=21.5\text{ MPa}$ and $f_y=520\text{MPa}$. The fragility analysis results showed that, the building will suffer 45 %, 43%, 12% and 0% higher probability of slight, moderate, severe and no collapse damage in building for Mandar's model. Whereas building will suffer 46 %, 43%, 10% and 1% higher probability of slight, moderate, severe and collapse damages in building for Kent and Park model, when $f_{ck}=23\text{MPa}$ and $f_y=520\text{MPa}$.

The results showed that, 47 %, 43%, 9% and 1% higher probability of slight, moderate, severe and collapse damage in building for Mandar's model. Whereas building will suffer 48 %, 47%, 7% and 0% higher probability of slight, moderate, severe and no collapse damage in building for Kent and Park model, when $f_{ck}=25\text{MPa}$ and $f_y=520\text{MPa}$. Building will suffer 48%, 46%, 6% and 0% higher probability of slight, moderate, severe and no collapse damage in building for Mandar's model. Whereas building will suffer 47 %, 46%, 7% and 0% higher

probability of slight, moderate, severe and no collapse damage in building for Kent and Park model, when $f_{ck}=27\text{MPa}$ and $f_y=520\text{MPa}$.

Similarly, fragility analysis results showed that, 48 %, 45%, 7% and 0% higher probability of slight, moderate, severe and no collapse damage in building for Mandar's model. Whereas building will suffer 48 %, 44%, 8% and 0% higher probability of slight, moderate, severe and no collapse damage in building for Kent and Park model, when $f_{ck}=28.5\text{MPa}$ and $f_y=520\text{MPa}$.

Lastly, the results showed that, 48 %, 44%, 8% and 0% higher probability of slight, moderate, severe and no collapse damage in building for code proposed response spectra. Whereas building will suffer 48 %, 45%, 7% and 0% higher probability of slight, moderate, severe and no collapse damage in building for Kent and Park model, when $f_{ck}=30\text{MPa}$ and $f_y=520\text{MPa}$.

From the fragility analysis for the considered building, the POA has been done for two properties (say code specified and user defined property), the results showed that, 40 %, 39%, 18% and 3% higher probability of slight, moderate, severe and collapse damage in building for code proposed response spectra. Whereas building will suffer 41%, 39%, 17% and 3% higher probability of slight, moderate, severe and collapse damage respectively in building for user defined response spectra, when $f_{ck}=20\text{MPa}$ and $f_y=520\text{MPa}$. The fragility analysis results showed that, 42 %, 41%, 15% and 2% higher probability of slight, moderate, severe and collapse damage in building for code proposed response spectra. Whereas building will suffer 44 %, 42%, 12% and 2% higher probability of slight, moderate, severe and collapse damage in building respectively for user defined response spectra, when $f_{ck}=21.5\text{MPa}$ and $f_y=520\text{MPa}$.

The results showed that, 45 %, 43%, 10% and 2% higher probability of slight, moderate, severe and collapse damage in building for code proposed response spectra. Whereas building will suffer 43 %, 42%, 13% and 2% higher probability of slight, moderate, severe and collapse damages in building respectively for user defined response spectra, when $f_{ck}=23\text{MPa}$ and $f_y=520\text{MPa}$.

Similarly, the fragility analysis for the considered building, the results showed that, 59 %, 34%, 6% and 1% higher probability of slight, moderate, severe and collapse damage in building for code proposed response spectra. Whereas building will suffer 47 %, 45%, 6% and 2% higher probability of slight, moderate, severe and collapse damage in building respectively for user defined response spectra, when $f_{ck}=25\text{MPa}$ and $f_y=520\text{MPa}$.

Also, fragility analysis results showed that, 53%, 40%, 7% and 0% higher probability of slight, moderate, severe and no collapse damage in building for code proposed response spectra. Whereas building will suffer 49 %, 44%, 6% and 1% higher probability of slight, moderate, severe and collapse damage in building respectively for user defined response spectra, when $f_{ck}=27\text{MPa}$ and $f_y=520\text{MPa}$. The building will suffer 56 %, 41%, 3% and 0% higher probability of slight, moderate, severe and no collapse damage in building for code proposed response spectra. Whereas building will suffer 47 %, 46%, 7% and 0% higher probability of slight, moderate, severe and no collapse damage in building respectively for user defined response spectra, when $f_{ck}=28.5\text{MPa}$ and $f_y=520\text{MPa}$.

Lastly, the fragility analysis results showed that, 53 %, 41%, 6% and 0% higher probability of slight, moderate, severe and no collapse damage in building for code proposed response spectra. Whereas building will suffer 49 %, 45%, 6% and 0% higher probability of slight, moderate, severe and collapse damage in building for user defined response spectra, when $f_{ck}=30\text{MPa}$ and $f_y=520\text{MPa}$.

The fragility analysis result shows that for the considered buildings with varying $f_{ck}(\text{MPa})$ and for constant $f_y=520 \text{ MPa}$, a high probability of slight, moderate damages can be observed and a low probability of severe and collapse damage states can be noted and is almost found to be similar in all the parametric studies (including both Mander and Kent and Park models and even in code proposed and user defined properties).

6.2 SCOPE FOR THE FUTURE WORK

In the present study, a frame has been studied under monotonic loads with inverted triangular load profile. The frame can be studied even under different loading conditions, that is, parabolic loading as load profile to monitor variation in load deflection curves.

Also, frame has been studied with variation in material strength under monotonic loads. The frame can be studied under cyclic-loading to monitor the variation in load-deflection curves at a given time history.

This study focuses on nonlinear static analysis procedure to check the performance of the structure. But, the study can be extended to nonlinear time history analysis and the results can be checked for more accuracy.

In this study, variation in material strength is dealt with; the work may be further extended by varying the cover of the reinforcement. Also, the study can be further extended by adopting advanced modelling techniques to develop fragility curves.

The accuracy of the proposed fragility curves can further be improved by introducing building damage data of neighbouring zones and the result of analytical studies.

REFERENCES

Books/ Journals Articles/ Reports:

Abhilash, R., Biju, V. and Rahul Leslie. (2009). "Effect of lateral load patterns in pushover analysis." *10th National Conference on Technological Trends (NCTT09)*, College of Engineering Trivandrum, Kerala, India, 138-142.

Ahmad, A Fallah., Abdoreza, S Moghadam. and Saeed Mohammad, Zadeh. (2009). "Reliability index for reinforced concrete frames using nonlinear pushover and dynamic analysis." *International Journal of Advanced Structural Engineering*, 1(2), 135-151.

Akanshu, Sharma. and Reddy, G.R. (2010). "A report on round robin exercise on experiment and analysis of four storey full scale reinforced concrete structure under monotonic pushover loads." Reactor Safety Division, *Bhabha Atomic Research Centre*, Mumbai.

Alfredo, H-S Ang. and Wilson, H. Ang. (2007). "Probability concepts in engineering-emphasis on applications in civil & environmental engineering." *John Wiley & Sons, Inc.*, USA.

Alexandra, Papailia. (2011). "Seismic fragility curves for reinforced concrete buildings." Master Degree in Earthquake Engineering and Engineering Seismology Thesis, University of Patras.

Amr S, Elnashai. and Luigi Di, Sarno. (2008). "Fundamentals of earthquake engineering." *John Wiley & Sons, Ltd.*, UK.

Anand S, Arya. (2000). "Recent developments toward earthquake reduction in India", *Current Science*, 79 (9), 1270-1277.

Angelo, Marinilli. (2008). "Simplified Stochastic Analysis of Reinforced Concrete frames under seismic loads." *14th World Conf. on Earthquake Eng.*, Beijing, China.

- Antoniou, S. and Pinho, R. (2004). "Development and verification of a displacement-based adaptive pushover procedure." *J. of Earthquake Engg.*, 8(5),643-661.
- Bai, Zhizhou. (2006). "Nonlinear analysis of reinforced concrete beams and columns with special reference to full-range and cyclic." *The University of Hong Kong*. <http://hdl.handle.net/10722/50666>.
- Bapat, A., Kulkarni,R. and Guha, S. (1983). "Catalogue of earthquakes in India and neighbourhood from historical period up to 1979." *J. Indian Society of Earthquake Technology*, Roorkee.
- Barbat, A.H., Pujades, L.G., and Lantada, N. (2006). "Performance of buildings under earthquakes in Barcelona, Spain." *Computer-Aided Civil and Infrastructure Engineering*, 21(8), 573–593.
- Barbat A, H., Pujades, L.G. and Lantada, N.(2008). "Seismic damage evaluation in urban areas using the capacity spectrum method: application to Barcelona." *Soil Dynamics and Earthquake Engineering*, 28(10), 851-865.
- Bakhshi, A . and Karimi, K.(2008). "Performance evaluation of masonry buildings using a probabilistic approach." *Scientia Iranica*, 15(3), 295-307.
- Beena Kumari. (2010). "Finite element modelling of reinforced concrete frame." *M.E in Structures Thesis*, Thapar University, Patiala, India.
- Bolotin, V.V. (1993). "Seismic risk assessment for structures with the Monte Carlo simulation." *Probabilistic Engineering Mechanics*, 8 (3), 69-177.
- Borzi, B., Pinho, R., and Crowley, H. (2006). "Simplified pushover-based vulnerability analysis for large-scale assessment of RC buildings." *Engineering Structures*, 30(3), 804–820.
- Cheng-Tzu, Thomas Hsu, "Moment-curvature characteristics for reinforced concrete", Dept. of Civil and Environmental Engineering, Chapter 3,New Jersey Institute of Technology, Newark, New Jersey, 89-130.
- Choudhary, M.R., Upton, M. and Haldar, A. (2001). "Seismic reliability assessment of reinforced concrete frames under seismic loading." *8th Int. Conf. on structural safety and reliability (ICOSSAR 2001)*, Paper No. 237.
- Dagang, Lu., Xiaohui, Yu., Mingming, Jia. and Guangyuan, Wang. (2013). "Seismic risk assessment for a reinforced concrete frame designed according to Chinese codes." *Structure*

and Infrastructure Engineering: Maintenance, Management, Life-Cycle Design and Performance. <http://dx.doi.org/10.1080/15732479.2013.791326>.

Dookie, Kim., Sandeep, Chaudhary., Charito, Fe Nocete., Feng, Wang. and Do, Hyung Lee. (2011). "A probabilistic capacity spectrum strategy for the reliability analysis of bridge pile shafts considering soil structure interaction", *Latin American Journal of Solids and Structures*, 8, 291-303.

El Ghoulbzouri, Abdelouafi., Khamlichi, Abdellatif., Bezzazi, Mohamed. and Lopez Almansa, Francisco. (2009). "Reliability Analysis for Seismic Performance Assessment of Concrete Reinforced Buildings." *Australian J. Basic and Applied Sciences*, 3(4), 4484-4489.

Faella, C., Lima, C. and Martinelli, E. (2008). "Non-linear static methods for seismic fragility analysis and reliability evaluation of existing Structures." *14Th World Conference on Earthquake Engineering*, Beijing, China.

Filippou, Filip. C. and Ahmad, Issa. (1988). "Nonlinear analysis of reinforced concrete frames under cyclic load reversals." Report No. UCB/EERC-88/12, *Earthquake Engineering Research Center*, College of Engineering, University of California, Berkeley.

Gencturk, B., Elnashai, A.S., and Song, J. (2008). "Improved fragility relationships for populations of buildings based on inelastic response." *14Th World Conference on Earthquake Engineering*, Beijing, China.

Giovinazzi, S. (2005). "The vulnerability assessment and the damage scenario in seismic risk analysis." Dissertation, *University of Florence and Technical University of Braunschweig*.

Haran Pragalath, D C., Robin, Davis, P., Pradip Sarkar and Monalisa, Priyadharshini (2014). "Seismic reliability assessment of RC frame in a high seismic zone- India." *Int. J. Emerging Technology and Advanced Engineering*, 4(4), 2250-2459.

Ioana, Olteanu., Yeudy Felipe, Vargas., Alex-Horia, Barbat., Mihai, Budescui. and Lluís Gonzaga, Pujades. (2011). "Vulnerability and risk evaluation for a reinforced concrete frame." *Bul. Inst. Polit. Iași*, t. LVII (LXI), f. 3.

Iyengar, R.N., and Ghosh, S. (2004). "Microzonation of earthquake hazard in Delhi area", *Current Science*, 87(9), 1193-1202.

- Kappos, A.J, Panagopoulos, G., Panagiotopoulos, C., and Penelis, G. (2006). "A hybrid method for the vulnerability assessment of R/C and URM buildings." *Bulletin of Earthquake Engineering*, 4(4), 391–413.
- Kircher, C.A., Reitherman, R.K., Whitman, R.V., and Arnold, C. (1997a). "Estimation of earthquake losses to buildings." *Earthquake Spectra*, 13(4), 703–720.
- Kircher, C.A., Nassar, A.A., Kustu, O. and Holmes, W.T. (1997b). "Development of building damage functions for earthquake loss estimation." *Earthquake Spectra*, 13(4), 663–682.
- Laura, Eads. "Pushover analysis of 2-story moment frame." *From Open Sees Wiki*, <http://opensees.berkeley.edu>
- Luna Ngeljaratan, P., Kamachi. and Nagesh R, Iyer. (2011). "A critical review on earthquake resistant design provisions of SNI 03-1726-2002 of Indonesia and IS 1893(Part 1)-2002 of India", *Journal of Structural Engineering*, 38(3), 285-296.
- Lu D.G, Yu X.H and Jia M.M. (2012). "Analytical Formulations of Fragility Functions with Applications to Probabilistic Seismic Risk Analysis". *The 15th World Conference on Earthquake Engineering*.
- Mashaly, E.A. and Datta, T. K. (1990). "Seismic risk analysis of buried pipelines." *Journal of Transportation Engineering*, 115(3), 232-252.
- Nasserasadi, K., Ghafory-Ashtiany, M., Eshghi, S. and Zolfaghari, M.R.(2009). "Developing seismic fragility function of structures by stochastic approach", *Asian J. Civil Eng., (Building and Housing)*, 10(2), 183-200.
- Nikos, D. Lagaros. (2012) "Fuzzy Fragility Analysis of Structures with Masonry Infill Walls." *The Open Construction and Building Technology Journal*, 6, (Suppl. 1-M18), 291-305.
- Oh-Sung Kwon., Amr S, Elnashai. (2007). "Probabilistic seismic assessment of structure, foundation, and soil interacting systems." *Ph.D Thesis*, Department of Civil and Environmental Engineering, University of Illinois, Urbana-Champaign Urbana, Illinois.
- Pauley, T. and Priestley, M.J.N. (1992). "Seismic design of reinforced concrete and masonry buildings." *John Wiley and Sons*, New York.
- Pavan Kumar, A. (2010). "Seismic performance evaluation and fragility analysis of reinforced concrete buildings." *M.Tech Thesis*, IIT Bombay, Mumbai.

- Ranganathan, R. (1990). "Reliability analysis and design of structures," *Tata McGraw-Hill Publishing Company Ltd.*, New Delhi.
- Ramesh Babu, R, Akanshu Sharma. and Reddy, G.R. (2009). "Significance of modelling techniques in pushover analysis of RC buildings." *ACSGE*, BITS Pilani, India, 25-27.
- Ravi Kanitkar. and Vasant Kanitkar. (2004). "Seismic performance of conventional multi-storey buildings with open ground floors for vehicular parking." *The Indian Concrete Journal*, 99-104.
- Rehan A, Khan., Naqvi, T. and Adeela, Afreen. (2011). "Seismic reliability analysis of RCC building frame." *Int. J. Earth Sciences and Eng.*, 6, 530-533.
- Richard Sharpe (2004). "(Chapter 16) - Supporting local seismic experts: experiences in Nepal and India." *OECD*, pp.205-207.
- Rohit, Bansal. (2011). "Pushover analysis of reinforced concrete frame." *M.E in Structures Thesis*, Thapar University, Patiala, Punjab, India.
- Ross, B. Corotis. and Holly, L. Bonstrom. "Structural reliability and community sustainability." <http://www.colorado.edu>
- Ruiz-Garcia, J., Teran-Gilmore, A. and Oscar, Zuniga-Cuevas. (2010). "Simplified drift-based fragility assessment of confined masonry buildings." *Proc., the 9th U.S. National and 10th Canadian Conf. on Earthquake Eng.*, Canada, Paper No. 1240.
- Seong-Hoon, Jeongaand. and Amr S, Elnashai. (2007). "Probabilistic fragility analysis parameterized by fundamental response quantities." *Engg., Structure*, 1238–1251.
- Shah, V.L and Karve, S.R. (2003). "Illustrated reinforced concrete design." *Structures Publications*, Pune.
- Shamim, A. Sheikh. and Yeh, C. C. (1992). "Analytical moment-curvature relations for tied concrete columns." *Journal of Structural Engineering*, 118 (2), 529- 544.
- Shinozuka, M., Mizutani, M., Takeda, M. and Kai. Y. (1989). "Seismic PRA procedure in Japan and its application to building performance safety estimation." Part 3. Estimation of Building and Equipment Performance Safety, Proc. ICOSAR 89, 5th *Int Conf on Structural Safety and Reliability*, Publ., by ASCE, New York, USA, 637-644.

Takeda, M., Kai, Y., Mizutani, M. (1989). "Seismic PRA procedure in Japan and its application to building performance safety estimation", Part 2, Fragility Analysis, Proc. ICOSSAR 89, *5th Int Conf on Structural Safety and Reliability*, Publ., by ASCE, New York, USA, 629-636.

Takemura, M., Ishida, H., Amano, A and Mizutani, M. (1989). "Seismic PRA procedure in Japan and its application to building performance safety estimation", Part 1, Fragility Analysis, Proc ICOSSAR 89, *5th Int. Conf. on Structural Safety and Reliability*, Publ., by ASCE, New York, USA, 629-636.

Varghese, P.C. (2005). "Advanced reinforced concrete design." *Prentice-Hall of India*, New Delhi.

Varpasuo, P. (2005)." The seismic response and floor spectra of OL3NPP buildings in Finland." *18th International Conference on Structural Mechanics in Reactor Technology (SMiRT 18)*, Beijing, China. August 7-12, SMiRT18-K07-3.

VipinUnnithan, U., Meher Prasad, A. and Rao, B.N. (2008). "Development of fragility curves using high dimensional model representation." *14th World Conf. on Earthquake Eng.*, Beijing, China.

Yeudy F, Vargas., Alex H, Barbat., Lluís G, Pujades. and Jorge E, Hurtado. (2013). "Probabilistic seismic risk evaluation of reinforced concrete buildings." *Structures and Buildings, Proceedings of the Institution of Civil Engineers*, Paper No. 1200031, 1-10.

Codes/ Standards/ Specifications

Applied Technology Council. (1982). “An investigation of the correlation between earthquake ground motion and building performance.” *Report No. ATC-10*, Redwood City, CA.

Applied Technology Council. (1985). “Earthquake damage evaluation data for California.” *Report No. ATC-13*, Redwood City, CA.

Applied Technology Council (1996). Seismic evaluation and retrofit of concrete buildings, *Report No. ATC-40*, Redwood City, CA.

Applied Technology Council. (2009). “Guidelines for seismic performance assessment of buildings.” *Report ATC-58*, April 2009, Redwood City, CA.

IS 456:2000. “Plain and reinforced concrete- code of practice”, *BIS*, New Delhi.

IS 875 (Part I):1987. “Code of practice for design loads (other than earthquake) for buildings and structures”, *BIS*, New Delhi.

IS 1893 (Part 1)-2002. “Criteria for earthquake resistant design of structures, Part 1 General provisions and buildings”, *BIS*, New Delhi.

IS 15988: 2013. “Seismic evaluation and strengthening of existing reinforced concrete buildings-guidelines”, *BIS*. New Delhi.

National Disaster Management Authority, Government of India, (2013). “Technical Document (*Tech-Doc*) on Seismic Vulnerability Assessment Methods for Buildings”, New Delhi.

National Disaster Management Authority, Government of India, (2007). “Technical Report on Development of Probabilistic Seismic Hazard Map of India”, New Delhi.

BMTPC, Ministry of Housing and Urban Poverty Alleviation, Government of India (2007). “Vulnerability Atlas of India”, New Delhi.

Durgesh C Rai. “Review of Documents on Seismic Evaluation of Existing Buildings”, Document No. IITK- GSDMA-EQ03-V1.0, Interim Report I: Earthquake Codes, IITK-GSDMA Project on Building Codes, IIT, Kanpur.

Durgesh C Rai. “Review of Documents on Seismic Strengthening of Existing Buildings”, Document No. IITK- GSDMA-EQ07-V1.0, Final Report: A- Earthquake Codes, IITK-GSDMA Project on Building Codes, IIT, Kanpur.

Federal Emergency Management Agency. (1997a). "NEHRP guidelines for the seismic rehabilitation of buildings." *FEMA 273*, Washington, D.C., October 1997.

Federal Emergency Management Agency. (1997b). "NEHRP Commentary on the Guidelines for the Seismic Rehabilitation of Buildings." *FEMA 274*, Washington, D.C., October 1997.

Federal Emergency Management Agency. (1997c). "HAZUS®97 Earthquake Loss Estimation Methodology, User Manual." *Federal Emergency Management Agency*, Washington, D.C., United States, 197.

Federal Emergency Management Agency. (1999). "HAZUS®99 Earthquake Loss Estimation Methodology, User Manual." *Federal Emergency Management Agency*, Washington, D.C., United States, 314.

Federal Emergency Management Agency. (2000). "Prestandard and commentary for the seismic rehabilitation of buildings." *FEMA 356*, Prepared by American Society of Civil Engineers, Reston, Virginia, United States, November 2000.

Federal Emergency Management Agency. (2001). "HAZUS®99-SR1 estimated annualized earthquake losses for the United States." *FEMA 366*, Report of the Federal Emergency Management Agency, Washington, DC, United States, 33.

Federal Emergency Management Agency. (2002). "HAZUS®99-SR2 (Service Release 2), Advanced Engineering Building Module, Technical and User's Manual." Federal Emergency Management Agency, *FEMA and National Institute of Building Sciences*, NIBS, Washington D.C.

Federal Emergency Management Agency. (2003). "HAZUS-MH MR4 Technical Manual." Washington, D.C.

Federal Emergency Management Agency. (2005). "Improvement of Nonlinear Static Seismic Analysis Procedures." *FEMA 440*, Prepared by Applied Technology Council (*ATC-55 Project*), Washington, D.C., United States, June 2005.

Federal Emergency Management Agency. (2008). "HAZUS-MH Estimated annualized earthquake losses for the United States." *FEMA 366*, Report of the Federal Emergency Management Agency, Washington, DC, United States, 66.

NIBS.(2003). "Multi-hazard loss estimation methodology, earthquake model-Hazus-MH: technical manual, report prepared for the Federal Emergency Management Agency(FEMA)." National Institute of Building Sciences, Washington, DC.

APPENDIX- I

Table I- Lateral Load Distribution as per IS-1893(2002)

Storey level	Lateral force distribution (N)
4 th floor	16227.66
3 rd floor	13088.25
2 nd floor	6101.95
1 st floor	1459.16

APPENDIX- II

Moment-curvature relationship for doubly reinforced concrete section developed in Matlab 7.1

```
b=input('enter the beam width in mm =');
d=input('enter the effective depth in mm =');
Asc=input('enter the area of rebars in compression mm2=');
Ast=input('enter the area of rebars in tension mm2=');
Fck=input('enter the characteristic strength or design strength of concrete in N/mm2 = ');
Fy=input('enter the yield strength or design stress of rebars in N/mm2 = ');
E=input('enter the value of modulus of elasticity in N/mm2 =');
d1=input('enter the distance of top reinforcement from top face mm=');
e0=0.002;
xu=5;          %initial guess of neutral axis%
phi=0:0.000000100:0.0002;
for i=1:2001;
if xu*phi(i)<=0.002& (d-xu)*phi(i)<=(fy/(E))& (xu-d1)*phi(i)<=(fy/(E));
f = @(xu)(b*fc*(((phi(i)*xu.^2)/e0)-(phi(i)/e0)^2*xu.^3/3)+(phi(i)*E*Asc*(xu-d1))-
(phi(i)*(d-xu)*E*Ast));
xu = fzero(f,xu);
M(i)=b*fc*(((2*phi(i)*xu.^3)/(3*e0))-(phi(i)/e0)^2*xu^4/4)+(E*phi(i)*Asc*(xu-
d1)^2)+(E*phi(i)*Ast*(d-xu)^2);
elseif xu*phi(i)<=0.002& (d-xu)*phi(i)<=(fy/(E))& (xu-d1)*phi(i)>(fy/(E))
f = @(xu)(b*fc*(((phi(i)*xu.^2)/e0)-(phi(i)/e0)^2*xu.^3/3)+(fy*Asc)-(phi(i)*(d-xu)*E*Ast));
xu = fzero(f,xu);
M(i)=b*fc*(((2*phi(i)*xu.^3)/(3*e0))-(phi(i)/e0)^2*xu^4/4)+(fy*Asc*(xu-
d1))+(E*phi(i)*Ast*(d-xu)^2);
elseif xu*phi(i)<=0.002& (d-xu)*phi(i)>(fy/(E))& (xu-d1)*phi(i)<=(fy/(E))
f = @(xu)((b*fc*(((phi(i)*xu.^2)/e0)-(phi(i)/e0)^2*xu.^3/3)+(phi(i)*E*Asc*(xu-d1))-
fy*Ast);
xu = fzero(f,xu);
M(i)=b*fc*(((2*phi(i)*xu.^3)/(3*e0))-(phi(i)/e0)^2*xu^4/4)+(E*phi(i)*Asc*(xu-
d1)^2)+fy*Ast*(d-xu);
elseif xu*phi(i)<=0.002& (d-xu)*phi(i)>(fy/(E))& (xu-d1)*phi(i)>(fy/(E))
```

```

f = @(xu)((b*fc*(((phi(i)*xu.^2)/e0)-(phi(i)/e0)^2*xu.^3/3))+(fy*Asc)-fy*Ast);
xu = fzero(f,xu);
M(i)=b*fc*(((2*phi(i)*xu.^3)/(3*e0))-(phi(i)/e0)^2*xu.^4/4)+(fy*Asc*(xu-d1))+fy*Ast*(d-
xu);
elseif xu*phi(i)>0.002& xu*phi(i)<0.003&(d-xu)*phi(i)<=(fy/(E))& (xu-d1)*phi(i)<=(fy/(E))
f = @(xu)((fc*b*(xu-(0.34*(0.002/phi(i)))))+(phi(i)*E*Asc*(xu-d1))-phi(i)*(d-xu)*E*Ast);
xu = fzero(f,xu);
M(i)=(fc*b*0.5*(xu^2-0.167*((0.002/phi(i))^2)))+(E*phi(i)*Asc*(xu-
d1)^2)+E*phi(i)*Ast*(d-xu)^2;
elseif xu*phi(i)>0.002& xu*phi(i)<0.003&(d-xu)*phi(i)<=(fy/(E))& (xu-d1)*phi(i)>(fy/(E))
f = @(xu)((fc*b*(xu-(0.34*(0.002/phi(i)))))+(fy*Asc)-phi(i)*(d-xu)*E*Ast); xu =
fzero(f,xu);
M(i)=(fc*b*0.5*(xu^2-0.167*((0.002/phi(i))^2)))+(fy*Asc*(xu-d1))+E*phi(i)*Ast*(d-xu)^2;
elseif xu*phi(i)>0.002& xu*phi(i)<0.0035&(d-xu)*phi(i)>(fy/(E))& (xu-
d1)*phi(i)<=(fy/(E))
f = @(xu)((fc*b*(xu-(0.34*(0.002/phi(i)))))+(phi(i)*E*Asc*(xu-d1))-fy*Ast);
xu = fzero(f,xu);
M(i)=(fc*b*0.5*(xu^2-0.167*((0.002/phi(i))^2)))+(E*phi(i)*Asc*(xu-d1)^2)+fy*Ast*(d-xu);
elseif xu*phi(i)>0.002& xu*phi(i)<0.0035&(d-xu)*phi(i)>(fy/(E))& (xu-d1)*phi(i)>(fy/(E))
f = @(xu)((fc*b*(xu-(0.34*(0.002/phi(i)))))+(fy*Asc)-fy*Ast);
xu = fzero(f,xu);
M(i)=(fc*b*0.5*(xu^2-0.167*((0.002/phi(i))^2)))+(fy*Asc*(xu-d1))+fy*Ast*(d-xu);
else
M(i)=0;
End
end
plot(phi,M/(10^6)),grid; xlabel('Curvature of the section (phi)');
ylabel('Moment of resistance of the section (M) in kN-m');
title('Moment Curvature Relation For RCC section');

```

APPENDIX- III

Table II: Available Indian strong motion records

SI	Earthquake Event	Date	Station	PGA
1	NE-India Earthquake	Aug 6,1988	Cherrapunji	0.511
2	Barkot (NW Himalaya)	March 29,1999	Chamoli	0.226
3	NE-India Earthquake	Aug 6,1988	Dauki	1.06
4	NE-India Earthquake	Aug 6,1988	Gunjung	0.919
5	NE-India Earthquake	Aug 6,1988	Panimur	1.22
6	Chamoli (NW Himalaya)	March 29, 1999	Uttarkashi	0.623
7	Chamoli (NW Himalaya)	March 29, 1999	Tehri	0.611
8	Uttarkashi Earthquake	Oct 20,1991	Srinagar	0.654
9	NE-India Earthquake	Feb 6,1988	Shillong	0.351
10	NE-India Earthquake	Feb 6,1988	Katakhal	0.92
11	Kashmir Earthquake	March 24, 1995	Rakh	0.247
12	Chamoli (NW Himalaya)	March 29, 1999	Joshimath	0.622
13	Uttarkashi Earthquake	Oct 20,1991	Almora	0.947
14	Uttarkashi Earthquake	Oct 20,1991	Barkot	0.242
15	Uttarkashi Earthquake	Oct 20,1991	Koteshwar	0.652
16	N.E. India Earthquake	May 08, 1997	Katakhal	1.053
17	Bhuj Earthquake	Jan 26, 2001	Ahemadabad	0.783
18	Uttarkashi Earthquake	Oct 20,1991	Uttarkashi	2.37
19	NE-India Earthquake	May 18,1987	Diphu	0.719
20	N.E. India Earthquake	May 08, 1997	Shillong	0.708

LIST OF PUBLICATIONS

JOURNALS

1. Ravi Kumar, C. M., Babu Narayan, K. S., Sujith, B. V. and Venkat Reddy, D. (2012). “Effect of irregular configurations on seismic vulnerability of RC buildings.” *Architecture Research*, 2(3), 20-26.
2. Ravi Kumar, C.M., Babu Narayan, K.S., Venkat Reddy, D. and Venkataramana, K. (2013). “Probabilistic format for seismic risk analysis of RC buildings in the Indian Context.” *The International Journal of Structural Engineering (The IUP Journal)*, VI (4), 7-22.
3. Ravi Kumar, C.M., Babu Narayan, K.S., Venkat Reddy, D. (2014). “Probabilistic seismic risk evaluation of RC buildings.” *International Journal of Research in Engineering and Technology*, 3(1), 485-495.
4. Ravi Kumar, C. M., Babu Narayan, K. S., Venkat Reddy, D. and Venkataramana, K. (2014). “Usage of 2-dimensional Gaussian Random variables in probabilistic seismic risk evaluation of RC buildings.” *American Journal of Civil and Structural Engineering*, 1(3), 62-70.
5. Ravi Kumar, C. M., Babu Narayan, K. S., Venkat Reddy, D. and Venkataramana, K. (2014). “Methodology for probabilistic seismic risk evaluation of RC buildings based on POA.” *Open Journal of Architecture Design*, 2(2), 13-20.
6. Ravi Kumar, C.M, Vimal Choudhary, Babu Narayan, K.S and Venkat Reddy D. (2014). “Moment Curvature Characteristics for Structural Elements of RC Buildings.” *Journal on Today’s Ideas –Tomorrow’s Technologies*, 1(1), 1–17.
7. Ravi Kumar, C. M., Babu Narayan, K. S. and Venkat Reddy, D. (2014). “Fragility estimates for RC buildings.” *Global Journal of Earth Sciences and Engineering*, 1, 49-56.

CONFERENCES

1. Ravi Kumar, C.M., Babu Narayan K.S. and Venkat Reddy, D. “Seismic performance evaluation of RC buildings with vertical irregularity.” *ISET Golden Jubilee Symposium, Indian Society of Earthquake Technology*, October 20-21, 2012, Department of Earthquake Engineering, Indian Institute of Technology, Roorkee.
2. Ravi Kumar, C.M., Babu Narayan, K.S. and Venkat Reddy, D. “Generation of 2-dimensional Gaussian random variables in probabilistic seismic risk evaluation of RC buildings.” Poster Presentation, *American Society of Civil Engineers Conference (Indian Chapter)*, 14th-16th March 2014, Vellore Institute of Technology, Tamil Nadu.
3. Ravi Kumar, C.M., Babu Narayan K.S. and Venkat Reddy, D. “Probabilistic seismic risk evaluation of RC buildings with probability of variation in material strength.” *Structural Engineering Convention-2014, Indian Association of Structural Engineering*, 22nd -24th December 2014, Indian Institute of Technology, Delhi.

CURRICULUM VITAE

1. Name: C.M. Ravi Kumar
2. Date of Birth: 03/02/1974
3. Nationality: Indian
4. Address

Office:

Assistant Professor
 Department of Civil Engineering
 University B.D.T College of Engineering
 (A Constituent College of Visvesvaraya
 Technological University)
 Davangere-577004
 Telephone (O):08192-226196 Fax: 08192-233412

Permanent:

Chattekamba
 Junjara Gunte (P.O)
 Challakere (Tq.)
 Chitradurga (Dist.)
 PIN: 577538

5. Mobile: 098450040
6. E-mail: cmravibdt@gmail.com,
7. Academic Qualifications:

Qualifying Degree	Specialization	Institute/University/ Board	Class Obtained	Year of Passing
B. E	Civil Engineering	SJCE, Mysore/ Mysore University	First class with Distinction	1996
M. Tech	Structural Engineering	N.ITK,Surathkal/ Mangalore University	First class with Distinction	2000

8. Professional Experience:

Address of the Organization/ Institute	Post held	Duration	
		From	To
National Institute of Technology Karnataka, Surathkal	Lecturer(Temporary)	10/08/2001	14/02/2006
University B.D.T College of Engineering (A Constituent College of Visvesvaraya Tecnological University, Belagavi) Davangere	Assistant Professor	15/02/2006	Till to date

I declare that above information is true and correct to best of my knowledge.

(C.M. Ravi Kumar)